Airborne Electromagnetics as a method for Arctic wide sea ice thickness retrieval

Luftgestützte elektromagnetische Verfahren zur arktisweiten Bestimmung von Meereisdicken

Cumulative Doctoral Thesis
Kumulative Doktorarbeit

written by

Lasse Rabenstein

Zur Vorlage am Fachbereich Geowissenschaften der
Universität Bremen

February 25, 2010

Contents

ABSTRACT

Improving methods for regular observations of the Arctic sea ice cover is the key to a comprehensive data base necessary for a better understanding of climatic processes. The area and extent of sea ice is routinely observed by satellite platforms, whereas sea ice thickness and the Arctic sea ice mass balance is not yet monitored on Arctic wide scales throughout the year. One method for sea ice thickness retrieval is airborne electromagnetics (AEM) which has been successfully applied from helicopters (HEM) during several expeditions. The purpose of this thesis was to improve AEM sensors in order to mount them under the wings of long range airplanes and to quantify sources of noise that limit the accuracy of the obtained thickness results. Another aim was to determine thickness distribution functions from HEM data of several regions in the central Arctic under summer conditions and to characterise them with respect to different ice regimes. The statistical reliability of spatial constrained HEM data for the evaluation of observed temporal and spatial changes of sea ice thickness are discussed, including the definition of minimum transect lengths necessary for a reliable thickness profile.

For the evaluation of a prototype fixed wing AEM system, the original HEM-Bird system served as a reference of accuracy, noise level and signal drift. Test flights were performed over open water in order to determine the fixed wing system's accuracy for a known ice thickness of zero metres. The test flight results were supported by numerical 3D finite element model studies. The accuracy of the HEM Bird was found to be ± 0.1 m and that of the fixed wing system ± 0.5 m. The author quantified additional noise sources at the fixed wing system caused by wing flexure and inductive coupling between the metallic airplane and the ocean. Wing flexure has a particularly strong contribution that is comprised of a geometric and an inductive part of equal importance, and produces noise which can be as high as the wanted ocean signal. Most of the weaker ocean airplane coupling signal can be removed by calibration. The author further quantified the effect of pitch and roll on the measurements, which can be as high as $\sim$10 percent of the signal. When recorded, pitch and roll can be easily corrected. It is suggested to take that component of the electromagnetic response signal which is 90° out of phase with the actively transmitted source signal, since wing flexure noise mainly is 180° out of phase with the source signal. In future, AEM antennas should be mounted on the more rigid fuselage instead on the wings and the relative positions of the antennas must be measured during flight.

Sea ice thickness distribution functions from the central Arctic were analysed with respect to existing modes, mean, 'full width at half maximum' and the decay of the function towards thicker ice. Furthermore, distribution functions of pressure ridge sail-spacing and -height were determined to evaluate the degree of deformation. Statistical reliability was quantified on the basis of standard errors which were calculated for different profile lengths and the parameters mean thickness, modal thickness as well as pressure ridge height and spacing. Mean/modal thickness standard errors as low as 0.2 m could be obtained for 10/50 km long profiles in less deformed ice, independently of the ice age. In heavily deformed multi year ice (MYI) regimes standard errors of mean/mode were as high as 0.2/0.6 for 100 km long profiles. These results show that a reduction of central Arctic mean/modal thickness by 0.8/0.6 m between 1991 and 2001 as well as a reduction by 1.0/1.0 m between 2001 and 2007 are higher than typical spatial variability within one field campaign, assuming a homogeneous age composition and a low degree of deformation, e.g. five sails per kilometre. Significantly lower thicknesses

occurred in a region where sea ice concentration was below 90% and should not be taken into account for interannual comparisons. The dramatic thickness decrease in the central Arctic between 2001 and 2007 was attributed to a regime shift from MYI to first year ice (FYI). Evidences suggest that 2007 FYI was not exceptionally thin, but remained constant within the fluctuation range of annual melting rates.

ZUSAMMENFASSUNG

Die Weiterentwicklung von Methoden zur Beobachtung der Arktischen Meereisdecke ist der Schlüssel zu einer umfassenden Datengrundlage, die für ein besseres Verständnis von klimarelevanten Prozessen unabdingbar ist. Meereisausdehnung und meereisbedeckte Fläche werden durchgehend von verschiedenen Satellitensystemen bestimmt. Dem hingegen sind Beobachtungen der Meereisdicke, welche für eine Kentnis über die arktische Meereismassenbilanz notwendig sind, weit davon entfernt auf regelmässiger und Arktis umfassender Basis stattzufinden. Eine Methode zur Bestimmung der Meereisdicke ist das luftgestützte elektromagnetische Verfahren (AEM), welches mit Hilfe von Helikoptern (HEM) bereits auf mehreren Expeditionen erfolgreich angewandt wurde. Der vorliegenden Arbeit ist die Verbesserung von AEM Sensoren zum Ziel gesetzt und zwar dahingehend, sie an die Tragflächen eines Langstreckenflugzeuges zu montieren. Insbesondere wurden sämtliche Störsignale die bei AEM Messungen vom Flugzeug auftreten quantifiziert, um ihren relativen Anteil am gesamten Rauschen eines solchen Systems zu bestimmen. Ein weiteres Ziel dieser Arbeit war die Bestimmung von sommerlichen Meereisdickenverteilungen für verschiedene Gebiete in der zentralen Arktis und ihre Charakterisierung in Hinsicht auf die Zugehörigkeit zu verschiedenen Meereisregimen. Weiterhin wurde während dieser Arbeit die Signifikanz von räumlich begrenzten HEM Messergebnissen abgeschätzt, um beobachtete zeitliche und räumliche Veränderungen der Meereisdicke auf ihre Repräsentativität hin zu bewerten. Passend dazu wurde die Frage diskutiert, wie lang ein Meereisdickenprofil sein sollte um repräsentative Ergebnisse zu liefern.

Für diese Studie diente das etablierte HEM-Bird System als Referenz, weswegen für dieses Parameter wie die Stärke der Signaldrift oder das Systemrauschen quantifiziert wurden. Weiterhin wurde im Zuge dieser Arbeit ein Prototyp AEM Gerät konstruiert, an die Tragflächen eines Flugzeuges montiert und für Testmessungen über offenem Wasser verwendet. Dabei wurde unter anderem die Genauigkeit des Systems untersucht, eine bekannte Eisdicke von null Metern zu messen. Die Testergebnisse des Flugzeugsystems wurden durch numerische 3D finite Elemente Modellierungen weiter untermauert. Die Messgenauigkeit des HEM Systems betrug ± 0.1 m und die des Flugzeugsystems ± 0.5 m. Gründe für die geringere Genauigkeit des Flugzeugsystems waren Störsignale, die durch Flügelschwingungen und durch eine induktive Kopplung zwischen dem Metallkörper des Flugzeuges und dem Meerwasser zustande kamen. Insbesondere Flügelschwingungen erzeugten ein erhebliches Störsignal, welches eine geometrische und eine induktive Komponente in der gleichen Grössenordnung aufzeigte und sogar in der Grössenordnung des Nutzsignales sein konnte. Das Kopplungssignal war deutlich schwächer und konnte durch Kalibrationsflüge über dem offenen Ozean berücksichtigt werden. Darüberhinaus wurde der Effekt von Rollen und Neigung des Flugzeuges bestimmt, was das Nutzsignal nocheinmal um bis zu 10% verändern kann. Da Rollen und Neigung während des Fluges aufgezeichnet wurde, konnte das Signal dahingegen korrigiert werden. Für die eigentliche Bestimmung der Meereisdicke mit Hilfe des Flugzeugsystems sollte der Teil des Nutzsignals genutzt werden, der 90° ausser Phase mit dem Quellsignal ist, da Störsignale durch Flügelbiegung vor allem 180° ausser Phase mit dem Quellsignal sind. Bei zukünftigen Flugzeugsystemen sollten die Antennen besser an den starren Rumpf des Flugzeuges montiert werden und die relative Entfernung zwischen den beiden Antennen während des gesamten Fluges gemessen werden.

Meereisdickenverteilungsfunktionen aus der zentralen Arktis wurden in Hinsicht auf vorhan-

dene Moden, Mittel, Halbwertsbreite und exponentiellem Abfall zu dickeren Dicken hin analysiert. Ausserdem wurden Verteilungsfunktionen von Presseisrückensegelabständen und Presseisrückensegelhöhen bestimmt um den Grad an Deformation innerhalb eines Gebietes abzuschätzen. Die statistische Zuverlässigkeit wurde mit Hilfe von Standardfehlern quantifiziert und zwar für verschiedene Profillängen und die Grössen modale und mittlere Dicke als auch für den Abstand und die Höhe von Presseisrücken. Die Standardfehler von mittleren und modalen Eisdicken erreichten den Wert von 0.2 m schon bei Profillängen von 10 und 50 km und zwar in einem einjährigen als auch in einem mehrjährigen Regime. Beide Regime waren relativ undeformiert. In einem stärker deformiertem mehrjährigem Eisregime konnte ein Standardfehler von 0.2 m für die mittlere Dicke erst für Profillängen von 100 km bestimmt werden, wobei die modale Dicke dann lediglich bei einem Standardfehler von 0.6 m landete. Anhand dieser Standardfehler konnte überprüft werden, ob beobachtete zeitliche Änderungen grösser waren als typische räumliche Variabilität. Der Rückgang der mittleren und modalen Eisdicke um 0.8 m und 0.6 m zwischen 1991 und 2001 ist demnach nicht mehr mit einer räumlichen Variabilität zu erklären. Gleiches gilt für den noch stärkeren Rückgang von modaler und mittlerer Dicke um 1.0 m zwischen 2001 und 2007. Dieser Vergleich setzt voraus, dass die Eisregime in ihrer Alterszusammensetzung homogen sind und nicht zu stark deformiert sind, z.B. nicht mehr als fünf Rücken pro km aufweisen. Signifikant geringere Eisdicken besass ein Gebiet in dem die Eiskonzentration bei unter 90% lag. Solche Gebiete sollten für interannuale Vergleiche nicht herangezogen werden. Der starke Rückgang der Meereisdicke zwischen 2001 und 2007 basiert auf einem Regimewechsel von mehrjährigem zu einjährigem Eis. HEM Eisdickenverteilungen deuten an, dass die 2007er einjährige Eisdicke im Rahmen typischer interannualer Schwankungen von Schmelz- und Wachstumsraten lag und nicht aussergewöhnlich dünn war.

LIST OF RELEVANT PAPERS

Paper I

Rabenstein, L., Hendricks, S., Martin, T. and Haas, C. Thickness and surface-properties of different sea-ice regimes within the Arctic Trans Polar Drift: Data from summers 2001, 2004 and 2007 , submitted 09/**2009** to Journal of Geophysical Research - Oceans

Paper II

Rabenstein, L., Hendricks, S., Lobach, J. and Haas, C. Noise characteristics of an electromagnetic sea-ice thickness sounder on a fixed wing airplane., , submitted 02/**2010** to Journal of Applied Geophysics

Paper III

Haas, C., Lobach, J., Hendricks, S., **Rabenstein, L.**, Pfaffling, A., Helicopter-borne measurements of sea ice thickness using a small and lightweight digital EM system, Journal of Applied Geophysics, **67**, 234-241, **2009**

Paper IV

Haas, C., Pfaffling, A., Hendricks, S., **Rabenstein, L.**, Etienne, J.L. and Rigor, I., Reduced ice thickness in the Arctic Transpolar Drift favors rapid ice retreat, Geophysical Research Letters, **35**, LI7501, **2008**

A complete publication list can be found in the appendix.

LIST OF ACRONYMS

AEM	-	Airborne Electromagnetics
AMSR	-	Advanced Microwave Scanning Radiometer
AUV	-	Autonomous Underwater Vehicle
AVHRR	-	Advanced Very High Resolution Radiometer
AW	-	Atlantic Water
AWI	-	Alfred Wegener Institute
BG	-	Beaufort Gyre
DC	-	Continuous Current
DGPS	-	Differential Global Positioning System
DLR	-	Deutsches Zentrum für Luft und Raumfahrt
DM	-	Drift Age Model
EM	-	Electromagnetic
Envisat	-	Environmental Satellite
ERS	-	European Remote Sensing Satellite
FDD	-	Freezing Degree Day
FEM	-	Finite Elements
FWHM	-	Full Width at Half Maximum
FYI	-	First Year Ice
GPR	-	Ground Penetrating Radar
HCP	-	Horizontal Coplanar
HEM	-	Helicopter Electromagnetics
ICESat	-	Ice, Cloud and Land Elevation Satellite
IPCC	-	Intergovernmental Panel on Climate Change
LIDAR	-	Light Detection and Ranging
MODIS	-	Moderate Resolution Imaging Spectroradiometer
MYI	-	Multi Year Ice
PDF	-	Probability Density Function
PSW	-	Polar Surface Water
QuickScat	-	Quick Scatterometer
RV	-	Research Vessel
Rx	-	Receiver
SAR	-	Synthetic Aperture Radar
SSM/I	-	Special Sensor Microwave/Imager
SYI	-	Second Year Ice
TPD	-	Arctic Trans Polar Drift
Tx	-	Transmitter
ULS	-	Upward Looking Sonar
VCP	-	Vertical Coplanar
VCX	-	Vertical Coaxial
VDC	-	Voltage of Continuous Current

LIST OF VARIABLES AND CONSTANTS

Synopsis:

A	-	Area fraction of a certain thickness interval
f	-	Thermodynamical growth function
L	-	Profile length
P	-	Thickness distribution function
Ψ	-	Thickness redistribution function
R	-	Area of sea ice thickness survey
t	-	Time
v	-	Drift velocity field
z	-	Sea ice thickness

Paper I:

A	-	Fitting parameter for the exponential decay of P
B	-	Fitting parameter for the exponential decay of P
C	-	Fitting parameter for the exponential decay of P_{sail}
D	-	Fitting parameter for the exponential decay of P_{sail}
ϵ	-	Standard error
h	-	Sail height
h_{cut}	-	Cut off sail height = 0.8 m
L	-	Latitude
l	-	Profile length
n	-	Number of profiles
μ	-	Fitting parameter for P_{spac}
P	-	Thickness distribution function
P_{rdg}	-	Thickness distribution for ranges thicker than the mode
P_{sail}	-	Distribution function of sail height
P_{spac}	-	Distribution function of sail spacing
P_{dens}	-	Distribution function of sail density
s	-	Sail spacing
σ	-	Fitting parameter for P_{spac}
θ	-	Fitting parameter for P_{spac}
W	-	Open Water Content
z,Z	-	Sea ice thickness
z_{mod}	-	Modal thickness

Paper II:

A	-	Amplitude
$\mathbf{A}$	-	Magnetic vector potential
$\mathbf{B}$	-	Magnetic field
d	-	Antenna separation distance
ϵ_r	-	Relative electrical permittivity
ϵ_0	-	Electrical permittivity of vacuum
h	-	Laser altimeter height
I	-	Inphase component
I_{Tx}	-	Transmitter current strength
i	-	Imaginary unit
L	-	Inductance
μ_0	-	Magnetic permeability of vacuum
μ_r	-	Relative magnetic permeability
N	-	Number of windings in antenna coils
ω	-	circular frequency
Q	-	Quadrature component
Φ	-	Magnetic Flux
r	-	Coil radius
ρ	-	Electrical resistivity
R	-	Pitch response ratio
$\mathbf{R}$	-	Rotation matrix
S	-	Measured sea water plus airplane response signal in parts per million
S_A	-	Modelled response signal from metallic airplane in parts per million
S_O	-	Modelled response signal from sea water in parts per million
S_{AO}	-	Modelled sea water plus airplnae response signal in parts per million
S_P	-	Modelled signal from the Primary Field at the receiver
S_F	-	Modelled coupling signal between airplane and ocean in parts per million
S_{PO}	-	Modelled primary signal plus sea water response signal
S_{PA}	-	Modelled primary signal plus airplane response signal
S_{POA}	-	Modelled primary plus airplane plus sea water plus coupling signal
σ	-	Electrical conductivity
Θ	-	Phase
U_{rec}	-	Recorded high altitude primary plus secondary signal at receiver in volts
U_{ref}	-	Reference voltage at transmitter
U_{calc}	-	Theoretically calculated primary signal in free space at receiver in volts
U_{sec}	-	Secondary field voltage, either calculated by $U_{PS} - U_{calc}$ or identical to U_S
U_S	-	Digitally compensated secondary field voltage at receiver
U_{PS}	-	Primary plus secondary field voltage at receiver
Z_0	-	Mutual Impedance between Tx and Rx

Paper III:

A	-	Amplitude
f1	-	Lower Tx frequency of 3.68 kHz
f2	-	Higher Tx frequency of 112 kHz
h_w	-	EM derived height over sea water
h_i	-	Laser altimeter height
I	-	Inphase component
P	-	Phase
Q	-	Quadrature component
Z	-	Sea ice thickness

Motivation and Key Hypotheses

The presence of Arctic sea ice influences the climate on regional and global scales. Its extent varies on seasonal but also on decadal time scales and can be taken as an indicator for climatic changes in the Arctic. However, for a complete understanding of the Arctic climate and the role of sea ice, regular observations of Arctic sea ice thickness are of importance. Various techniques for sea ice thickness determination exist, ranging from local scale methods like drilling to submarine sonar measurements or Arctic wide scale satellite altimetry. This thesis addresses airborne electromagnetic (AEM) induction sounding, an approach for direct sea ice thickness retrieval by aircrafts. None of these techniques are performed on a routinely basis making the interpretation of thickness data difficult due to spatial and temporal data gaps. The knowledge of the sea ice mass budget is of particular importance because the sea ice thickness distribution is a crucial parameter in Arctic climate models. Without knowledge about the actual thickness of sea ice in the Arctic, predictions of the future state of the Arctic sea ice cover remain uncertain.

In order to evaluate thickness measurements with respect to their accuracy and applicability further research is necessary towards an improvement and better understanding of the particular techniques. The motivation of this thesis is to evaluate the potential of AEM to deliver significant information about sea-ice thickness distributions on Arctic wide scales. On the one hand this thesis deals with technical improvements of AEM systems, primarily to increase the spatial coverage of the method by the usage of long range airplanes instead of helicopters which were previously used during several campaigns. On the other hand a statistical analysis of several AEM sea ice thickness data from the central Arctic is performed in order to evaluate the significance of observed spatial and temporal thickness changes.

Two key hypotheses define the outline of the thesis and are addressed by several approaches.

1. **AEM sea-ice thickness measurements can be performed with antennas mounted under the wings of the polar airplane** *Polar 2* **of the Alfred Wegener Institute.**
   A prototype AEM instrument was constructed and test flights were performed over the North Sea in order to determine the systems accuracy to obtain a known ice thickness of zero. The noise level of the airplane system was compared to that of helicopter systems using a towed EM Bird. Additional noise sources were quantified, by means of test flights and 3D finite element modelling, and the possibility to reduce them by additional data processing was discussed.

2. **On the basis of EM sea-ice thickness data significant spatial and temporal changes can be observed on interannual and decadal scales.**
   A total length of 4000 km ice thickness profiles were obtained by means of helicopter electromagnetics (HEM) in the central Arctic in summer 2007. In addition EM thickness data ranging back to 1991 were used to evaluate trends towards thinner ice in the Arctic Trans Polar Drift (TPD). Ice thickness distribution functions were calculated and compared with respect to their mean and modal thicknesses and with respect to their content of open water and deformed ice. As an important parameter, the standard error of mean and modal thickness and of sea ice pressure ridge parameters were calculated as a measure for natural spatial variability within different ice regimes. These standard

errors were taken as thresholds for significant changes in the sea ice cover.

Introduction

Sea Ice as an Indicator for Climatic Changes

Between 3-6 % of the earths surface is covered with sea-ice (*Comiso and Dieckmann*, 2010) and most of it is situated in the Polar regions. In the southern hemisphere the extent of sea-ice reaches its annual maximum during September and in the northern hemisphere in February-March. Sea-ice forms when the ocean temperature falls below the freezing point which is for a salinity of 34 ‰ at -1.86°C. The colder the air temperature is relative to the ocean the faster sea-ice grows and reaches an equilibrium thickness when the conductive heat transfer through the sea-ice into the atmosphere is equal to the oceanic heat flux coming from e.g. heat reservoirs in the deeper sea (*Petrich et al.*, 2010). Therefore the formation of sea-ice depends on the heat budget of air and ocean and consequently the extent and thickness of sea-ice varies seasonally. For the same reason sea-ice reflects climatic changes and a warmer climate will necessarily lead to a smaller and thinner sea-ice cover possibly resulting in a solely seasonal ice cover in the Arctic. Such a development would have serious consequences for ecosystem and economics in the Arctic. Thus, regular observation of the state of the worlds varying sea-ice cover can be seen as an early warning system indicating changes in the worlds climate earlier than they appear in lower latitudes. However, air temperature and oceanic heat flux are not the only parameters influencing the thermodynamic growth of sea ice. Further parameters are incoming short- and long wave radiation, outgoing longwave radiation, sensible and latent heat fluxes as well as heat fluxes due to surface melting (*Maykut*, 1986).

Sea Ice as a Driver for the Climate

Furthermore sea-ice itself is a driver for the climate in a specific region and even worldwide. In most cases sea ice has a white surface and therefore a high albedo of between 0.4 and 0.8 (*Perovich et al.*, 2006). Thus, over an ice covered area, a huge amount of incident solar energy is reflected and does not contribute to a warming of the earth surface. In comparison, open ocean has a lower albedo and absorbs more solar energy which leads to an accumulation of solar heat which in turn causes more sea ice to melt due to an increased oceanic heat flux. In other words, sea-ice keeps the earth cool and its disappearance would lead to an accelerated warming. This interaction is called the ice albedo feedback.

When sea ice is present the heat exchange between ocean and atmosphere is limited to heat conduction through the sea-ice. I.e. sea-ice decreases the turbulent and radiative heat fluxes between ocean and atmosphere significantly or, if thick enough, it suppresses them entirely. The ocean heat loss over open water for instance is two order of magnitudes larger than over a thick perennial sea-ice cover (*Badgley*, 1966). Hence, sea-ice acts as a lid on the ocean, and the sheer presence of a sea-ice cover reduces the moderating effect of oceans on regional climates. A coast with a year round sea-ice cover has rather a continental climate than an

oceanic one.

Last but not least the formation of sea-ice influences the thermohaline circulation due to salt release during freezing and fresh water release during melting. Thus, sea-ice formation in the Arctic and Antarctic together drives a system of global thermohaline ocean circulation (*Brandon et al.*, 2010).

The Dynamics of Sea Ice

The evolution of a sea-ice cover is always driven by thermodynamic (e.g. heat content of ocean and air) and dynamic processes (e.g. windfields and ocean currents). A low pressure system for instance moving over a closed sea-ice cover causes divergent or convergent ice drift. Such changes can occur even within a time frame of days (e.g. *Bruemmer et al.*, 2008). A wind driven reduction in ice-covered area can be explained by compaction of ice, which in turn leads to an increase in mean thickness by means of pressure ridge formation and rafting of entire ice floes. A dynamical change in the extent of sea-ice can be explained by winds drifting ice for instance north- or southwards or by winds scattering a regional and closed ice cover into several single floes, which in turn is accompanied by an increase in open water fraction within the ice cover, which again reduces the overall albedo and increases the heat content of the upper ocean. This chain of causation could be continued and demonstrates the complexity of the interaction of dynamics and thermodynamics. Two years with the same temperature evolution but with different dominant atmospheric circulation regimes can show significant differences in the minimum sea-ice extent. The fact, that for instance in the 1990's the summer with the largest Arctic sea-ice extent (1996) succeeded the one with the lowest (1995) further express the complexity of the involved processes (*Haas and Eicken*, 2001). The sensitivity of a sea-ice cover to dynamical processes has to be taken into account before the state of a sea-ice cover is put into a climatological context or in particular in a global warming context. *Maslanik et al.* (2007) for instance highlighted the importance of regional atmospheric circulation to a reduction of the Arctic ice cover. This sensibility to dynamical processes makes a year to year prediction of sea-ice extent difficult if not impossible. In any case, sea-ice extent alone is a questionable indicator for the state of the entire sea-ice cover. The mass budget of the sea-ice cover in contrary is less influenced by short term dynamical processes and therefore a better parameter to evaluate the state of an ice cover. This underlines the importance of sea ice thickness retrieval methods.

Sea Ice Thickness, the Missing Parameter

None of the models mentioned in the 4th assessment report of the Intergovernmental Panel on Climate Change (IPCC) predicted the rapid decline of the Arctic summer sea-ice extent during the last years correctly. Those models closest to reality incorporated a detailed parameterisation of sea-ice thickness (*Stroeve et al.*, 2007). Several modelling studies highlighted a sensitivity of the summer sea-ice evolution to the sea-ice volume at the beginning of the melting period (*Dorn et al.*, 2007). An assimilation of observational thickness data into numerical models would increase the chance to predict the evolution of a sea-ice cover at least

on a seasonal scale significantly, as long as the data encompass wide areas. The high sensitivity of numerical models to sea-ice thickness is not surprising when we consider the processes influenced by sea-ice thickness. In first order all kind of heat exchanges between atmosphere and ocean reduces with increasing thickness. Radiative transfer of energy for instance follows a negative exponential dependence on thickness and the conductive heat flux a 1/x behaviour (e.g. *Petrich et al.*, 2010). The mechanical strength of ice and its drag against wind and ocean currents and therefore drift and pressure ridge formation is a function of thickness too (e.g. *Hibler III*, 1986). Last but not least thickness of ice determines the trafficability of ice covered shipping routes like the Arctic North-East and North-West passages.

Methods for Sea Ice Thickness Retrieval

There are several methods to obtain sea-ice thickness. Every method has a certain accuracy, coverage and logistical effort. The one with the highest accuracy certainly is drilling. However, drilling is not applicable for arctic wide operations, and the obtained ice thickness information is very local. Especially thicker ice in form of pressure ridges is hard to drill. The task to get full 3D information of the structure of even a single pressure ridge by drilling alone is quite challenging and can take several days of field work on the ice.

Since 1958 sea ice thickness is measured using upward looking sonar (ULS) from nuclear submarines (e.g. *Wadhams and Horne*, 1980; *Bourke and Garrett*, 1987). The principle of such an instrument is based on the emission of an acoustic pulse and the recording of its reflection from the ice underside. With known travel time, sound velocity and depth under the sea surface the draft of sea-ice can be obtained. Between the 1960s and 1980s ULS submarine cruises were the only arctic wide sea-ice thickness data source. The accuracy of this method with respect to mean thicknesses is in the range of ± 0.25 m (*Rothrock and Wensnahan*, 2007), the logistical effort is enormous and depend on the cooperation with the military. Very often such data are considered as top-secret and are released not before years after the survey. Unfortunately during the 2000s the number of ULS expeditions decreased and only a few recent submarine ULS draft data from the Arctic are published. As an alternative ULS instruments can be mounted on moorings installed on the ocean floor (e.g. *Fissel et al.*, 2008). Such measurement provide good time series but are not suitable for the determination of an areal sea-ice thickness distribution. Recent developments focus on the installation of wide swath ULS instruments on autonomous underwater vehicles (AUV) (*Doble et al.*, 2009).

Alternatively to draft measurements from submarines the idea to measure sea-ice freeboard from aircrafts and satellites by means of laser or radar altimetry emerged. The accuracy of freeboard measurements from air and space is limited to accurate knowledge of the dynamic sea level reference height, the snow thickness on top of the ice and the density of sea-ice and snow. Furthermore, freeboard is on average only 1/9 of the total sea-ice thickness and all inaccuracies of the measurement itself are approximately ten fold. *Kwok and Cunningham* (2008) have estimated the accuracy of thickness data derived from satellite laser altimetry with respect to the uncertainty of all included parameters to 0.7 m. Nevertheless, satellite based altimetry is the only method capable to deliver circumpolar sea-ice thickness data within monthly time frames. So far four satellite systems have been used for freeboard

estimations, the radar altimtery based "ERS-1", "ERS-2" and "Envisat" satellites (e.g. *Laxon et al.*, 2003) and the laser altimetry based "ICESat" (*Kwok and Cunningham*, 2008; *Farrell et al.*, 2009). A future radar satellite mission, the CryoSat2, is scheduled for 2010. All satellite missions have a latitudinal limit due to their orbit which is 81.5° for the ERS and Envisat , 86° for ICESat and 88° for CryoSat2. Furthermore, each altimeter system has a certain footprint (ICESat 70m, ERS1&2 and Envisat several kilometers, CryoSat2 300m) for which the freeboard is averaged. It is still not clear whether this averaged freeboard corresponds to the mean or to the most frequent freeboard within the footprint. Another issue is the penetration characteristic of each system. ICESat is reflected at the uppermost surface, whereas radar systems penetrate a certain depth into the snow cover. Ideally, a radar signal is reflected at the snow-ice interface but ground validation measurements of airborne radar altimetry have shown that the penetration depth can be reduced due to moist snow or compacted ice-like layers within the snow profile (*Makynen and Hallikainen*, 2009). The operation of satellites certainly has the highest logistical effort connected to the largest costs. Furthermore, the involved instrumentation is fragile and occuring system failures cannot be repaired easily. For instance, ICEsat is not running continuously due to battery problems and its operation time is limited to chosen time windows, where cloud density over the Arctic is expected to be low in order to reduce the influence of clouds on the measurements. The predecessor of CrySat2, CryoSat1, did not reach the orbit at all due to a failure of the carrier rocket.

Other satellite methods are based on the measurement of different surface properties. Thermal infrared sensors (e.g. AVHRR (Advanced Very High Resolution Radiometer) or MODIS (Moderate Resolution Imaging Spectroradiometeer)) measure the surface temperature of sea-ice from which thin ice thicknesses up to 0.5 m can be estimated (e.g. *Yu and Rothrock*, 1996) when the survey area is cloud free. Other sensors (SSM/I (Special Sensor Microwave/Imager) or AMSR (Advanced Microwave Scanning Radiometer) measure microwave brightness temperatures, which are directly connected to surface temperatures. Thin sea-ice thicknesses of up to 0.2 m can be estimated from these kind of measurements (e.g. *Martin et al.*, 2004). Measurements of low brightness temperatures and radar backscatter (QuikScat Satellite) are suitable to differentiate between first year ice and ice which survived a melting season (*Haarpaintner and Spreen*, 2007). This is a qualitative approach to the sea-ice thickness problem assuming that older ice is thicker than first year ice. Such measurements deliver important evidences for the retreat of multi year ice from the Arctic. A last method widely used for studies of the sea-ice cover is SAR (Synthetic Aperture Radar) imagery. SAR delivers high resolution images of the sea-ice surface where the difference between young ice and older ice is clearly visible due to different radar backscatter (e.g. *Holmes et al.*, 1984).

Methods from the field of Applied Geophysics, like ground penetrating radar (GPR), DC-Geoelectrics, Electromagnetics (EM) or Seismics, were tested for sea ice thickness measurements during several studies. Methods capable to obtain sea-ice thickness were DC-Geoelectrics, EM and for certain prerequisites GPR. DC-Geoelectrics involves a lot of in-situ field work where several electrodes have to be placed on the ice surface (*Flinsbach*, 2005). This intensive field work makes the coverage of Geoelectrics similar small to those of simple drilling. The interpretation of GPR radargrams of sea-ice is difficult due to scattering effects. Brine channels and the loose structure of pressure ridges cause scattering and attenuation of

the radar wave, therefore a reflection from the ice-ocean interface is not visible for young salty ice and for heavily deformed ice. However, recent studies by *Holt et al.* (2009) dealing with ultra wide band GPR are promising with respect to the detection of the ice-ocean interface on first year ice. Ground EM was first applied on sea-ice by *Sinha* (1976). As it turned out to be a suitable method, with an accuracy of 0.1 m on level ice, further studies followed (*Kovacs and Morey*, 1991; *Haas et al.*, 1997). The main advantage of the EM method is its feasibility to do airborne surveys and therefore to cover larger areas. First successful helicopter EM sea-ice thickness measurement were already performed by *Kovacs et al.* (1987). Airborne EM then spreaded out and several other case studies were performed (*Kovacs and Holladay*, 1990; *Liu et al.*, 1991; *Kovacs et al.*, 1995; *Multala et al.*, 1996; *Prinsenberg et al.*, 1996 2002; *Pedersen et al.*, 2009). Since the early 2000s the Alfred Wegener Institute performs regular helicopter electromagnetic measurements in the Antarctic and Arctic, under winter as well as summer conditions (*Haas et al.*, 2006 2008 2009; *Pfaffling et al.*, 2007; *Pfaffling and Reid*, 2009; *Rabenstein et al.*, 2010). The method of airborne EM is further explained in the chapter 'The Method of Airborne Electromagnetics'.

Another interesting approach is the passive recording of the propagation of low amplitude and low frequency intragravity waves in a sea-ice covered ocean (*Wadhams and Doble*, 2009). Such waves are triggered by ocean surface waves approaching the sea-ice margin. The recording itself is done with a basin wide array of e.g. gravimeters, accelerometers or tilt buoys placed on the ice. The idea is to invert a thickness dependent travel time between two recording stations into a mean thickness along the wave travel path. It is likely that the so derived thickness represents the most frequent thickness in the area of wave propagation and not the mean thickness.

A very new approach is the offbeam recording of the diffusive return of actively tranmitted LIDAR pulses (*Varnai and Cahalan*, 2007) during airborne operations. The size and intensity of halos (annular oriented spread of light around an illuminated spot) depends on the thickness of the underlying sea-ice and snow layer. The existence of halos can be explained by volume scattering of light. The signal emerging from scattering processes in sea-ice is so weak, that LIDAR measurements have to be conducted during night. Applications of LIDAR are still in an experimental status and further validation measurements are necessary.

Sea Ice in the Arctic Ocean

The biggest difference between Arctic and Antarctic sea ice is the fact that Arctic sea ice is limited in its extent and drift by the Eurasian and American continents, whereas the ring of sea ice around the Antarctic continent is not constrained by land masses on its outer boundary. These different settings have consequences on the dominant weather situations and on the oceanographic situation. The Arctic Ocean has three connections to the worldwide ocean system. The biggest is Fram Strait and Barents Sea together, ranging from Greenland to Svalbard and Scandinavia. The second entry for water masses into the Arctic Ocean is the shallow and narrow Bering Strait between Alaska and Siberia and the third connection to southern oceans consists of a system of narrow channels between the islands of the Canadian archipelago. In terms of water mass exchange the opening to the Atlantic Ocean is the most

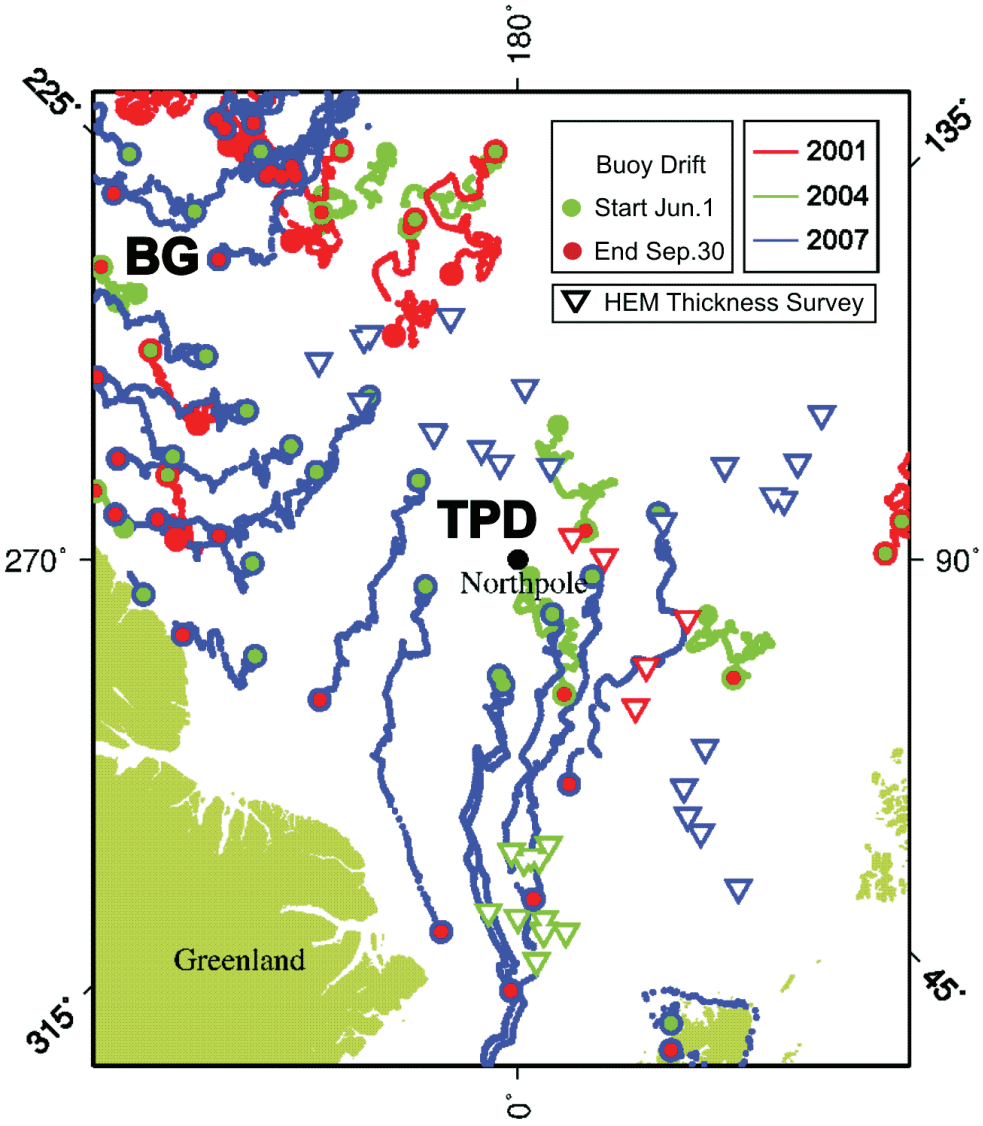

Figure 1: Drift buoy data from the central Arctic of a four month period during the summers of 2001, 2004 and 2007. Green dots mark the starting point on June 1 and red dots the buoy position after a four month drift on September 30. Triangles mark positions where helicopter electromagnetic (HEM) surveys were flown during the same period. In 2007 buoys drifted twice the distance between start and end point as in 2001 and 2004. The 2001 and 2004 drift trajectories are more chaotic reflecting less persistent wind fields during this particular summers. Furthermore, in 2001 the BG was not well developed, and even buoys north of the archipelago drifted towards Fram Strait during the four month period. In contrast the 2007 drift shows a well developed anticyclonic BG together with a strong TPD. (Drift data base: *http://iabp.apl.washington.edu/*)

important one (*Brandon et al.*, 2010). Warm and saline Atlantic Water (AW) from southern latitudes is transported through the eastern Fram Srait and the Barents Sea into the Arctic

Ocean and spreads into the Arctic basins. Measurements in the central Arctic ocean shows that the AW is overlaid by a layer of fresh and cold Polar surface water (PSW). Fresh, because it is influenced by the river run-off from Siberia, Alaska and Northern Canada. AW and PSW are separated by the so called Arctic halocline, which existence maintains the Arctic sea ice cover. In regions where the halocline is not well developed (e.g. Svalbard) increased oceanic heat flux from the AW often prevents the formation of a sea ice cover even in winter. The main outflow of cold PSW, an with it the main export of sea-ice, takes place through the western Fram Strait. This outflow is the extended arm of a surface current system covering the central Arctic and the regions east of the North Pole, the Trans Polar Drift (TPD). The TPD acts as a gigantic conveyor belt exporting sea-ice from the eastern and central Arctic into the North Atlantic. The velocity of the TPD varies for different years and sea ice can last in the TPD between one, two or even more than two years. A good example is the different endurance of two TPD drift experiments: The drift of Fridtjof Nansens *Fram* which lasted from autumn 1893 to spring 1896 and the recent *Tara* drift experiment which lasted one year less from autumn 2006 to spring 2008. Sea-ice drift in the central Arctic during a four month period for three different years is shown in Figure 1. In some years the TPD is extremely accelerated and ice is extensively flushed out of the Arctic Ocean into the North Atlantic, as happened e.g. in the winters 05/06 & 06/07 (*Nghiem et al.*, 2007). In years with a dominant TPD its influence reaches as far as western Greenland and huge amounts of perennial ice from North of Greenland drift into the Fram Strait. In other years the direction of the TPD can be on short term even reversed depending on the actual weather situation. The regions north of Alaska and the western archipelago up to the North Pole are dominated by the anticylonic Beaufort Gyre (BG). Sea-ice can last in the BG for many years. TPD and BG both push ice on a long term towards Greenland and the coasts of the archipelago. The ice export through the narrow straits of the archipelago is smaller than the ice advection from TPD and BG causing the formation of thicker and older perennial sea-ice zones north of Greenland and north of the Canadian Islands. Depending on the dominant atmospheric circulation in a year the BG can be quite expanded or limited to a small region (see Figure 1). These complex interactions have consequences for the appearance of sea-ice. For instance in Fram Strait where the ice streams of the TPD converge a higher degree of deformation can be expected and therefore a higher number of pressure ridges.

Long Term Changes of the Arctic Sea Ice Cover

Since the beginning of sea-ice satellite observations in 1979 the seasonal cycle of sea-ice extent in the Arctic is superimposed with a negative trend. This trend even accelerated from -2.2% per decade between 1979-1996 to -10.1% per decade in the last 10 years (*Comiso et al.*, 2008). Particular dramatic is the evolution of the summer minimum sea-ice extent, which reached a record minimum of only 62% of a climatological average in 2007 . So far there is no sign of a substantial recovery and also in 2008 and 2009 the summer extent was below the long term average. According to the 4th IPCC report and other publications this reduction is connected to global warming. Some observation can be interpreted as a direct impact of warming, e.g. the overall increase in Arctic melt season by more than one week per decade since 1979 (*Stroeve et al.*, 2006) or by 5 days per decade for the perennial ice zone between 1979 and 1996 (*Smith*, 1998). The question raises whether the Arctic sea-ice cover develops towards an

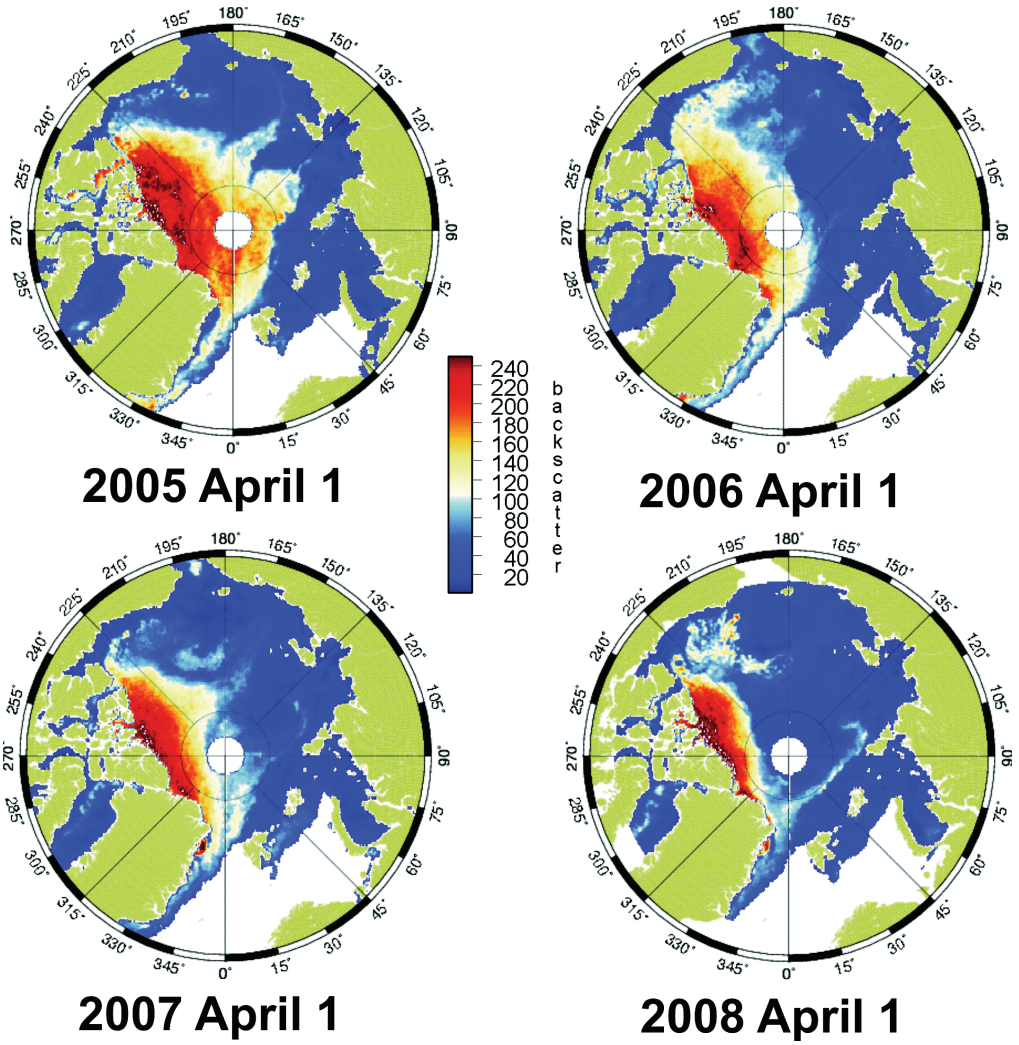

Figure 2: Circumpolar maps of radar backscatter intensity over sea ice for April 1 between 2005 and 2008. Backscatter strength is given in relative strengths. Higher backscatter regions (yellow and red) coincide with multi year ice (MYI) which survived the previous summer melt season. Blue colours coincide with first year ice. Clearly visible is the steady decrease of the MYI fraction. (Data base: *http://cersat.ifremer.fr/data/discovery/by_parameter/sea_ice/psi_quikscat*)

ice free Arctic Ocean or whether the observed changes are part of natural variability. Nobody can give a definite answer but if the observed development of the last 30 years continues or even accelerates the Arctic ocean will be ice free sooner than later. Some model studies predict an ice free arctic ocean in summer before the end of the 21st century (*Boe et al.*, 2009). However, the 2007 minimum e.g. could not be predicted by any of the IPCC climate models demonstrating how little is understood of the processes in the Arctic. This motivated many studies to deal with processes leading to the record minimum in 2007. Some studies highlighted the importance of regional atmospheric circulation (*Ogi et al.*, 2008; *L'Heureux et al.*, 2008) other referred to exceptional heat gain of the Arctic ocean (*Steele et al.*, 2008;

Perovich et al., 2008). Probably the most prominent change of the Arctic sea ice cover during the last five years was the disappearance of large areas of perennial sea ice. *Nghiem et al.* (2006 2007) showed that the fraction of perennial sea ice in the Arctic decreased by 23% from 2005 to 2007 (see Figure 2). It is assumed that such a reduction in MYI is accompanied by an overall thinning and therefore by a potential rapid reduction of sea-ice extent during future melt seasons.

Whether thickness and therefore volume of the Arctic sea-ice cover decreases with the same intensity as the extent is controversially discussed (e.g. *Gerdes and Koeberle*, 2007; *Lindsay et al.*, 2009). During the last four decades of the 20th century extensive ULS measurements of sea-ice draft from nuclear submarines were performed resulting in a series of publications. Most of them indicate an overall thinning of ice in the Arctic. E.g. 43% thinning of mean draft in the Fram Strait between 1976 and 1996 (*Wadhams and Davis*, 2000a) and 1.5 m thinning of mean draft in the Western Arctic between the mid-1980s and early 1990s (*Tucker et al.*, 2001). In the central Arctic a comparison of the periods 1958-1970 and 1993-1997 indicated a shift of ice thicker than 2 m to thinner ice between 1-2 m accompanied with a volume loss of 32% (*Yu et al.*, 2004). Contrasting to this, two studies published in 1992 and 2002 refer to the high interannual variability of sea-ice thickness in the central Arctic and conclude that in this region no significant reduction in mean thickness could be observed for the period 1977 to 1990 (*McLaren et al.*, 1992) and that mean ice thickness between 1986 and 1997 remained constant (*Winsor*, 2001). So the same data base lead to different conclusions. *Rothrock et al.* (2008) found that previous interpretations of submarine data often ignored the seasonal influence or compared different locations. Therefore they published an analysis of all available submarine data (36 cruises since 1958 in the central and western Arctic) and determined their spatial, annual and interannual variability with the result that the annual mean draft declined from a peak of 3.42m in 1980 to a minimum of 2.29m in 2000. In the 2000s the ULS submarine activities in the Arctic were reduced to only sporadic experiments and the need for alternatives emerged.

Two alternative methods which produced results worth to mention in the context of a thickness trend is ground and airborne EM and laser and radar satellite altimetry. Already in the 90's extensive ground EM thickness measurements were done in the TPD by *Haas* (2004). He found in accordance with the results of *Rothrock et al.* (2008) a decrease of mean thickness in the central Arctic from 3.11 m to 2.41 m (22.5%) between 1991 and 2001. Satellite radar altimetry derived sea-ice thickness for regions below 81.5° North showed a high interannual variation and no significant trend for the winters between 1994 and 2001 (*Laxon et al.*, 2003). Ice thickness observations of the last 10 years however, all agree in a substantial thinning of Arctic sea-ice. ICESat measurements indicate a circumpolar freeboard reduction of -1.8cm per year of autumn sea ice and -1.6cm per year of spring sea ice between 2003 and 2008 (*Farrell et al.*, 2009). Based on the same dataset *Kwok* (2009) quantified the reduction in terms of MYI and FYI thickness and volume. MYI thickness decreased during the observation period by 0.6 m whereas FYI thickness remained constant. In terms of volume this means a net reduction of total ice volume of 42% for autumn sea ice and 21% for winter sea ice. Interestingly the loss of MYI volume is larger than the overall volume loss, which is only partially compensated by an increase in FYI volume. The strongest reduction in MYI volume took place during the record minimum summer in 2007 which is also supported by the results

of *Giles et al.* (2008). They analysed radar altimetry based sea-ice thickness for latitudes below 81.5° North between 2003 and 2008 and found a constant mean sea ice thickness for the period before summer 2007 and a an abrupt step towards a 0.26 m thinner circumpolar mean thickness and towards a 0.49 m thinner mean thickness in the western Arctic.

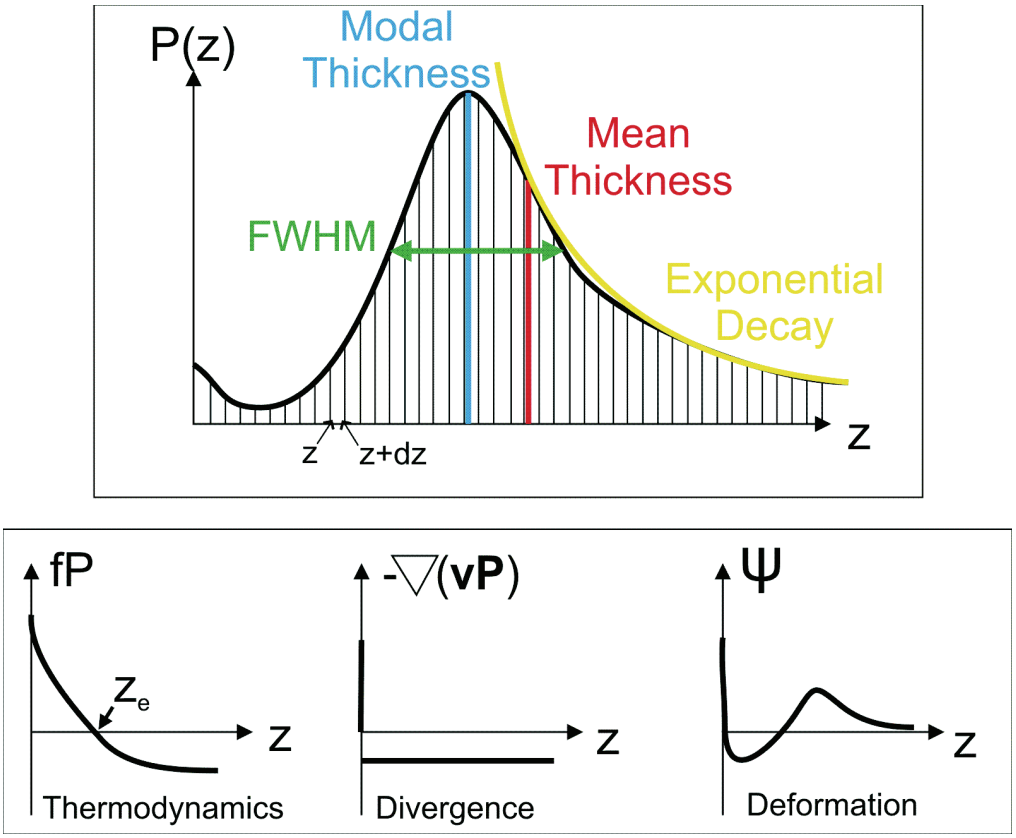

Figure 3: A typical sea ice thickness distribution P with the characteristic quantities mean, mode, "full width at half maximum" (FWHM) and exponential decay. In case of a discrete distribution function P is defined for intervals dz. Furthermore the single terms of equation 0.2 are illustrated. z_e is the thermal equilibrium thickness.

Theory of Ice Thickness Distribution

The complex interaction of thermodynamic and dynamic processes create a non homogeneous distribution of thickness in a survey area **R**. Thickness varies between very thin ice formed recently on open leads, seasonal ice from the autumn freeze up reaching thicknesses of ∼1.6 m in spring or perennial sea ice which can be significantly thicker than 1.6 m. Every ice class can be subject to deformation processes leading to rafting of ice thinner than 0.5 m or to ridging events creating ice of thicknesses up to 20m and even more (*Wadhams and Davis*, 2000a). In order to estimate the thickness distribution of a survey area **R** the distribution function P has to be determined. The fraction of **R** with ice thickness z and $z_1 < z < z_2$ is

given by:

$$\int_{z_1}^{z_2} P(z)dz = \frac{1}{R}A(z_1, z_2). \tag{0.1}$$

with **A** the area fraction of **R** where ice thickness is between z_1 and z_2. From a large enough number of statistical independent thickness measurement taken within **R** a discrete version of $P(z)$ can be formed, a so called histogram with the discretization dz. *Thorndike et al.* (1975) for the first time described a theory in order to interpret $P(z)$ with respect to the responsible processes. The evolution of $P(z)$ can be described by the following formula:

$$\frac{dP}{dt} = -P\nabla \cdot \mathbf{v} - \frac{d}{dz}(fP) + \psi \tag{0.2}$$

where $\mathbf{v}$ is the velocity field of the drifting ice, f is a thermodynamic growth function and ψ is called the redistribution function. The first term describes the divergence of ice, the second the thermodynamic growth and the third deformation of sea ice. In Figure 3 a sample thickness distribution function and the three terms of equation 0.2 are shown. If both, the divergence and deformation term would be somehow suppressed the sea-ice thickness distribution would appear as a delta pulse at $z = 0$ to the time of autumn freeze up and would reach an equilibrium thickness z_e at the moment when oceanic heat fluxes equals the heat transfer through the ice. The shape of f in Figure 3 includes the thickness dependence of ice growth. The position where f becomes zero reflects z_e and ice thicker than z_e melts even in winter. The divergence term accounts for the advection and export of ice within **R**. It has a delta peak at $z = 0$ simulating cracks and open leads emerging due to a divergent sea-ice drift. In case of a convergent ice regime the divergence term shown in Figure 3 is mirrored at the y-axis. ψ can be seen as a sink for thinner ice, which is easier to deform, and a source for thicker ice and therefore it describes the redistribution of level ice into pressure ridges. Furthermore ψ is volume conserving and area changes due to ψ must equal the net divergence. *Thorndike et al.* (1975) found a plausible description of the evolution of $P(z)$: '*The thermodynamic seeks the mean and the mechanics the extremes. The thickness distribution is an historical integral of the continuous and simultaneous action of these two processes.*'.

From the sample distribution function in Figure 3 can be seen that $P(z)$ is not normal distributed around the mean. Therefore we differentiate between a mean thickness, which is also influenced by the degree of deformation, and a modal thickness, which reflects the most frequent ice thickness. Ideally, the modal thickness is related to huge areas of undeformed ice emerged during the same autumn freeze up. Then the modal thickness is a direct measure for the thermodynamic growth conditions. Probably this relation becomes weaker for perennial sea ice, which has survived several seasonal cycles and the dynamical terms had more time to act on the thickness distribution.

Statistics of Sea Ice Thickness Sampling

A question concerning all in-situ sea-ice thickness measurements is that of undersampling. Can a measurement based on certain profiles be representative for an entire region? With the representativeness of even shorter ice thickness drilling profiles dealt a study by *Eicken and Lange* (1989). They compared the thickness distribution of two profiles from the Fram

Strait region: a 1.23 km long drilling profile (5m spacing) and a 2845 km submarine profile. Both distributions showed the same characteristic maximum of 3 m. *Eicken and Lange* (1989) attributed this similarity to the topography of sea-ice in Fram Strait, and stated that even smaller floes potentially reflect the thickness evolution of the overall perennial sea-ice of this region.

A quantification of the significance of variability is the standard error, which is the standard deviation of a number of mean values corresponding to subsections of certain length. If the standard error remains high for even longer subsections in one area, the assignment of a mean thickness to the complete survey area is questionable and even more questionable is the comparison of two mean thickness values of subsequent years. *Wadhams* (1997) determined standard errors for 50km long subsections of four submarine expeditions between 1977 and 1990 and found that the standard error around the North Pole during one expedition was with 0.492m (12.75% of mean thickness) in the same order of magnitude as the variability of mean thickness between different years and therefore too high to justify a significant reduction in mean thickness for this period.

Another quantity of importance is the sampling interval in order to assure statistical independence of a result. Therefore a sampling interval should exceed the autocorrelation length of a thickness distribution which can be between e.g. 185 m on a single drilling profile in Fram Strait (*Eicken and Lange*, 1989) or larger than 1000 m for more homogeneous regions e.g. in the Beaufort Sea (*Rothrock and Thorndike*, 1980). However, keeping the example of *Eicken and Lange* (1989) in mind even shorter profiles with a shorter sampling interval can be representative for an entire region but unfortunately there are no grounds to know this in advance.

One question remains concerning the length of a profile necessary to obtain mean and modal thickness with a satisfying standard error. *Wadhams* (1997) suggested to take his 12.75% reference standard error for 50km sections and the assumption that the standard error decreases with profile length like $L^{-0.5}$ in order to determine the length necessary for significant results. A recent study by *Percival et al.* (2008) showed that the standard error decreases with $0.29^2 \cdot (\frac{L}{50})^{-0.46}$ as well based on 50km subsections. The *Percival* relation implies that the standard error decreases by a factor of 3.5 slower than suggested by *Wadhams*. However, both relations assume that the significant morphological properties occur on small scales below 50km segments. Such an ice field can be referred to as well mixed. When significant changes occur on larger scales the ice pack is poorly mixed due to e.g. two converging ice regimes, for instance a seasonal and a perennial one.

Surface Properties of Sea Ice

Further parameters of an ice cover than area, extent and thickness have to be obtained for a complete understanding of sea ice related processes.

The number and distribution of pressure ridges reflects the degree of deformation, influences the drag against wind and ocean current and is furthermore an important parameter for navigation in ice covered shipping routes. Height and spacing of pressure ridges can be

profiled by laser altimetry or ULS submarine measurements. According to previous studies the spacing of pressure ridges follows a lognormal distribution function (*Davis and Wadhams*, 1995; *Wadhams and Davy*, 1986) and sail height a negative exponential one (*Tucker et al.*, 1979). It was found that spacing of pressure ridges is subject to strong spatial variations whereas the height of pressure ridge sails is fairly constant at a given time (*Tucker et al.*, 1979). The height of pressure ridge sails is often interpreted as a measure for the thickness of an ice cover during visual observations, which is true for the thickness of deformed ice (*Timco and Burden*, 1997) but whether there is a connection between sail height and level ice thickness within an ice regime is not clear by implication.

In summer when the air temperature increases, the surface of a sea-ice cover starts to melt and melt ponds appear. The surface of melts ponds is darker which in turn lowers the albedo of the sea-ice cover and accelerates its solar heat gain (ice albedo feedback). The mean albedo of a snow covered surface is determined to be 0.8 and that of a ponded surface on thick MYI to be 0.4 (*Perovich et al.*, 2006) and even less on a thinner FYI cover. The contribution of melt ponds to an accelerated surface melt of sea-ice is still not entirely understood but nevertheless intensively studied. *Perovich et al.* (2003) for instance found an on average 0.21 m larger total amount of surface melt on ponded ice in comparison to unponded ice.

The Method of Airborne Electromagnetics

Electromagnetic (EM) Surveying is a method from the field of Applied Geophysics and uses the response of conductive bodies to a propagating electromagnetic field in order to determine the size, conductivity and distance of the body. Classical targets are conductive ore bodies in a high resistive ground as they appear in Scandinavia and Canada where this method was first applied in the 1920s. The coupling between antennas and ground is of inductive nature making mechanical contact unnecessary. This characteristic makes EM methods suitable for airborne operations. The first successful airborne EM (AEM) survey was flown in the 1950s in Canada to qualitatively detect conductivity anomalies in the shallow subsurface. Within AEM most systems are so called active systems i.e. that both transmitter and receiver are mounted on the aircraft. Furthermore some systems transmit and record continuously at the same time, so called frequency domain systems, and other record the response of a transient EM pulse during transmitter off time, so called time domain systems. Frequency domain systems used for geological mapping and ore exploration usually own several frequencies in order to get EM responses from different depth levels. For sea-ice thickness retrieval only frequency domain systems are used so far and in this special case even single frequency systems deliver useful results. Suitable airborne platforms are aeroplanes as well as helicopters both connected with different implication problems. Very often helicopter EM (HEM) makes use of a towed Bird system. An EM-Bird includes all antennas, transmitter and receiver, as well as a compensation coil in order to suppress the primary signal from the transmitter to obtain a clear residual response signal from the ground. The rigidity of the Bird is of advantage, since separation changes between transmitter and receiver influence the response signal with d^3. In principal, an EM-Bird realisation is feasible for aeroplane systems, provided that a winch exists and that the aeroplane is certified to carry external swing loads. However, in the past some fixed wing antenna systems were constructed as well. Today the fixed wing

EM system of the Geological Survey of Finland and the British Geological Survey is the only frequency domain fixed wing instrument available for scientific purposes (*Levaniemi et al.*, 2009). For the sea-ice application the advantage of a long range aeroplane over the shorter ranged helicopters is obvious, since sea ice thickness data have to be obtained on wide areas to be significant. A method to reach the central arctic even with HEM is the usage of an ice breaker as a helicopter landing platform. However, even with an ice breaker the thicker perennial sea-ice zone cannot be reached easily.

The transmitter itself consists of a coil supplied with an alternating electrical current which in turn creates an alternating magnetic dipole field (the primary field). The magnetic moment of the transmitter increases with current strength, coil diameter and the number of windings. The actively transmitted EM field causes via induction a corresponding alternating current on the receiver coil. In homogeneous space the response on the receiver coil can be calculated analytical (e.g. *Keller and Frischknecht*, 1966). When conductive structures are within the range of the primary field, the receiver signal consists of the primary signal plus a secondary signal caused by induced eddy currents in the conductivity structure. The secondary field response can be calculated analytically for simple geometries like a homogeneous halfspace or a layered subsurface. If the subsurface structure becomes more complicated numerical methods have to be used to simulate the response signal and to proper invert EM response into conductivity of the subsurface. The orientation of the coils is of importance since it determines the orientation of the magnetic dipole. Usual configurations have a pair of horizontal coplanar loops (HCP), vertical coplanar loops (VCP) or vertical coaxial loops (VCX). The EM method can be described with the quasi static approximation of the Maxwell equations. This approximation is valid as long as the involved wavelengths of the EM signal are much larger than the dimension of the problem. Frequencies of EM methods usually lie in the range of 2 kHz to 100 kHz.

Airborne EM systems have to be calibrated over targets of known response. Alternatively this can be done by the help of a calibration coil installed within the instrument (*Fitterman*, 1998). After calibration every change of the systems configuration causes the calibration to be invalid. Possible changes are the resistivity of the coils due to temperature changes, a change in antenna separation due to mechanical forces or pitch, roll and yaw movements of the instruments which changes the orientation of the magnetic dipole relative to the ground. Low frequency changes of system parameters cause drift, which is mainly driven by the operation temperature of the antennas and the in turn changing resistivities of transmitter and receiver coil. Drift of a system is clearly visible during flights in high altitude where the response signal should be zero. So the drift during high altitude flight sections can be extrapolated in order to correct for drift during low altitude survey sections.

AEM measurements are relative measurements and record the secondary or response field in parts per million (ppm) of the actively transmitted primary magnetic field. The involved magnetic fields are in the order of 10^{-7} Tesla. Furthermore, the phase shift between primary and secondary magnetic field is of importance. An alternative description to the Phase-Amplitude description is the Inphase-Quadrature nomenclature. The inphase and quadrature component are that parts of the secondary field which are 180° and 90° out of phase with the primary field. The higher the conductivity of the subsurface, which is the ocean in the sea ice application, the larger is the inphase component relative to the quadrature component.

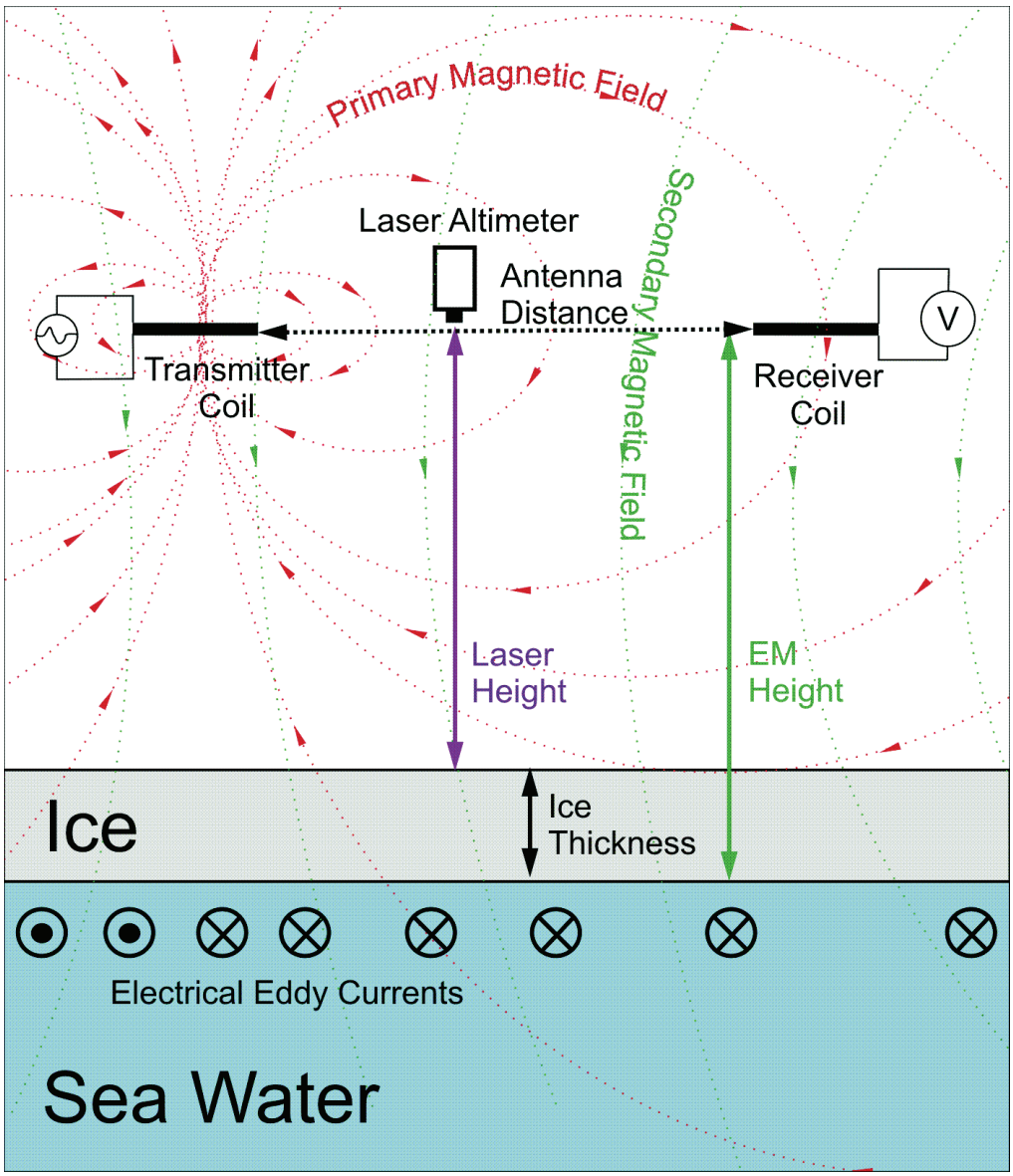

Figure 4: Principle of AEM sea ice thickness sounding for the HCP case. Two heights, laser height and EM height are subtracted from each other in order to obtain ice thickness. An AC current on a horizontally oriented transmitter coil creates a primary magnetic vertical dipole field which induces electrical eddy currents in the ocean. Those in turn cause a secondary magnetic field which can be measured as an induced current on the passive receiver coil. The EM height can be derived from the strength of the secondary magnetic field. The method is highly sensitive on the antenna distance. In EM Birds a third coil is placed close to the receiver in order to compensate the primary magnetic field physically at the receiver location (not shown in the picture).

Specifics of Electromagnetics on Sea Ice

The application of AEM on sea-ice is special for two reasons: 1. Ice thickness is a highly quantitative measure and 2. the presence of the high conductive ocean makes calibration

easier. The principle of AEM for sea ice thickness determination is sketched in Figure 4. The quantity that has to be measured with a desired accuracy of 10 cm is the distance of the instrument to the ocean. Ice thickness is then derived by a second measurement of the distance between instrument and uppermost snow or ice surface. Ice thickness is the difference of both distances. A 10 cm accuracy can only be reached if the systems calibration can be rechecked frequently and here the second reason for speciality comes into play. The ocean can bee seen as a homogeneous good conducting halfspace. Therefore flights in different altitude over open water result in well known responses, assuming that the height (measured with a laser altimeter) and the conductivity (measured with a ship based salinometer) is known. Remaining noise sources which cannot be handled by frequent calibration is pitch, roll and yaw. Therefore a stable flight is of importance. A lot of up and down manoeuvres during flight causes an EM-Bird to tilt. For a fixed wing antenna system the change in antenna distance due to wing flexure is of particular importance in order to maintain a noise level required for a 10 cm accuracy.

Interpretation of AEM sea-ice thickness data have to take into account the footprint of the system. Studies by *Kovacs et al.* (1995) characterised the footprint for HCP configurations as 3.7 times the flight height and for a VCX configuration as 1.35 time the flight height. *Reid et al.* (2006) have further improved the footprint definition by a dependency on the so called induction number with the result of realistic footprint ratios for the HCP sea-ice case of 2.7 and 4.6 times the flight height for Quadrature and Inphase respectively. Consequently ice thickness values are averaged over the area of the footprint and maximum thicknesses of pressure ridges are underestimated by up to 50%. Nevertheless, studies by *Hendricks* (2009) showed that on longer profiles the measured modal and mean thickness agree with the true thicknesses within ±0.1 m.

For the determination of the distance between instrument and ocean the on average two magnitude smaller conducting sea-ice layer can be neglected for frequencies usually used for sea ice thickness determination (*Pfaffling et al.*, 2007).

Key Findings of the Thesis

Requirements for HEM Sea Ice Thickness Sounding

Paper III can be taken as the methods part of the thesis, since it includes the description of the AWI EM Bird system used for all thickness measurements mentioned in Paper I and IV. To meet the quantitative nature of sea ice thickness measurements an EM system need certain requirements and proper handling in the field. A feasible realisation of a sea-ice thickness sounder is the EM Bird solution due to the rigidity of the antenna system and the large distance to the metallic aircraft. In Paper III an analysis of noise and drift characteristics of the AWI EM Bird is presented. Furthermore our experience and advises for a proper handling are introduced. For sea-ice thickness determination generally the inphase component of a single frequency is sufficient, as long as the noise level is not larger than ±10 ppm and the drift below 200 ppm per hour. Those requirements are only met if a two hour warming phase prior to the actual survey flight is maintained. The warming phase reduced the drift by up to

75%. When those requirements are fulfilled an ice thickness accuracy over undeformed level ice of 0.1 m can be guaranteed as long as flight height does not exceed 20 metres and other parameters like antenna distance and transmitter dipole moment are oriented on the AWI EM Bird.

The AWI EM Bird was operated during several field campaigns under polar summer and winter conditions. Our experience shows that the noise level of the 3.68 kHz signal varies between ± 10 and ± 5 ppm independently of the weather conditions. The residual drift remaining after the warming phase never exceeded 200 ppm per hour, was sometimes positive, sometimes negative and could not be attributed to temperature or any weather situation. We conclude that this level of noise and drift is the minimum level reachable with the AWI EM Bird system. Under these circumstances we suggest to recalibrate the EM Bird system approximately every 15 minutes during a 3 to 5 minute flight in altitudes higher than 300m on the basis of the internal calibration coil. In addition, during sections of low altitude thickness surveying open water spots within the ice cover should be over flown in different altitudes in order to get additional data for a post flight adjustment of phase and gain on the basis of a 1D model curve. However, it is of importance to avoid strong course correction and therefore tilting of the EM Bird which is of higher priority than measurements over open water spots.

Quantitative Measurements with Fixed Wing Antenna Systems

So far EM systems mounted on the wings of airplanes were used for qualitative measurements of conductivity anomalies only. The results of Paper II have to be seen in context with the work of *Multala et al.* (1996), which is the only exception where a fixed wing antenna system was used for sea-ice thickness measurements. Motivated by the accuracy of ±0.2 m *Multala* reached, the AWI initiated a feasibility study to install a sea-ice thickness EM system on the available pylons under the wings of the institutes own polar airplane, the "Polar 2" which is a Dornier 228. A prototype instrument was constructed and test flights over the North Sea and in Spitsbergen were performed. The prototype instrument could not meet the noise requirements mentioned in Paper III and reached an accuracy of ±0.5 m only but the experiments gave new insights into the nature of AEM measurements and their interaction with the aircraft.

Studies from *Suppala et al.* (2005) and *Levaniemi et al.* (2009) mentioned noise caused by wing flexure which contributed to the total noise of ∼30 ppm ppm of the "AEM-05" system of the Finish and Britsh Geological Survey. Furthermore *Suppala* stated that the main part of the airplane EM response could be handled by calibration and that a coupling between airplane and ground could be neglected. However, none of these studies further quantified their statements. Based on test flights with the prototype system over the North Sea and 3D FEM modelling we estimated the contributions of wing flexure, of pitch and roll and of electromagnetic coupling between ocean and airplane to the total noise.

The "Polar2" causes an additional EM signal with an amplitude of 35,000 ppm. Most of it is constant and can therefore be subtracted from the ocean signal. In comparison to geological surveying over comparable low conductive ground ice thickness surveying over the ocean as a good conducting halfspace (2.0 - 4.5 S/m) includes a significant coupling signal between

airplane and ocean. Over the North Sea the inphase coupling signal was between 200 ppm in 50m height and 2000 ppm in 15m flight height. For the coupling signal can be accounted when the results of calibration flights over open water in different flight heights are taken as the reference for the sea-ice thickness determination instead of a 1D model curve. This method is only suitable as long as other major noise sources are suppressed. Alternatively, a 3D FEM model curve can be taken. Here the conductivity value of the airplane body in the model has to be chosen carefully on the basis of best fits to calibration flight results.

For a VCP coil configuration roll has a neglecting influence, whereas pitch causes reductions of the ocean response signal by up to 7% and 9% for the inphase and quadrature component respectively, for typical pitch values during stable flight and for typical flight heights of 30m. We used the FEM results to create a specific pitch correction chart for the prototype EM instrument on the "Polar2".

From all noise sources wing flexure has the strongest contribution. In this context *Levaniemi et al.* (2009) only mentioned the varying coil separation distance due to wing flexure. In addition to this geometrical component we found a significant inductive component of wing flexure noise. Assuming an airplane conductivity similar to aluminum the geometrical and inductive components are of the same order of magnitude. For a wing deflection angle of 5° for instance the geometrical component is in the order of 10,000 ppm and the inductive component of 8,000 ppm. This results are supported by a test flight where wing flexure was triggered by heavy up and down movements of the airplane which caused noise on the inphase by up to 8,000 ppm. The geometrical part of wing flexure noise, ideally, has no influence on the quadrautre in free space and also the inductive component has a much weaker effect on the quadrature than on the inphase component due to the high electrical conductivity of the airplane body. Hence, for sea ice thickness retrieval with a fixed wing antenna system the quadrature component is superior to the inphase component, even when the inphase produces a stronger ocean response.

Further Thinning in the Trans Polar Drift

During an ice breaker expedition of the German research vessel "FS Polarstern" into the central Arctic Ocean in summer 2007 extensive HEM ice thickness data were collected. Together with data from 2004 these results are a continuation of a series of irregular EM ice thickness measurements under summer conditions in the Trans Polar Drift (TPD) between 1991 and 2001 (*Haas*, 2004). In Paper IV the 2007 data were analysed with respect to this time series. Between 1991 and 2001 the mean and modal thickness decreased from 3.11 m and 2.50 m to 2.41 m and 1.95 m, which is a reduction by 22.5% and 22% respectively. 2004 showed the same modal thickness and even a larger mean thickness than 2001, which may be accounted for the different region farther downstream the TPD closer to the Fram Strait. Significantly smaller than 2001 are mean and modal thickness of the 2007 surveys with a reduction of 53% and 44% respectively to values of 0.9 m and 1.27 m. This abrupt reduction is in accordance to a regime shift from multi year ice (MYI) to first year ice (FYI) (*Nghiem et al.*, 2007) in this region and further support the results of *Kwok* (2009) who found a dramatic volume loss of sea-ice in the arctic during summer 2007. The 2004 data were collected in the region north

of Fram Strait and confirm a continuation of the thinning of Fram Strait ice (*Wadhams and Davis*, 2000a) by another 22% since 1996.

Paper IV further deals with the question whether the regime shift to FYI is the only reason for the thinning of the 2007 sea ice or whether MYI in this region was thinner as well. For this purpose HEM measurements over second year ice (SYI) during the preceding spring at the North Pole were seasonally adjusted by North Pole melting rates reported by *Perovich et al.* (2008). According to this examination, 2007 SYI mean thickness was 22% thinner than the mean thickness in 2001. Thus, the changes are not only based on a regime shift but also on a thermodynamical thinning of MYI. Remains the question whether FYI ice thinned as well? Comparison with ground based EM measurements on FYI in the Laptev Sea in 1995 indicate a decrease of FYI modal thickness from 1.25 m by about 0.35 m to the 2007 thickness values, which is almost within the natural variability of annual growth and melting rates which were as high as 0.3 m in previous years (*Haas and Eicken*, 2001; *Perovich et al.*, 2008). Therefore, I would not consider the 2007 FYI thickness as considerably lower than in previous years. The thickness of FYI is further discussed in Paper I. For thickness distributions considering only level ice a second modal thickness of 1.1m was visible in the 2001 data which can be interpreted as a FYI mode. This as well suggest that 2007 FYI was indeed not significant thinner than in previous years, which is furthermore supported by satellite freeboard measurements by *Kwok* (2009). Only exception were significant thinner modal thicknesses from single flights close to the sea ice margin where ice concentration was below 90%.

Characteristics of Younger and Older Ice Regimes

Paper I presents a detailed analysis of HEM thickness profiles flown in the central Arctic in 2001, 2004 and 2007. Ice age maps presented in Paper IV on the basis of a drift-age model (*Rigor and Wallace*, 2004) indicate the different age regimes in which these HEM surveys were taken. Thus, these three datasets represent the rare opportunity to compare thickness distributions and other surface parameters in first year ice regimes (2007) and in MYI regimes (2001,2004). Thickness distribution functions (P) are characterised by their mean and modes, by their exponential decay and by their width at half maximum (FWHM) (see Fig. 3). In none of these years a second mode (except the open water mode at z=0) is present, indicating that the majority of the ice in each year experienced a similar thermal history. We found equal modal thicknesses for both MYI regimes and a significant thinner mode for the FYI regime. Despite equal modal thickness both MYI regimes differed in their mean thickness by 0.35 m indicating different dynamical histories with at the same time similar thermodynamic histories. With respect to exponential decay and FWHM both the survey areas close to the North Pole, the FYI (2007) and the MYI (2001) regime, were self consistent with each other. The MYI regime further downstream the TPD close to the Fram Strait showed a slower decay and a broader FWHM, indicating a heavier degree of deformation.

Following the theory of thickness evolution by *Thorndike et al.* (1975) we state that the growth function f acted similar on both MYI regimes, but the redistribution function ψ differed significantly. Thus, there is no predictable time dependence of ψ. In fact deformation of sea-ice, and with it a lower exponential decay of the P and a larger mean thickness rather

depend on the position within the Arctic than on the age of the ice. Thinking of ψ as a sink for thinner ice and a source for thicker ice, a lower exponential decay and a broader FWHM in deformed regimes is obvious. Nevertheless, both quantities can also be increased when the thickness survey is flown in a region where different MYI sea ice regimes mix. In that case the maximum of the distribution function would be flat since it reflects level ice thicknesses with different thermal histories. Different modes for every age class are not necessarily pronounced in a region covering different MYI regimes.

Even when modal thickness is a good indicator in order to distinguish between FYI and MYI, pressure ridge parameters and melt pond coverage are not. The mean height of pressure ridge sails e.g. differed by a maximum of only 0.13 m in all regimes and can therefore not be taken as a reference, neither for the age nor for the modal ice thickness of a particular regime. However, all data are based on summer measurements, in winter the conditions can be different. The number of pressure ridge sails per kilometre on the other hand is a good indicator for the degree of deformation but as well not for the age and differed between $\sim$5 in undeformed FYI and MYI regimes and $\sim$7 in a deformed MYI regime. The distribution of sail spacing follows a lognormal behaviour and has a maximum in the range of 10 $\pm$ 5 m independently of the regime. Considering the lower number of sails per kilometre an obvious conclusion is that sails emerge in clusters within one pressure ridge with the consequence that mean sail spacing is not a suitable measure for the mean distance of pressure ridges in a regime.

Significance of Ice Thickness Sampling

With the question of representativeness of obtained mean and modal thicknesses deals Paper I. We derived standard errors for different profile lengths of mean and modal thickness, sail height, sail spacing and sail density. We have chosen the EM Bird accuracy of $\pm$ 0.1m as the level of significance which is even harder to meet than the 0.497m suggested by *Wadhams* (1997). In Paper IV we mention the remarkable similarity of all ice thickness distributions obtained in summer 2007. The standard error can be seen as a quantification of this similarity. In general, a significant mean thickness is easier to obtain than a significant modal thickness as higher standard errors of modal thickness indicate. In the relative undeformed regimes of 2001 and 2007 mean thicknesses representative for the entire expedition could be obtained for 10 km long sections, which reflects indeed a remarkable similarity. In the heavier deformed 2004 MYI regime 100 km were necessary. In contrast, representative modal thicknesses could not be obtained before profile lengths of 50 km in the undeformed regimes and not even with 100 km long profiles in the deformed 2004 regime. The high standard error in the 2004 regime is also attributed to the fact that in the region north of Fram Strait sea ice regimes of different origin merge together. Thus, the interpretation of a single modal thickness as the thermodynamical grown ice thickness is questionable in and around Fram Strait with the consequence that modal thicknesses obtained on 100 km long profiles must differ by at least 0.6 m (whether temporal or spatial) to exceed the natural spatial variability in this region.

The representativeness of pressure ridge parameters differ from quantitiy to quantity. Mean sail spacing e.g. is already obtained with a standard error of less than 12% for 5 km long sections independently of the regime. The typical sail interval of $\sim$10m within pressure

ridges dominates the spacing distribution already on short distances. Standard errors of mean sail height drops to 12% for sections longer than 5 km. The number of ridges per kilometre has standard errors of more than 12% even for sections exceeding 100 km. Only for the shorter 2001 total profile length the number of ridges reaches a representative level reflecting the higher probability of smaller areas to be homogeneous. For longer survey areas a representative number of ridges per kilometre cannot be assigned.

We summarize that mean thickness and sail height can be representative even for larger regions, whereas the number of sails per kilometre does not distribute homogeneously enough over larger survey areas in order to have a representative character. Representative modal thicknesses can be found for large areas as long as deformation stays below a certain level and as long as the age composition of the ice is dominated by one age class.

Spatial Thickness Gradients

When entering the Arctic pack ice with an ice breaker we intuitively expect thinner ice in the beginning close to the margin and thicker and denser ice conditions the more north we travel. In 2004 "RV Polarstern" experienced the opposite north of Fram Strait, with the thickest ice with modal thicknesses of 2.4 m close to the sea-ice margin at a latitude of 82° North and much thinner ice with modal thicknesses of down to 1.5 m two latitudes farther north. North of Fram Strait this can be explained with convergent ice drift where a tongue of younger ice drifted from the east into the area and ended up north of the older ice which probably advected from the MYI belt north of Greenland.

When "Polarstern" left the pack ice on the Pacific side of the ice cover in 2007 it found a situation where the ice concentration and with it the ice thickness decreased gradually towards the ice edge. This situation can be explained with the unusual high sea surface temperatures in the summer 2007 (*Steele et al.*, 2008), heavy bottom melting (*Perovich et al.*, 2008) in this part of the Arctic Ocean and extreme thin modal thicknesses of 0.9 m in the closed pack. On thin ice melt ponds tend to transform into thaw holes which in turn reduces the sea ice concentration. Then an albedo feedback process is triggered which lead to further melting. Thaw holes emerged equally distributed over the ice cover along the ice margin. Therefore open water content distributed in a similar way. In comparison, equally high open water fractions in 2001 close to the North Pole did not trigger additional thinning and modal sea ice thicknesses remained at a level of approximately 2 m. One plausible solution is the fact that in 2001 at the North Pole open water existed in form of a few but huge open leads of several kilometres width and much more kilometres length which lead to a smaller heat gain of the ocean as for the case where vast fractions of the ice cover starts to disintegrate due to thaw holes like in 2007.

Melt Ponds

During data processing of the HEM data we observed laser altimeter drop-outs for all these thickness profiles where visual observations recorded a significant amount of open melt ponds. Based on these drop outs and the obtained sea-ice thickness we estimated the concentration

of melt ponds in August 2004 and 2007. Both years and regions did not show a significant difference in melt pond concentration which amounted to 15% ± 14%. The error of ± 14% is the standard error for 35 km long transects. However, melt ponds on the thicker 2004 MYI did not have the potential to transform into thaw holes, thus a thinner ice cover can melt away on vast dimensions more easily. The potential for future rapid sea-ice area reductions is also discussed in Paper IV. The laser drop-out method is still not established and further validation is pending. Comparisons with aerial photography indicate an underestimation of the real pond concentration.

Conclusions

To conclude this thesis I resume to the key hypotheses proposed in the first section.

1. In this thesis a feasibility study for a new fixed wing AEM instrument was performed on the basis of a prototype instrument and 3D finite element modelling. In principle such a system is capable to measure sea-ice thickness but with more technical efforts than for a towed bird solution. The accuracy achieved with the prototype instrument was ±0.5 m in comparison to ±0.1 m of the AWI EM Bird system.

   Data processing differs in some crucial steps to that of an EM Bird. The primary magnetic field is not attenuated by a bucking coil and has therefore to be subtracted from the receiver signal during a post flight processing step. Furthermore a 1D analytical model cannot be taken as a reference in order to adjust phase and amplitude of data obtained over open water. The reason is a significant electromagnetic coupling between airplane and ocean which is not considered in a 1D approach. In order to obtain a reasonable model curve, calibration flights over open water have to be compared with results of 3D models where the conductive airplane is included in the model. The coupling signal between airplane and ocean depends on the flight height and is added on a constant airplane signal of $\sim 35,000$ ppm.

   The noise level of the prototype instrument differed significantly for inphase and quadrature component. After data processing the quadrature signal noise could be redued to ± 50 ppm whereas the inphase noise was in the order ± 500 ppm. In a 3D model we quantified the effect of wing flexure and showed that it has the potential to disturb the EM inphase signal in the order of the wanted ocean signal. Because of wing flexure the quadrature is more suitable for sea ice thickness determination even when the inphase component of the ocean signal is stronger. We suggest to either measure the wing deflection and the relative coil positions during flight and/or to mount the antennas on nose and tail of the fusealge.

2. Several HEM thickness profiles from the central Arctic have been analysed. It has been found that thickness distributions from single HEM flights within a two month period can be remarkable similar over an area ranging from North of Svalbard to the Pacific side of the summer sea ice cover. However, thickness distributions further downstream the TPD between Greenland and Svalbard showed larger spatial variability for an even less extended area. We conclude that sea-ice thickness information from HEM profiles

in less deformed thickness regimes can be representative for entire regions where the ice is classified as being of same age. In regions where MYI with different histories is mixed and a convergent drift causes deformation, profiles of 100 km can be necessary in order to obtain mean thicknesses with a low standard error and modal thicknesses are most probably not representative enough at all to be valid for the entire region.

Since 1991 the AWI performs measurements in the central Arctic Ocean and the 2007 summer expedition, as a main part of this thesis, contributed to this time series. Taking into account typical standard errors of HEM surveys in the North Pole region, a reduction of modal ice thickness by 44% between 2001 and 2007 represents a significant decrease. This decrease can be explained by a regime shift from MYI to FYI. As well significant is the decrease of mean thickness by 22% between 1991 and 2001, which is definitely higher than typical spatial variabilities of mean thickness for the surveyed area. Mean thickness of MYI in the Fram Strait region in 2004 was 0.7 m lower than mean thickness obtained by ULS submarines in the same region in 1996. This decrease is significantly higher than the typical spatial variability in this region for profiles of that length. In summary, HEM, when repeated annually, performed during icebreaker cruises in the central Arctic are a suitable tool for long term observation of ice thickness in order to evaluate thickness trends for entire regions. Nevertheless, HEM thickness measurements must be interpreted in connection with results from remote sensing techniques, drift buoys or in situ measurements in order to assign them to regions with the same ice history and in order to find plausible explanations for abrupt changes.

Outlook

Even 50 years after the first ULS submarine profile in the Arctic sea ice thickness observations are not performed on a routine basis. Nevertheless, more and more efforts will be directed towards the development of new methods and the establishment of known methods. The launch of CryoSat2 is scheduled for 2010 and new EM Birds are about to be purchased by further research institutions. Every year several research ice breakers are on expeditions within the Arctic and most of them have helicopters on board. The 2007 Polarstern expedition has shown the potential of HEM to cover large areas of the Arctic Ocean. While the EM Bird technology spreads out in the sea-ice community an increasing amount of thickness data will be available from different regions in the Arctic Ocean.

My efforts towards a fixed wing realisation of an EM sea-ice thickness sounder are a basis for the construction of a beta system including a method to measure wing flexure and relative antenna position, by means of e.g. laser distance meters pointing on the antennas. As an alternative the antennas could be mounted on tail and nose of the fuselage. During the writing of this thesis the AWI decommissioned the 'Polar 2' and purchased a 'Basler BT-67' (called 'Polar 5'). The 'Polar 5' has a 500 km longer range and is licensed to carry an external swing load, e.g. an EM Bird. In 2009 first Polar 5 EM Bird measurements were completed and further thickness surveys are planned for the upcoming years.

Own Contribution to the Publications

Paper I

HEM thickness data were collected during three expeditions into the Arctic (2001,2004,2007). The 2007 measurements were planned and conducted by Dr. Stefan Hendricks (that time PhD student) and myself which included a 11 weeks cruise into the central Arctic ocean. During that cruise a total amount of ∼4000 km of HEM thickness profiling was performed which represents an unprecedented coverage of Arctic HEM thickness data. Data processing was done by us two during the cruise on the basis of processing software developed in the sea-ice physics group of the Alfred Wegener Institute. Analysis of ice thickness from all three expeditions was done by myself only. This included gathering of data, unification of data formats, creation of programs for statistical evaluation of the data on the basis of IDL (Interactic Data Language) and the placement of the results into the context of the actual state of Arctic research. The paper itself was written by myself during a two month research stay at the University of Edmonton, Canada, funded by the German Academic Exchange Service (DAAD). All figures were created by myself.

Paper II

The presented results were obtained with a prototype instrument which was constructed under specifications which I worked out together with Prof. Dr. Christian Haas (that time AWI) and John Lobach (Fera Dynmaic Inc.). I was heavily involved in the construction of the prototype system, which included tuning of the antenna coils and test measurements on ground. The electronic components were constructed by Ferra Dynamics Inc., mounting and certification was done by 'Optimare Sensorsysteme AG', construction of the shell was done by 'Leichtwerk AG' and the airplane was operated by DLR (Deusches Zentrum für Luft und Raumfahrt). All test flights, over the North Sea and in Spitsbergen, were planned by myself. Especially the choice of flight manoeuvres was important in order to obtain meaningful results.

All post flight processing work was done by myself under initial advice of Ferra Dynamics Inc.. Due to the prototype nature of the instrument no prior processing software existed, hence all programs necessary were created by myself on the basis of IDL. In order to further quantify the physics of the fixed wing system 3D finite element modelling was done by myself on the basis of Comsol Multiphysics under initial advice of my colleague Stefan Hendricks, who used Comsol for his thesis one year earlier. The paper and all included figures was written by myself only.

Paper III

Paper III is based on the experience of several field campaigns using the AWI EM Bird. I participated one of these expeditions into the Canadian Arctic in 2006. I was responsible for the noise analysis part of this paper. This included gathering and processing of HEM data

from all considered field campaigns. Paper III comprises work I did during my first year in the sea ice physics group. Later studies (Paper I + II) based on the experience of this early work. The publication was written by Prof. Dr. Christian Haas, since he is the 'father' of the AWI EM Birds and Paper I is the first publication solely referring to this technology.

Paper IV

Paper IV is based on ground EM and HEM thickness data from the Arctic Trans Polar Drift between 1991 and 2007. I was, as in Paper I, responsible for the measurements done in summer 2007, which is the data set most conclusions in Paper IV are based on. Since Paper IV includes a 16 years long time series it was written by Prof. Dr. Christian Haas, who was responsible for most of these measurements especially in the 1990s. However, Christian Haas wrote this paper on the basis of discussions with all involved authors and it was only published after reviewing by myself and the other responsible authors.

Bibliography

Badgley, F., Heat balance at the surface of the arctic ocean, *Proceedings of the Symposium on the Arctic Heat Budget and Atmospheric Circulation, Santa Monica , Calif., RM-5233-NSF*, 267–278, 1966, edited by J.O. Fletcher.

Boe, J., A. Hall, and X. Qu, September sea-ice cover in the Arctic Ocean projected to vanish by 2100, *Nature Geoscience*, *2*, 341–343, 2009.

Bourke, R., and R. Garrett, Sea ice thickness distribution in the arctic ocean, *Cold Reg. Sci. Technol.*, *13*, 259–280, 1987.

Brandon, M., F. Cottier, F. E. D. T. Nilsen, and G. Dieckmann, *Sea Ice and Oceanography*, chap. 3, Wiley-Blackwell, Oxford, United Kingdom, 2010, 2nd edition.

Bruemmer, B., D. Schroeder, G. Mueller, G. Spreen, A. Jahnke-Bornemann, and J. Launiainen, Impact of a Fram Strait cyclone on ice edge, drift, divergence, and concentration: Possibilities and limits of an observational analysis, *Journal of Geophysical Research - Oceans*, *113*, 2008.

Comiso, J. C., C. L. Parkinson, R. Gersten, and L. Stock, Accelerated decline in the Arctic Sea ice cover, *Geophys. Res. Lett.*, *35*, 2008.

Comiso, J. E. D. T., and G. Dieckmann, *Variability and Trends of the Global Sea Ice Cover*, chap. 6, Wiley-Blackwell, Oxford, United Kingdom, 2010, 2nd edition.

Davis, N., and P. Wadhams, A statistical-analysis of Arctic pressure ridge morphology, *J. Geophys. Res.*, *100*, 10,915–10,925, 1995.

Doble, M., A. Forrest, P. Wadhams, and B. Laval, Through-ice AUV deployment: Operational and technical experience from two seasons of Arctic fieldwork, *Cold Regions Science And Technology*, *56*, 90–97, 2009.

Dorn, W., K. Dethloff, A. Rinke, S. Frickenhaus, R. Gerdes, M. Karcher, and F. Kauker, Sensitivities and uncertainties in a coupled regional atmosphere-ocean-ice model with respect to the simulation of Arctic sea ice, *Journal of Geophysical Research - Athmospheres*, *112*, 2007.

Eicken, H., and M. Lange, Sea ice thickness data - the many vs the few, *Geophy. Res. Lett.*, *16*, 495–498, 1989.

Farrell, S. L., S. W. Laxon, D. C. McAdoo, D. Yi, and H. J. Zwally, Five years of Arctic sea ice freeboard measurements from the Ice, Cloud and land Elevation Satellite, *J. Geophys. Res.*, *114*, 2009.

Fissel, D. B., J. R. Marko, and H. Melling, Advances in upward looking sonar technology for studying the processes of change in Arctic Ocean ice climate, *Journal of Operational Oceanography*, *1*, 9–18, 2008.

Fitterman, D., Sources of calibration errors in helicopter em data, *Exploration Geophysics*, *29*, 65–70, 1998.

Flinsbach, D., Gleichstromgeoelektrik zur erkundung der inneren struktur und der dicke von meereis, Master's thesis, Ludwig-Maximilian Universitaet, Munich, Germany, 2005.

Gerdes, R., and C. Koeberle, Comparison of Arctic sea ice thickness variability in IPCC Climate of the 20th Century experiments and in ocean - sea ice hindcasts, *J. Geophys. Res.*, *112*, 2007.

Giles, K. A., S. W. Laxon, and A. L. Ridout, Circumpolar thinning of Arctic sea ice following the 2007 record ice extent minimum, *Geophy. Res. Lett.*, *35*, 2008.

Haarpaintner, J., and G. Spreen, Use of enhanced-resolution QuikSCAT/SeaWinds data for operational ice services and climate research: Sea ice edge, type, concentration, and drift, *IEEE Transactions on Geoscience and Remote Sensing*, *45*, 3131–3137, 2007.

Haas, C., Late-summer sea ice thickness variability in the Arctic Transpolar Drift 1991-2001 derived from ground-based electromagnetic sounding, *Geophy. Res. Lett.*, *31*, 2004.

Haas, C., and H. Eicken, Interannual variability of summer sea ice thickness in the Siberian and central Arctic under different atmospheric circulation regimes, *J. Geophys. Res.*, *106*, 4449–4462, 2001.

Haas, C., S. Gerland, H. Eicken, and H. Miller, Comparison of sea-ice thickness measurements under summer and winter conditions in the Arctic using a small electromagnetic induction device, *Geophysics*, *62*, 749–757, 1997.

Haas, C., S. Hendricks, and M. Doble, Comparison of sea ice thickness distribution in the Lincoln Sea and adjacent Arctic Ocean in 2004 and 2005, in *Ann. Glaciol., VOL 44*, edited by Langhorne, P. and Squire, V., vol. 44 of *Ann. Glaciol.*, pp. 247–252, 2006.

Haas, C., A. Pfaffling, S. Hendricks, L. Rabenstein, J.-L. Etienne, and I. Rigor, Reduced ice thickness in Arctic Transpolar Drift favors rapid ice retreat, *Geophys. Res. Lett.*, *35*, 2008.

Haas, C., J. Lobach, S. Hendricks, L. Rabenstein, and A. Pfaffling, Helicopter-borne measurements of sea ice thickness, using a small and lightweight, digital EM system, *J. Appl. Geophys.*, *67*, 234–241, 2009.

Hendricks, S., Validierung von altimetrischen Meereisdickenmessungen mit einem helikopterbasierten elektromagnetischen Induktionsverfahren, Ph.D. thesis, University Bremen, 2009, in german.

Hibler III, W., *Ice Dynamics*, chap. pp.577-640, Martinus Nijhoff Publishers, dordrecht (NATO ASI B146) Ed. N. Untersteiner, 1986.

Holmes, Q., D. Nuesch, and R. Shuchman, Textural analysis and real-time classification of sea ice types using digital SAR data, *IEEE Transactions on Geoscience and Remote Sensing*, *22*, 113–120, 1984.

Holt, B., P. Kanagaratnam, S. P. Gogineni, V. C. Ramasami, A. Mahoney, and V. Lytle, Sea ice thickness measurements by ultrawideband penetrating radar: First results, *Cold Reg. Sci. Technol.*, *55*, 33–46, 2009.

Keller, G., and F. Frischknecht, *Electrical methods in geophysical prospecting*, Oxford Pergamon Press, 1966.

Kovacs, A., and J. Holladay, Sea-ice thickness measurement using a small airborne electromagnetic sounding system, *Geophysics*, *55*, 1327–1337, 1990.

Kovacs, A., and R. Morey, Sounding sea ice thickness using a portable electromagnetic induction instrument, *Geophysics*, *56*, 1992–1998, 1991.

Kovacs, A., N. Valleau, and J. Holladay, Airborne electromagnetic sounding of sea ice thickness and sub-ice bathymetry, *Cold Reg. Sci. Technol.*, *14*, 289–311, 1987.

Kovacs, A., J. Holladay, and C. Bergeron, The footprint altitude ratio for helicopter electromagnetic sounding of sea-ice thickness - Comparison of theoretical and field estimates, *Geophysics*, *60*, 374–380, 1995.

Kwok, R., Outflow of Arctic Ocean Sea Ice into the Greenland and Barents Seas: 1979-2007, *J. Climate*, *22*, 2438–2457, 2009.

Kwok, R., and G. F. Cunningham, ICESat over Arctic sea ice: Estimation of snow depth and ice thickness, *J. Geophys. Res.*, *113*, 2008.

Laxon, S., N. Peacock, and D. Smith, High interannual variability of sea ice thickness in the Arctic region, *Nature*, *425*, 947–950, 2003.

Levaniemi, H., D. Beamish, H. Hautaniemi, M. Kurimo, I. Suppala, J. Vironmaki, R. J. Cuss, M. Lahti, and E. Tartaras, The JAC airborne EM system: AEM-05, *Journal of Applied Geophysics*, *67*, 219–233, 2009.

L'Heureux, M. L., A. Kumar, G. D. Bell, M. S. Halpert, and R. W. Higgins, Role of the Pacific-North American (PNA) pattern in the 2007 Arctic sea ice decline, *Geophy. Res. Lett.*, *35*, 2008.

Lindsay, R. W., J. Zhang, A. Schweiger, M. Steele, and H. Stern, Arctic Sea Ice Retreat in 2007 Follows Thinning Trend, *J. Climate*, *22*, 165–176, 2009.

Liu, G., A. Kovacs, and A. Becker, Inversion of airborne electromagnetic survey data for sea-ice keel shape, *Geophysics*, *56*, 1986–1991, 1991.

Makynen, M., and M. Hallikainen, Simulation of ASIRAS Altimeter Echoes for Snow-Covered First-Year Sea Ice, *IEEE Geoscience and Remote Sensing Letters*, *6*, 486–490, 2009.

Martin, S., R. Drucker, R. Kwok, and B. Holt, Estimation of the thin ice thickness and heat flux for the Chukchi Sea Alaskan coast polynya from Special Sensor Microwave/Imager data, 1990-2001, *Journal of Geophysical Research - Oceans*, *109*, 2004.

Maslanik, J. A., C. Fowler, J. Stroeve, S. Drobot, J. Zwally, D. Yi, and W. Emery, A younger, thinner Arctic ice cover: Increased potential for rapid, extensive sea-ice loss, *Geophy. Res. Lett.*, *34*, 2007.

Maykut, G., *The surface heat and mass balance*, chap. pp.395-463, Martinus Nijhoff Publishers, dordrecht (NATO ASI B146) Ed. N. Untersteiner, 1986.

McLaren, A., J. Walsh, R. Bourke, R. Weaver, and W. Wittmann, Variability in sea-ice thickness over the north-pole from 1977 to 1990, *Nature*, *358*, 224–226, 1992.

Multala, J., H. Hautaniemi, M. Oksama, M. Lepparanta, J. Haapala, A. Herlevi, K. Riska, and M. Lensu, An airborne electromagnetic system on a fixed wing aircraft for sea ice thickness mapping, *Cold Regions Science and Technology*, *24*, 355–373, 1996.

Nghiem, S. V., Y. Chao, G. Neumann, P. Li, D. K. Perovich, T. Street, and P. Clemente-Colon, Depletion of perennial sea ice in the East Arctic Ocean, *Geophy. Res. Lett.*, *33*, 2006.

Nghiem, S. V., I. G. Rigor, D. K. Perovich, P. Clemente-Colon, J. W. Weatherly, and G. Neumann, Rapid reduction of Arctic perennial sea ice, *Geophy. Res. Lett.*, *34*, 2007.

Ogi, M., I. G. Rigor, M. G. McPhee, and J. M. Wallace, Summer retreat of Arctic sea ice: Role of summer winds, *Geophy. Res. Lett.*, *35*, 2008.

Pedersen, C. A., R. Hall, S. Gerland, A. H. Sivertsen, T. Svenoe, and C. Haas, Combined airborne profiling over Fram Strait sea ice: Fractional sea-ice types, albedo and thickness measurements, *Cold Reg. Sci. Technol.*, *55*, 23–32, 2009.

Percival, D. B., D. A. Rothrock, A. S. Thorndike, and T. Gneiting, The variance of mean sea-ice thickness: Effect of long-range dependence, *J. Geophys. Res.*, *113*, 2008.

Perovich, D., T. Grenfell, J. Richter-Menge, B. Light, W. Tucker, and H. Eicken, Thin and thinner: Sea ice mass balance measurements during SHEBA, *J. Geophys. Res.-Oceans*, *108*, 2003.

Perovich, D., S. Nghiem, T. Markus, and A. Schweiger, Seasonal evolution and interannual variability of the local solar energy absorbed by the Arctic sea ice-ocean system, *J. Geophys. Res.*, *112*, 2006.

Perovich, D. K., J. A. Richter-Menge, K. F. Jones, and B. Light, Sunlight, water, and ice: Extreme Arctic sea ice melt during the summer of 2007, *Geophy. Res. Lett.*, *35*, 2008.

Petrich, C., H. Eicken, E. D. Thomas, and G. Dieckmann, *Growth, Structure and Properties of Sea Ice*, chap. 2, Wiley-Blackwell, Oxford, United Kingdom, 2010, 2nd edition.

Pfaffling, A., and J. E. Reid, Sea ice as an evaluation target for HEM modelling and inversion, *J. Appl. Geophys.*, *67*, 242–249, 2009.

Pfaffling, A., C. Haas, and J. E. Reid, Direct helicopter EM - Sea-ice thickness inversion assessed with synthetic and field data, *Geophysics*, *72*, F127–F137, 2007.

Prinsenberg, S., J. Holladay, and J. Lee, Measuring ice thickness with eisflow^{TM}, a fixed-mounted helicopter electromagnetic-laser system, *12th International Offshore and Polar Engineering Conference, Conference Proceedings*, *1*, 737–740, 2002.

Prinsenberg, S., I. Peterson, and S. Holladay, Comparison of airborne electromagnetic ice thickness data with NOAA/AVHRR and ERS-1/SAR images, *Athmosphere-Ocean*, *34*, 185–205, 1996.

Rabenstein, L., S. Hendricks, T. Martin, and C. Haas, Thickness and surface-properties of different sea-ice regimes within the Arctic Trans Polar Drift: Data from summers 2001, 2004 and 2007., *J. Geophys. Res.*, , 2010, in press.

Reid, J., A. Pfaffling, and J. Vrbancich, Airborne electromagnetic footprints in 1D earths, *Geophysics*, *71*, G63–G72, 2006.

Rigor, I., and J. Wallace, Variations in the age of Arctic sea-ice and summer sea-ice extent, *Geophysicsl Research Letters*, *31*, 2004.

Rothrock, D., and A. Thorndike, Geometric properties of the underside of sea ice , *J. Geophys. Res.*, *85*, 3955–3963, 1980.

Rothrock, D. A., and M. Wensnahan, The accuracy of sea ice drafts measured from US Navy submarines, *J. Atmos. Ocean. Tech.* , *24*, 1936–1949, 2007.

Rothrock, D. A., D. B. Percival, and M. Wensnahan, The decline in arctic sea-ice thickness: Separating the spatial, annual, and interannual variability in a quarter century of submarine data, *J. Geophys. Res.*, *113*, 2008.

Sinha, A., A field study for sea-ice thickness determination by electromagnetic means, *Geological Survey of Canada Paper*, *76(1C)*, 225–228, 1976.

Smith, D., Recent increase in the length of the melt season of perennial Arctic sea ice, *Geophysicsl Research Letters*, *25*, 655–658, 1998.

Steele, M., W. Ermold, and J. Zhang, Arctic Ocean surface warming trends over the past 100 years, *Geophy. Res. Lett.*, *35*, 2008.

Stroeve, J., T. Markus, W. Meier, and J. Miller, Recent changes in the arctic melt season, *Annals of Glaciology*, *44*, 367–374, 2006.

Stroeve, J., M. M. Holland, W. Meier, T. Scambos, and M. Serreze, Arctic sea ice decline: Faster than forecast, *Geophys. Res. Lett.*, *34*, 2007.

Suppala, I., M. Oksama, and M. E. Hongisto, H. in Airo, Gtk airborne em system: characteristics and interpretation guidelines, *Geological Survey of Finland, Special paper*, *39*, 103–118, 2005.

Thorndike, A., D. Rothrock, G. Maykut, and R. Colony, Thickness distribution of sea ice, *J. Geophys. Res.- Oc. Atm.*, *80*, 4501–4513, 1975.

Timco, G., and R. Burden, An analysis of the shapes of sea ice ridges, *Cold Regions Science and Technology*, *25*, 65–77, 1997.

Tucker, W., W. Weeks, and M. Frank, Sea Ice Ridging over the Alaskan Continental-Shelf, *J. Geoph. Res. - Oceans and Atmospheres*, *84*, 4885–4897, 1979.

Tucker, W., J. Weatherly, D. Eppler, L. Farmer, and D. Bentley, Evidence for rapid thinning of sea ice in the western Arctic Ocean at the end of the 1980s, *Geophysical Research Letters*, *28*, 2851–2854, 2001.

Varnai, T., and R. Cahalan, Potential for airborne offbeam lidar measurements of snow and sea ice thickness, *Journal of Gophysical Research - Oceans*, *112*, 2007.

Wadhams, P., Ice thickness in the Arctic Ocean: The statistical reliability of experimental data, *J. Geophys. Res.-Oceans*, *102*, 27,951–27,959, 1997.

Wadhams, P., and N. Davis, Further evidence of ice thinning in the Arctic Ocean, *Geophy. Res. Lett.*, *27*, 3973–3975, 2000a.

Wadhams, P., and T. Davy, On the Spacing and Draft Distriubtions for Pressure Ridge Keels, *J. Geophys. Res.-Oceans*, *91*, 10,697–10,708, 1986.

Wadhams, P., and M. Doble, Sea ice thickness measurement using episodic infragravity waves from distant storms, *Cold Regions Science And Technology*, *56*, 98–101, 2009.

Wadhams, P., and R. Horne, An analysis of ice profiles obtained by submarine sonar in the beaufort sea, *J. Glaciol.*, *25*, 401–424, 1980.

Winsor, P., Arctic sea ice thickness remained constant during the 1990s, *Geophy. Res. Lett.*, *28*, 1039–1041, 2001.

Yu, Y., and D. Rothrock, Thin ice thickness from satellite thermal imagery, *Journal of Geophysical Research - Oceans*, *101*, 25,753–25,766, 1996.

Yu, Y., G. Maykut, and D. Rothrock, Changes in the thickness distribution of Arctic sea ice between 1958-1970 and 1993-1997, *J. Geophys. Res.*, *109*, 2004.

ACKNOWLEDGEMENTS

This thesis would have never been written without its promoter Christian Haas. He was the supervisor of this thesis and helped with words and deeds even when he left the AWI for a professorship at the University of Alberta in Canada. He introduced me into the topic of sea ice during a field campaign to the Lincoln Sea in 2006 and aroused my interest for this fascinating topic. He at first had the idea to mount EM antennas on the *Polar 2* and without his preceding negotiations and efforts the realisation of a prototype instrument would have been impossible. Especially helpful was a two month research stay in the working group of Christian Haas at the University of Alberta which was funded by the DAAD.

I would like to thank my colleagues Stefan Hendricks and Thomas Krumpen. It were the three of us who temporarily managed the measuring part of the sea-ice physics division from 2007 to 2008. Many of the results and interpretations presented in this study based on fruitful discussions with them. Furthermore, together with them I conducted several measurement campaigns into the Arctic, e.g. a 11 weeks cruise into the central Arctic in 2007 and a four weeks stay in the Laptev Sea, Siberia in 2008. The fact, that I continued with my thesis even in times when the sea ice physics group was temporarily disintegrating, was mainly attributed to the excellent collaboration with them.

Furthermore I am grateful to Prof. Dr. H. Miller who accepted my PhD proposal at the University Bremen and agreed to be the first referee of this thesis and to Prof. Dr. P. Lemke who accepted to be the second referee of my thesis.

I pretty much enjoyed the cooperation with John Lobach of Ferra Dynamics Inc., Canada. He introduced me into basic engineering work necessary for the development of AEM instruments and further avoided me from starving to death by initiating the PhD student feeding program which will obviously run out during the following weeks.

Dr. Wolfgang Dierking was in charge of the sea ice physics department for a 6 months period in 2008 followed by Prof. Dr. Ruediger Gerdes who is the head of the sea ice physics department down to the present day. Both guaranteed a productive working environment.

General thanks go to all my colleagues at the Alfred Wegener Institute. Many of them contributed to the positive and fruitful time I had in Bremerhaven. In particular I would like to thank Polona Roszman, Thomas Busche, Maddalena Bayer, Marcel Nicolaus, Susi Haase, Hartmut Hellmer, Malte Thoma, Torge Martin, Veit Helm, Sandra Schwegmanm, Ursula Schauer, Benjamin Rabe, Dirk Kalmbach and many others.

Proofreading of the manuscripts was done by Christian Haas, Stefan Hendricks, Thomas Krumpen, Torge Martin, John Lobach and Marc Taylor.

This thesis was mainly funded by the EU project DAMOCLES (Developing Arctic Modeling and Observing Capabilities for Long-term Environmental Studies) which was a contribution to the International Polar Year 2007-2008.

Finally I want to thank my parents who always encouraged me to proceed with my scientific career. Without their support I would have never been working in the fields of Geophysics.

APPENDIX

- Paper I
- Paper II
- Paper III
- Paper IV

Paper I

Thickness and surface-properties of different sea-ice regimes within the Arctic Trans Polar Drift: data from summers 2001, 2004 and 2007.

L. Rabenstein,[1,5] S. Hendricks,[1] T. Martin,[2] A. Pfaffhuber,[3] C. Haas[4]

Abstract.

Large scale sea-ice thickness and surface-property data were obtained in three summers and in three different sea-ice regimes in the Arctic Trans Polar Drift (TPD) by means of helicopter electromagnetic sounding. Distribution functions P of sea-ice thickness and of the height, spacing and density of sails were analysed to characterize ice regimes of different age and deformation. Results suggest that modal ice thickness is affected by the age of a sea-ice regime and that the degree of deformation is represented by the shape of P. Mean thickness changes with both age and deformation. Standard error calculations showed that representative mean and modal thickness could be obtained with transect lengths of 15 km and 50 km respectively in less deformed ice regimes such as those around the North Pole. In heavier deformed ice regimes closer to Greenland 100 km transects were necessary for mean thickness determination and a representative modal thickness could not be obtained at all. Mean sail height did not differ between ice regimes whereas sail density increased with the degree of deformation. Furthermore the fraction of level-ice, open melt-ponds and open water along the transects were determined. Although overall ice thickness in the central TPD was 50% thinner in 2007 than in 2001, first-year ice (FYI) was not significantly thinner in 2007 than FYI in 2001, with a decrease of only 0.3 m. Thinner FYI in 2007 only occurred close to the sea-ice edge where open water covered more than 10% of the surface. Melt pond coverage retrieved from laser measurements was 15% in both the 2004 MYI regime and the 2007 FYI regime.

1. Introduction

Sea-ice thickness is an important parameter with a great influence on climatic processes in the Arctic [*Holland et al.*, 2006]. Only two of the climate models mentioned in the 4th assessment report of the Intergovernmental Panel on Climate Change (IPCC) incorporate high resolution sea-ice thickness distributions [*McLaren et al.*, 2006; *Meehl et al.*, 2006]. These two best predicted the decline in arctic sea-ice extent [*Stroeve et al.*, 2007]. Satellite observations of the aerial extent and concentration of Arctic sea ice have been available on a regular basis since 1979. They reveal strong interannual variability of the sea-ice extent, which is superimposed by a decreasing trend of 3.7 % per decade for all seasons since the beginning of the record until 2006 [*Parkinson and Cavalieri*, 2008]. The decrease even accelerated within the last decade to 10.1 % [*Comiso et al.*, 2008], and was particularly pronounced during September 2007 when an abrupt decline in sea-ice extent to only 62% of the climatological average emerged. Despite this observed decrease in ice extent a long term decrease in sea-ice volume remains unclear. Although a negative trend of sea ice volume within the 20th century is supported by several submarine based upward looking sonar (ULS) sea ice draft measurements [e.g. *Wadhams and Davis*, 2000a; *Tucker et al.*, 2001; *Yu et al.*, 2004], with an average decrease of 33% from a peak in 1980 to a minimum in 2000 [*Rothrock et al.*, 2008], other publications discuss a controversial decrease of sea ice volume in the 20th century [e.g. *Winsor*, 2001; *Gerdes and Koeberle*, 2007]. Due to the progress of satellite altimetry techniques since the beginning of the 21st century, sea ice thickness data are available on an Arctic wide scale, indicating an increased loss of sea ice volume. Based on "ICESat" laser altimetry data, *Kwok et al.* [2009] found a volume loss of Arctic sea ice of more than 40% since 2005. As for the decrease of sea ice extent, this decrease was especially pronounced in 2007, which is also supported by the results of *Giles et al.* [2008] for the western Arctic, who obtained sea ice thickness on the basis of satellite radar altimetry. In addition to remote sensing studies of sea ice volume, a number of in-situ sea ice thickness data sets were collected by means of helicopter electromagnetics (HEM) in the Arctic Trans Polar Drift (TPD) between 2001 and 2007. Based on HEM data, *Haas et al.* [2008] have shown a decrease of mean summer sea-ice thickness in the Trans Polar Drift (TPD) from 2.2 m in 2001 to 1.3 m in 2007 which is a decrease by 44%. This dramatic thickness decline is mainly the consequence of a regime shift from multi-year to first-year ice in the TPD, which accompanied a significant reduction of perennial sea ice in the Arctic between March 2005 and March 2007 [*Nghiem et al.*, 2007] and a trend towards an accelerated TPD [*Rampal et al.*, 2009].

The study presented here is based on partially the same HEM data sets as the study of *Haas et al.* [2008], namely on HEM data taken in the TPD during the summers of 2001,2004 and 2007. However, here we study the HEM data in more detail, to investigate particular characteristics of sea

[1]Alfred Wegener Institute for Polar and Marine Research, Bremerhaven, Germany

[2]Leibniz Institute of Marine Sciences IFM-GEOMAR , Kiel, Germany

[3]Norwegian Geotechnical Institute, Oslo, Norway

[4]Department of Earth Sciences, University of Alberta, Edmonton, Alberta, Canada

[5]Now at: Swiss Federal Institute of Technology, Institute of Geophysics, Zürich, Switzerland

0148-0227/10/$9.00

ice thickness and pressure ridge distributions and their relation to melt pond coverage and sea ice concentration. In particular we are interested in the shape of the distribution functions, the thickness and amount of undeformed ice, the amount of deformed ice, the dependence of thickness on concentration of sea ice and in latitudinal gradients within the distribution. Furthermore, in this study we compare thickness and pressure ridge distribution functions with respect to the sea ice regimes in which they were taken and with respect to their representativeness on the basis of standard errors. We discriminate between multi year ice (MYI) and first year ice (FYI) regimes [*Haas et al.*, 2008] and between regimes with a mainly convergent ice drift north of Fram Strait or a mainly free ice drift in the region of the North Pole. Although we do not focus on the analysis of ice thickness trends in the TPD, which was the main goal of the preceding study by *Haas et al.* [2008], our results are important for the understanding of sea ice thickness changes in the Arctic. It provides details about the thickness distribution of seasonal ice in the record minimum year 2007 and compares them to the distribution functions of sea ice in the same region six years earlier. In addition it compares sea ice thickness distributions north of Fram Strait with earlier ULS measurements by *Wadhams and Davis* [2000a].

We follow the theory of sea-ice thickness distribution by *Thorndike et al.* [1975] and describe our results by calculating discrete probability density functions $P(z)$. Variations in $P(z)$ describe sea-ice conditions in different study areas and periods. An important parameter of the thickness distribution is the modal thickness, which is associated with local maxima in $P(z)$. It can be assumed that in FYI regimes the modal thickness reflects vast areas of undeformed level sea ice which were formed at the same time during the autumn freeze-up. Multiple modes give evidence for the presence of larger sea ice areas in the survey area which were formed during different times. A mode of $P(z)$ located at z=0 represents open water. Due to a longer melting and freezing period, undeformed sea ice in MYI regimes may not be considered as level any longer, such that a greater variety of undeformed ice thicknesses can be expected, i.e. $P(z)$ would be characterised by a broader mode.

We performed a detailed level-ice study with the motivation to compare level-ice thickness and level-ice occurrence between the three expeditions into the Arctic Ocean during the three summers of 2001, 2004 and 2007. In particular we examine whether 2007 FYI was significantly thinner than a small amount of FYI found in 2001 in the same region, as indicated by low ice extent and strong bottom melting reported in the Beaufort Sea [*Perovich et al.*, 2008], or whether it differed within the range of natural variability. Level FYI thicknesses between two preceding summers may vary by as much as 0.3 m [*Haas and Eicken*, 2001]. To extract level ice in the data, a carefully tailored level ice filter was applied, which ensures that eroded pressure ridges are filtered out and do not contribute to the modal thicknesses.

In addition we calculated distribution functions of ridge-sail height, spacing and density, which is the number of sails per kilometer. For this we used surface roughness data measured with a laser altimeter which is incorporated in the HEM instrument, similar to a study by *Peterson et al.* [2008]. A laser altimeter produces accurate measures of surface roughness after making corrections to account for variations in aircraft flight height. The technique is described in more detail in section 2.3. Ridge-draft and ridge-spacing distributions based on ULS data were intensively studied by *Wadhams and Horne* [1980]; *Bourke and Garrett* [1987] and *Davis and Wadhams* [1995]. These studies found that ridge-draft fits a negative exponential distribution and ridge-spacing a log-normal distribution. Here we verify whether these findings can be applied to laser derived sail heights and spacing.

During the summer months melting of sea ice creates melt ponds at the sea-ice surface. Melt ponds modify thickness distributions, as they result in enhanced local thinning due to their low albedo. *Perovich et al.* [2006], for instance, showed albedo values of 0.4 for a ponded surface at the beginning of August compared to 0.8 for a surface covered with dry snow. *Haas and Eicken* [2001] studied the influence of melt ponds on sea-ice thickness distributions and found that melt ponds are primarily located on the thinnest ice. Similar to our study *Inoue et al.* [2008] analyzed melt pond concentrations on sea ice of different ages in July 2003 in the Beaufort Sea and found typical concentrations of 25% on FYI and 30% on MYI. In this paper we introduce a new method to estimate the amount of meltpond concentration by analysing drop outs of the laser altimeter signal.

Our 2007 HEM measurements are the only extensive thickness data obtained during the summer of 2007 and therefore represent a unique possibility to study the spatial and temporal changes of sea-ice thickness while the sea-ice extent was at its minimum. *Steele et al.* [2008] showed sea-surface temperature anomalies for the Pacific side of the Arctic ocean of up to 5^o C in 2007. At the same time *Perovich et al.* [2008] measured 2.1 m of bottom melt on an individual ice floe close to the sea ice margin in the Beaufort Sea, which is more than 6 times the 1990s average. During the same period bottom melting on an ice floe close to the North Pole was comparable to previous years [*Perovich et al.*, 2008]. The difference between these two measurements suggests that the proximity to the sea-ice margin and the resulting lower sea-ice concentration accelerated the bottom melt. We analyze the 2007 thickness data with respect to enhanced thinning due to lower sea-ice concentrations and their relation to small distances to the sea-ice edge. We also compare our results to those of *Perovich et al.* [2008].

Another focus of the present study is on the statistical reliability of the measurements. For the first time we evaluate larger data sets of HEM sea ice thickness to determine the significance of the obtained mean and modal thicknesses and mean pressure ridge sail parameters. Here an important quantity is the standard error ϵ. The standard error is the standard deviation of an ensemble of mean or modal values obtained for transect subsections of the same lengths. When ϵ is calculated for section-ensembles of different lengths, it is a measure of the transect lengths necessary to obtain mean and modal values which are representative for the entire data set. So we answer the question as to how long HEM profiles should be in order to obtain reliable mean and modal thicknesses. Evaluation of standard errors for ULS submarine measurements was previously done by *Wadhams* [1997], who showed that for 50 km long profiles obtained in essentially the same ice regime around the North Pole in a time window of 55 hours, the standard error of ice draft is about 12.75 % of the mean thickness. *Wadhams* took this result as a reference standard error, which when exceeded indicates significant spatial or temporal variability.

2. Data and Methods

2.1. Location and Period

The data sets presented here are from the three expeditions ARK17/2, ARK20/2 and ARK22/2 of the German research ice breaker "RV Polarstern" (Fig. 1). ARK17 took place along the Gakkel Ridge and east of the North Pole in August-September 2001 [*Thiede*, 2002], ARK20/2 north of the Fram Strait in July-August 2004 [*Budéus and Lemke*, 2007] and ARK22/2 north of the Barents Sea and at the Pacific-Siberian side of the North Pole in August-September 2007 [*Schauer*, 2008]. The 2007 helicopter flight tracks were split into two regions, because they were widely separated and were surveyed three weeks apart from each

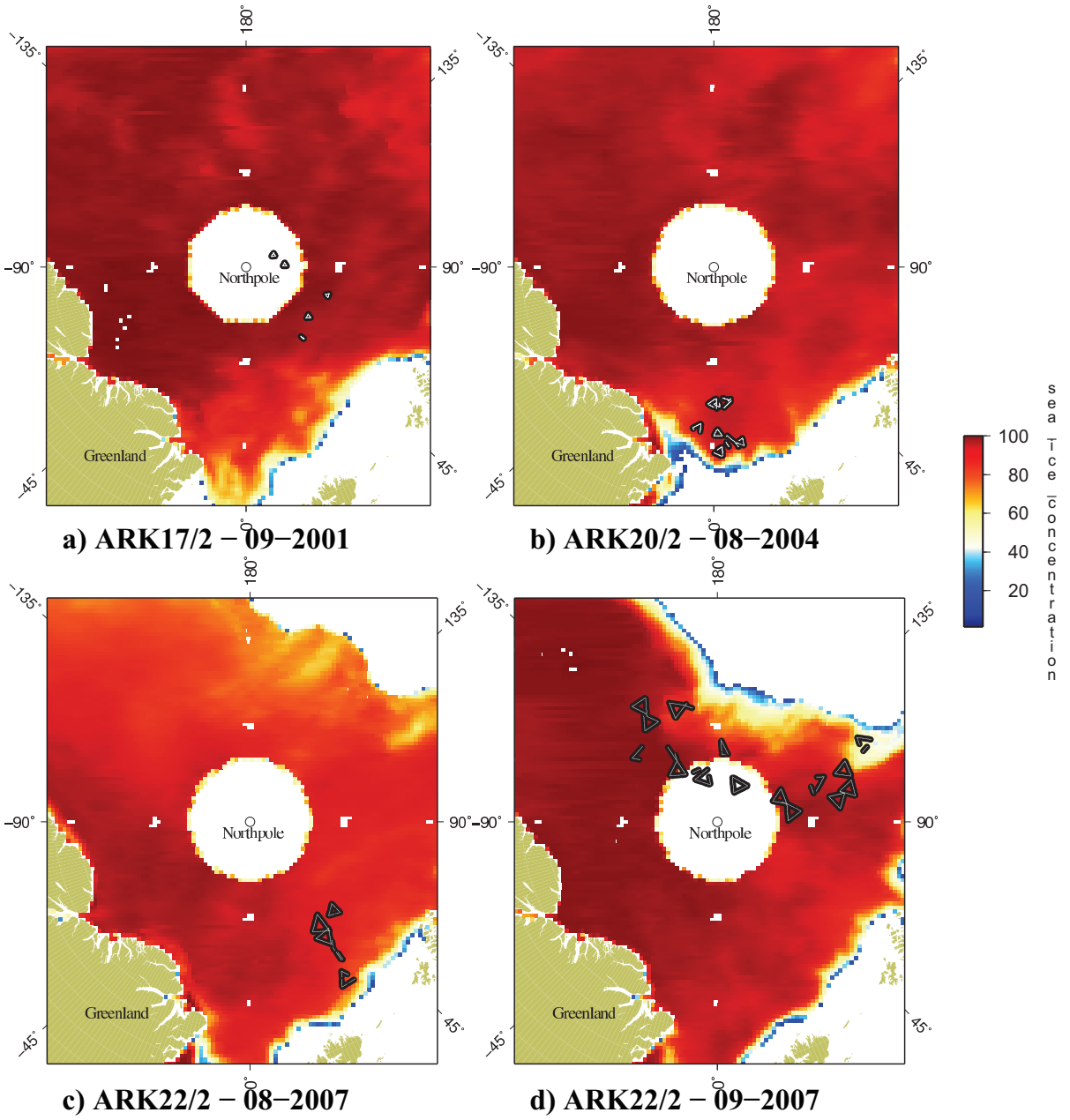

Figure 1. Maps of all HEM flights and respective SSM/I sea-ice concentration during each campaign

other (Table 1). HEM sea-ice thickness surveys were performed along the cruise track as often as weather conditions allowed. Flight tracks were arranged along triangles (see Fig. 1) with side lengths between 18.5 km (2001), 35 km (2004) and 70 km (2007). The increasing lengths of flights over the years demonstrates the operational advance in doing these measurements. Total survey lengths are listed in Table 1.

2.2. Helicopter-borne Electromagnetic Sounding

HEM was pioneered in the 1950's in order to detect ore deposits and was first applied over sea ice by *Kovacs and Holladay* [1990]. Since then the method has been frequently used for sea ice thickness determinations in the Arctic [e.g. *Prinsenberg et al.*, 2002; *Haas et al.*, 2006; *Peterson et al.*, 2008; *Haas et al.*, 2008]. Detailed information about the HEM instrument for measuring sea ice thickness was already given by *Haas et al.* [2009], hence we will only briefly summarize the HEM method here. A pair of transmitter and receiver coils operating at 4 kHz is used to estimate the distance of the instrument to the ice-ocean interface. The dominant EM induction process takes place in the conductive sea water [*Pfaffling et al.*, 2007]. In addition, a laser altimeter yields the distance to the uppermost snow surface, hence snow plus ice thickness is obtained by the difference of laser- and EM-distance measurements. During all three expeditions no snow cover was observed in August and on average 10 cm of new snow accumulated in September, which is in agreement with climatological snow depth data by *Warren et al.* [1999]. Snow depth was measured during several ground surveys on the ice and observed during continuous observations from the bridge of "RV Polarstern" [*Thiede*, 2002; *Budéus and Lemke*, 2007; *Schauer*, 2008]. Significant formation of drift banks could not be observed on the fresh snow cover. However, we cannot exclude the possibility that single samples of sea-ice thickness are biased by more than 10 cm, due to local snow accumulations.

Table 1. Parameters of the HEM surveys and results of the thickness measurements. FWHM is the full-width-half-maximum of the thickness distribution function. Open water content is the percentage of ice thinner than 0.1 m. Level-ice content is calculated with an adapted level-ice filter (see section 3.5.). Curvature B describes the tail of the thickness distribution function. Open melt ponds are determined using the algorithm as explained in section 3.4.

Year	Time Period (dd.mm)	Region	Total Length (km)	Overall Mean Thickness (m)	Overall Modal Thickness (m)	FWHM (m)	Open Water Content (%)	Level Ice content (%)	Curvature B	Open Melt Ponds (%)
2001	30.08-20.09	Gakkel Ridge & East of North Pole	260	2.28 ± 0.95	2.0	0.7	4	16	1.28	1
2004	23.07-14.08	North of Fram Strait	812	2.63 ± 1.32	2.1	1.3	1.8	9.5	0.86	15
2007a	03.08-10.08	North of Barents Sea	931	1.36 ± 0.73	0.9	0.8	0.5	20.5	1.47	15
2007b	28.08-18.09	Northpole towards Pacific / Siberia	3180	1.22 ± 0.79	0.9	0.8	5.4	19.1	1.44	0

Compared to other HEM "birds" typically used in mineral exploration and geological mapping, the EM-bird used here is small and easy to handle from the helicopter deck of a research vessel. The EM derived distance is sampled at 10 Hz which yields an average point spacing of 4 m with a typical helicopter speed of 40 m/s. The laser altimeter beam has a wavelength of 905 nm and is sampled at 100 Hz which results in a point spacing of 0.4 m. Due to the diffusive nature of the EM induction process, every thickness sample has a certain footprint over which the ice thickness is averaged [*Kovacs et al.*, 1995; *Reid et al.*, 2006]. In this case it is approximately 3.7 times the flight height of 10-15 m and leads to an underestimation of the maximum thickness of ridged ice by as much as 50%; open water spots smaller than the footprint cannot be detected at all. Furthermore 3D numerical modelling studies showed, that over long profiles of deformed ice the true mean thickness and the HEM mean thickness are in good agreement [*Hendricks*, 2009], and validation experiments showed that determination of modal thickness is achieved with an accuracy of 0.1 m [*Pfaffling and Reid*, 2009]. As a consequence of the instrument error, ice thickness samples thinner than 0.1 m are considered as open water.

2.3. Laser Profiling of Pressure Ridge Sails and Melt Ponds

Using a nadir looking 100 Hz laser altimeter we measured ridge-sail heights and spacing along the HEM profile. For ridge detection a combination of low and high pass filters was applied to the laser data in order to remove signals due to altitude variations of the helicopter [*Hibler*, 1972]. Local maxima in the filtered laser signal are inferred to represent pressure-ridge sails if they exceed a cut-off height of 0.8 m above the local level-ice height. In addition, two adjacent sails have to fulfil the Rayleigh criterion, i.e. they have to be separated by a data point of more than half their height to be considered as separate features.

Furthermore we identify drop-outs in the laser signal in order to estimate the fraction along the HEM transect, which was covered with open melt ponds. Over snow and ice a diffusive laser reflection can be expected whereas a specular return or an absorption of the laser energy in the water column occurs over open water [*Hoefle et al.*, 2009]. Hence laser drop-outs may occur over open water and melt ponds due to absorption or when specular reflections are missed by the laser altimeter due to small pitch and roll movements of the bird. Since the sample frequency of the laser is 100 Hz and that of the EM signal is 10 Hz, 10 laser samples are merged with one EM sample. When at least one of these 10 samples is a drop-out, and when ice thickness is larger than 0.1 m, we classify the particular thickness sample as a melt-pond measurement. This classification may fail where open leads and thaw holes are much smaller than the footprint of the EM-bird, as this may result in thickness values of more than 0.1 m. In such cases, open water spots and melt ponds cannot be distinguished. Although the accuracy of the absolute meltpond concentration is uncertain, due to a lack of validating data, we show relative changes between the years. Over melt ponds, extensive drill-hole studies showed that EM-derived ice thicknesses agree with the ice plus meltwater thickness within 0.1 m, as long as melt pond salinities are low [*Haas et al.*, 1997] [*Eicken et al.*, 2001].

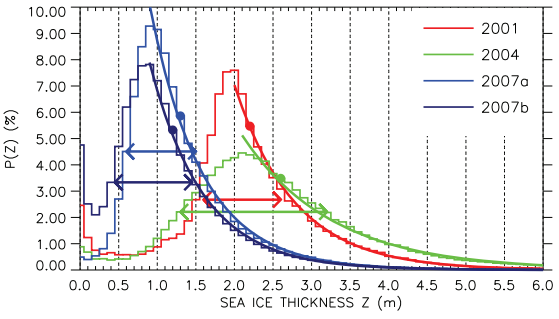

Figure 2. Overall sea-ice thickness distributions including open water. Circles mark the mean ice thickness and arrows the full width at half maximum (FWHM). Exponential fits for the tails of the distributions are plotted as solid lines.

3. Results & Discussion

3.1. General Sea Ice Conditions

As shown by *Haas et al.* [2008], all data from 2001 and 2004 were collected over predominantly multi-year ice (MYI) and 2007 data over predominantly first-year ice (FYI). Most data were recorded in regions with high ice concentrations of $> 90\%$, except those profiles located close to the Siberian-Pacific sea-ice margin in September 2007 (Fig. 1d). Ice concentrations shown in Figure 1 are negatively biased by melt ponds in a way as described by *Inoue et al.* [2008]. Not visible in Figure 1 are leads around the North Pole in 2001, which led to measured open water content for individual flights of up to 15% [*Thiede*, 2002]. The profiles flown in August 2007 (Figure 1c) were originally intended to extend farther north, but the "RV Polarstern" had difficulties breaking through the ice even though mean thickness

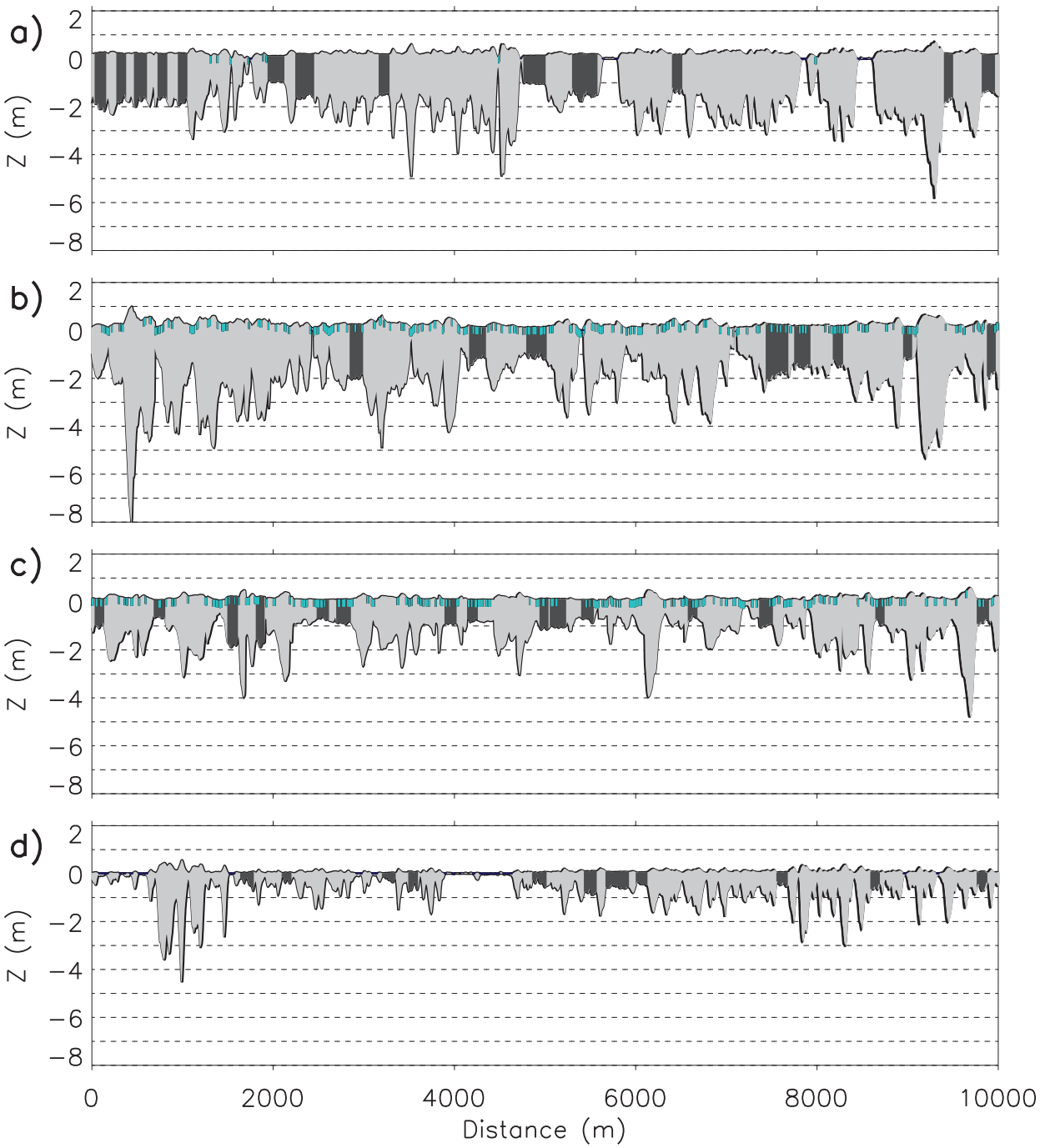

Figure 3. 10km long sea-ice sections representing typical profiles obtained during each campaign, where Z=0 marks the sea level. A freeboard to draft ratio of 0.89 was assumed in order to convert ice thickness into freeboard and draft. Dark sea-ice sections mark level ice as identified with the level-ice filter. Blue bars at the sea-ice surface are melt ponds located by laser drop-outs. Most of the larger ridges are melt pond free. **a)** 03/09/2001, 86.5°N/72°E. Level ice sections at 2 km and 5 km are first-year ice. **b)** 03/08/2004, 83.4.°N/4.7°W. Melt ponds are present and level-ice thickness ranges from one to two meters. **c)** 03/08/2007a, 82.8°N/31°E. Melt ponds are present. **d)** 17/09/2007b, 82.2°N/109°E. This section was obtained at the marginal sea ice zone

was below 1.4m (Table 1). By contrast, in September 2007, "RV Polarstern" steamed without any difficulties through ice which was on average only 15 cm thinner. Additional details of the four data sets are given in Table 1.

3.2. Thickness Distribution

The thickness distributions $P(z)$ of the 2001, 2004 and 2007 HEM surveys, together with their means, exponential decays and full-width-at-half-maximum (FWHM) values, are shown in Figure 2. FWHM is the width of $P(z)$ where it is at 50% of the maximum. For all four data sets the distribution was asymmetric, with most of the ice dis-

tributed in the thicker part. None of the four distributions showed more than a single maximum, open water, i.e. the maximum at z=0, not included. Typical sea-ice sections for each data set are shown in Figure 3.

Although 2001 was dominated by MYI and 2007 by FYI, both distribution functions were surprisingly similar in shape, as demonstrated by the similar FWHM (Table 1). This is an indicator for a common dynamic history of both sea-ice regimes, since according to *Thorndike et al.* [1975] only dynamic components are responsible for a redistribution of thinner ice towards thicker ice and therefore for a broadening of $P(z)$. The larger FWHM of the 2004 data either indicates a larger degree of deformation in the ice cover or the presence of several ice-thickness classes with different histories. Both explanations are typical for a MYI cover in the region north of Fram Strait, where sea ice from all over the Arctic Ocean converges, due to a constriction by the land masses of Greenland and Svalbard. This convergent ice regime includes sea ice from e.g. North of Greenland which probably remained there for multiple years but also younger MYI which advects from the central Arctic Ocean.

The most prominent difference between the years was the position of the maxima of $P(z)$, which represents the modal thickness. Modal thickness differed by as much as 1.2 m between the thinner maxima of 0.9 m in 2007 and the thicker ones of 2.0 m and 2.1 m in 2001 and 2004. This reduction was a consequence of the disappearance of MYI from this part of the Arctic Ocean in 2007 [*Nghiem et al.*, 2007]. The mean thickness also decreased from 2.3 m in 2001 to 1.3 m in 2007. The 2004 mean thickness was particularly large, differing from the 2001 mean thickness by 0.35 m, although the modal thickness was similar. This indicates similar thermal but different dynamic histories of the two MYI regimes. The reduction of mean and modal thickness in the central Arctic Ocean within the last 16 years was further studied by *Haas* [2004] and *Haas et al.* [2008], who used data ranging back to 1991, including the data presented here. They found a decrease of mean thickness in the central Arctic of 58% between 1991 and 2007.

As for sea-ice draft distributions from ULS data [*Wadhams and Davy*, 1986], the tail of the thickness distribution $P_{rdg}(z)$ can be fitted by a negative exponential function (Fig. 2)

$$P(z) = Ae^{-B(z-z_{mod})} \quad (1)$$

where z_{mod} is the modal sea-ice thickness, z the sea-ice thickness and A and B are two fitting parameters. The curvature B is the inverse of the standard deviation of the mean sea-ice thickness. The lower the curvature of B, the higher the amount of thicker deformed ice. Accordingly, B indicates there was a higher amount of deformed ice in the MYI cover of 2001 than in the FYI cover of 2007 and the degree of deformation of the MYI cover of 2004 was considerably higher than that of both, 2001 and 2007. All B values are listed in Table 1. A direct comparison of our curvatures with B values obtained from ULS measurements is difficult, since B is influenced by the different footprint averaging of HEM systems and ULS systems; the HEM method may underestimate the thickness of pressure ridges by up to 50%.

To summarize, we can state that the 2007 FYI and the 2001 MYI distributions are similar in shape but not in mean and modal thickness, for which 2001 showed a higher agreement with the 2004 MYI. The most plausible explanation is, that 2001 MYI and 2007 FYI experienced similar dynamic but different thermodynamic histories, namely different ice growth periods. The opposite is true for 2001 and 2004 MYI, where similar modal thicknesses were produced thermodynamically, but both regimes were subject to different dynamics in that the 2004 regime was subject to heavier deformation, due to the location in a convergent drift regime north of Fram Strait.

As a further conclusion we hypothesise, that the tail of thickness distributions $P_{rdg}(z)$ and the FWHM value do not necessarily increase with age, as shown by the comparison between 2001 MYI and 2007 FYI. The transition into a convergent stage has a stronger effect on both parameters as demonstrated by the 2004 data. However, the connection of curvature B and the amount of deformed ice in 2004 could be biased by the broad FWHM. In other words, we can think of the 2004 $P(z)$ as a superposition of several $P(z)$ from different ice regimes, each with a slightly different mode. Each ice thickness mode has an associated tail due to deformed ice and therefore modes might be influenced by tails. Moreover, we conclude that in a MYI regime only the FYI mode would be distinctly separated from the dominant one. A mode related to sea ice older than two years simply increases the FWHM, as the 2004 thickness distribution implies. $P(0)$ determines the amount of open water with only 2001 with 2.5% and 2007b with 4.9% showing a significant amount.

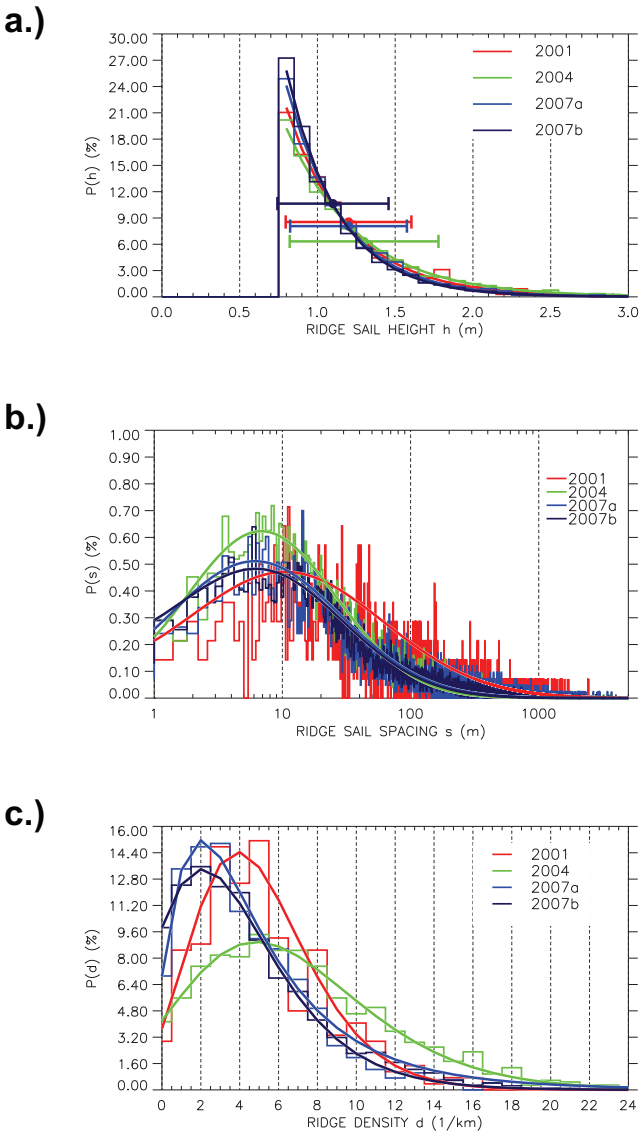

Figure 4. a) Distribution of sail heights fitted with a negative exponential function. No sails lower than the cut-off height of 0.8 m are detected. b) Histograms of sail spacing plotted with a bin width of 0.4 m together with the log-normal fits. c) Histograms of sail density in sails per kilometer with a bin size of 1 together with the lognormal fits.

Table 2. Ridge-sail parameters. Numbers following a ± symbol are standard deviations of the particular quantity. D is the curvature of the sail-height distribution

Year	Mean Sail Height (m)	Max Sail Height (m)	Curvature D	Mean Sail Spacing (m)	Min/Max Spacing (m)	Modal Sail Spacing (m)	Mean Sail Density (1/km)	Modal Sail Density (1/km)	Min/Max Density (1/km)
2001	1.21 ± 0.40	4.61	2.47	193 ± 254	0.88/2433	11	5.17 ± 3.27	3&5	0/16
2004	1.27 ± 0.48	4.90	2.15	139 ± 230	0.22/5662	8	7.20 ± 5.10	5	0/40
2007a	1.17 ± 0.38	4.36	2.75	233 ± 322	0.72/3686	6	4.28 ± 3.35	2	0/23
2007b	1.14 ± 0.36	4.97	2.93	220 ± 353	0.64/5021	6	4.50 ± 3.83	2	0/28

Compared to earlier ULS measurements of late summer sea-ice thickness between Fram Strait and the North Pole [*Wadhams and Davis*, 2000a], the 2004 mean sea-ice thickness between 82°N and 85°N is 60% thinner than in 1976 and 22% thinner than in 1996.

3.3. Ridge Distribution

Even when modal thickness is a good indicator for distinguishing between FYI and MYI, pressure ridge parameters are not. The mean height of pressure ridge sails differed by a maximum of only 0.13 m in all regimes and therefore cannot be taken as a reference, either for the age or for the modal or mean ice thickness of a regime. However, all data are based on summer measurements; in winter the conditions may be different due to an absence of surface melting. Nevertheless, pressure-ridge-sail distributions provide information about the degree of deformation within a sea-ice regime. Intuitively we expect higher sails, a higher sail density and a smaller spacing between the sails in a more deformed ice regime, such as in the 2004 survey area north of Fram Strait where we observed the highest mean sail height and the highest mean sail density or lowest mean sail spacing respectively. The histograms and the fitted distribution functions of the three sail parameters are shown in Figure 4. Further statistical ridge parameters are listed in Table 2.

Of the three ridge parameters, sail height h differs least between the three different ice regimes. For instance in the 2001 MYI regime with a modal thickness of 2.0 m, mean sail height was just 0.04 m or 10% higher than in the 2007a FYI regime with a modal thickness of 0.9 m. As for the tail of the thickness distribution, the distribution of sail heights can be described by a negative exponential fit for all data sets (Fig. 4a). The fitting function is

$$P_{sail}(h) = Ce^{-D(h-h_{cut})} \tag{2}$$

where C and D are the fitting parameters and h_{cut} the cut-off height of 0.8 m. The curvature D of the distribution and mean sail height plus its standard deviation for every year are shown in Table 2. The correlation r between fitted and calculated sail height distributions is higher than 0.99 for all years.

The spacing s and density d of pressure-ridges can be approximated by a log-normal distribution [*Wadhams and Davy*, 1986]

$$P(x) = \frac{1}{\sqrt{2\pi}\sigma(x+\theta)} e^{-\frac{(ln(x+\theta)-\mu)^2}{2\sigma^2}} \tag{3}$$

where μ, σ and θ are the fitting parameters and x represents s or d respectively. The maximum of $P(x)$ is at

$$x_{max} = \theta + e^{(\mu-\sigma^2)} \tag{4}$$

and the mean is at

$$x_{mean} = \theta + e^{(\mu+\frac{\sigma^2}{2})}. \tag{5}$$

The fitting parameters for $P(s)$ and $P(d)$ are listed in Table 3 and 4. Mean spacing and density are directly related whereas the modes differed significantly. Modal spacing in relation to mean spacing was with 6 to 11 m almost equal for all data sets, but differences in modal density were with 2 to 5 sails per kilometer in the same order of magnitude as differences in mean density. This is evidence that ridge sails tend to emerge in clusters, with a preferential spacing between 6 and 11 m within the cluster. Those clusters are probably associated with a single deformation zone in which the number of keels is not necessarily equal to the number of sails. Larger sail spacing in the distribution function can be assigned to level-ice areas which separate two deformation zones from each other. The correlations r between the true distributions of s and d and the log-normal fits are higher than 0.9 and 0.99 respectively for all data except 2001 where it is 0.69 and 0.95 respectively. The lower correlation for 2001 most probably results from the smaller number of samples and the consequently coarser distribution histogram and not from the fact that the 2001 sail distribution follows a different functionality, which would be in contrast to previous publications [e.g. *Davis and Wadhams*, 1995; *Wadhams*, 2000b].

3.4. Standard Errors

In order to quantify how representative the obtained results are, we calculate the standard error ε of the modal and mean thickness as well as of the means of the examined ridge parameters [*Wadhams*, 1997]. The standard error ε is given by

$$\varepsilon_{\bar{Z}}(l) = \left\{ \sum_{i=1}^{n} (\bar{Z} - Z_i)^2 / n \right\}^{\frac{1}{2}} \tag{6}$$

Table 3. The three log-normal fit parameters for sail spacing, the mean and modal sail spacing and the correlation r between fit and measurements.

Year	σ	μ	θ	s_{mean} (m)	s_{max} (m)	r
2001	1.93	6.09	0.19	1038.80	10.90	0.70
2004	1.33	3.69	0.00	104.03	6.83	0.97
2007a	1.51	4.10	0.00	212.99	6.10	0.91
2007b	∗1.48	4.08	0.50	177.28	7.18	0.97

Table 4. The three log-normal fit parameters for sail density, the mean and modal sail density and the correlation r between fit and measurements.

Year	σ	μ	θ	d_{mean} (m)	d_{max} (m)	r
2001	0.25	2.52	7.80	5.01	3.90	0.95
2004	0.24	3.01	14.35	6.52	4.85	0.99
2007a	0.65	1.70	1.60	5.15	2.00	0.99
2007b	0.33	2.32	7.10	3.68	2.08	0.99

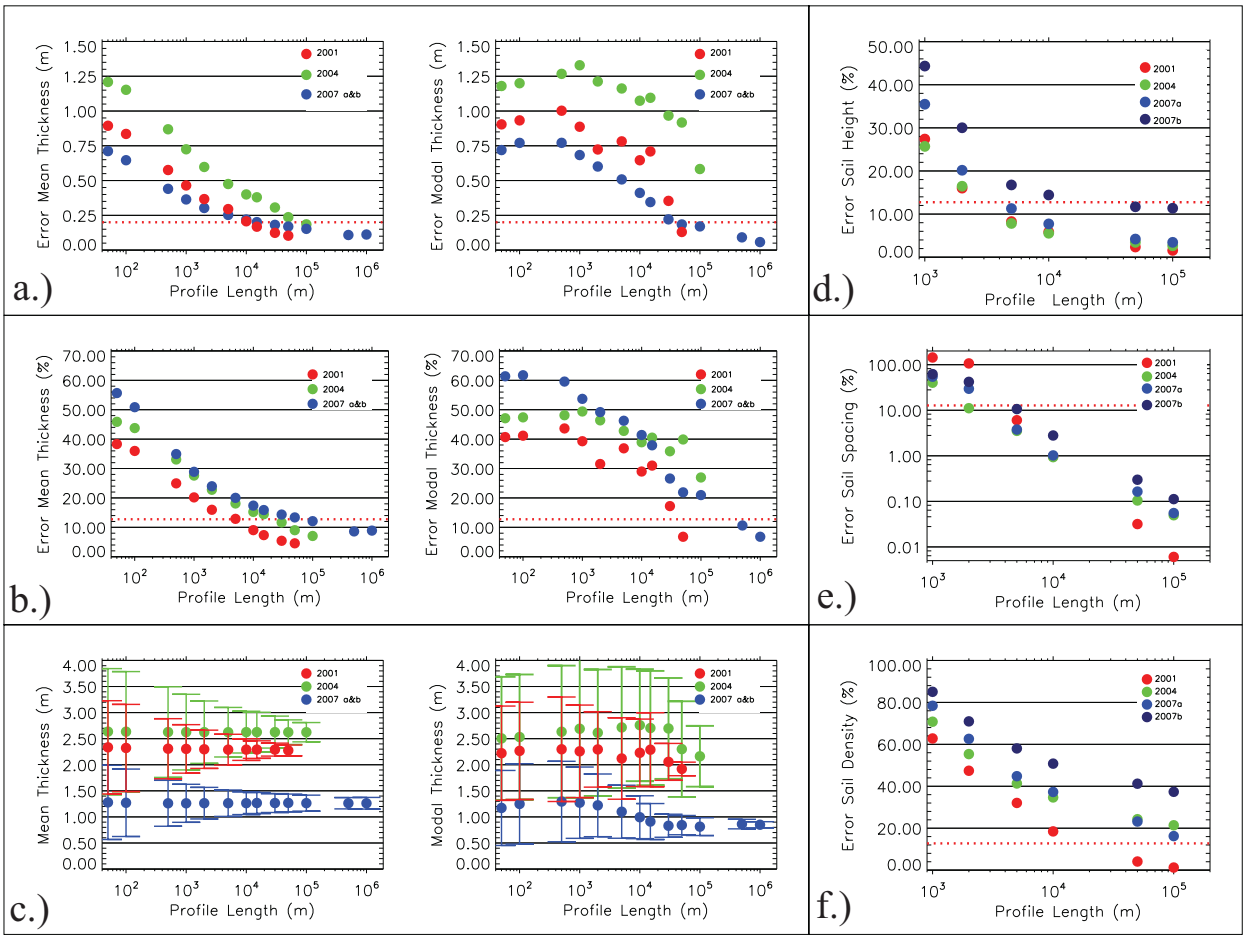

Figure 5. Standard Error ε versus profile length. **a.)** Absolute value of ε of mean thickness (left) and modal thickness (right). The red line denotes the threshold for reliability of 0.2 m. **b.)** ε in percent of the mean thickness (left) or modal thickness (right). **c.)** Circles are mean thickness (left) and modal thickness (right) and error bars indicate ε. **d.)** ε of mean ridge-sail heights as percentage of the mean. **e.)** ε of mean ridge spacing as percentage of the mean. **f.)** ε of mean ridge density in percent of the mean. Except in a.) the red dotted line mark a 12.75% threshold. This threshold is aligned with the threshold for reliable mean-thickness measurements of *Wadhams* [1997].

where $\bar{Z}$ is the mean or mode of the complete data set, Z_i the mean or mode of the ith subsection of the data set, n the number of subsections and l the length of the particular subsection. Thus the standard error is the standard deviation of an ensemble of subsection means or modes where all subsections concatenate to form the complete data set. The standard error ε is a function of the subsection length l, but also of the degree of homogeneity of the ice regime, expressed by e.g. multiple modes in the distribution function or a large FWHM. As a consequence, different ice regimes require different section lengths in order to determine the overall mean or the overall mode with a certain statistical reliability. For the determination of ε we subdivided the flights into smaller sections ranging from 50 m to the maximum flight length and even longer sections by concatenating all flights in a particular year. Results of all standard error determinations are shown in Figure 5.

In the following we denote ε of the mean and the modal thickness by ε_{mean} and ε_{mod}. For thickness determination the error is limited to the maximum accuracy of the HEM bird of ± 0.1 m which represents a 0.2 m thickness interval. Therefore we consider a measurement of mean or modal thickness as representative for a particular ice regime if ε is equal to or below the interval of 0.2 m. Previous thickness studies suggested an ε_{mean} as a percentage of the overall mean thickness of 12.75% as the threshold for representativeness [*Wadhams*, 1997]. We test for both criteria to evaluate our results. ε_{mean} decreases steadily as l increases and reaches the accuracy of 0.2 m at a length of 10km in 2001, at 100 km in 2004 and at 15 km in 2007 (Fig. 5a left). All data sets fulfil the *Wadhams* [1997] requirement for representativeness at profile lengths of 5 km for 2001, 30 km for 2004 and 100 km for 2007 (Fig. 5b left). However, we prefer the absolute standard error since an error of for instance 0.2 m should have the same weight in thicker and thinner ice regimes. Furthermore the comparison of absolute standard errors obtained in different thickness regimes is justified due to the non dependency of the standard error on mean thickness [*Wadhams*, 1997; *Percival et al.*, 2008]. All ε_{mean} values are shown on the left side of Figure 5 a-c. The decrease of ε_{mean} with profile length is a measure for the wavelength of thickness variations within the data set, with space and time information mixed. In $\varepsilon_{mean}(50m)$ for example all wavelengths greater than 50 m are included. A comparison of the two less deformed ice regimes (2001,2007) shows, that for short profile lengths $\varepsilon_{mean2001}$ was higher than $\varepsilon_{mean2007}$ and vice versa for longer profile lengths (Fig. 5a left side). This indicates that spatial variability in the 2001 data set occurred on shorter length scales than in the 2007 data set. In other words, on length scales longer than 10 km the MYI

cover in 2001 was even more homogeneous than the FYI cover in 2007. But 2007 covered a much larger area and a much longer time span i.e. larger variations can naturally be expected. So this conclusion is only valid for the data sets themselves and cannot be taken as a statement for the complete ice-thickness distribution of the TPD in the particular year. *Haas et al.* [2008] highlighted the remarkable self-similarity of all 2007 profiles. ε_{mean} can be taken as a quantification of this similarity. In the area covered in 2007, on 100 km sections over a time span of 1.5 months, the deviation of the section means to the overall mean was not greater than 0.15 m, which is indeed remarkably low. For 2001 the same applies to profile lengths of even 15 km, but here a time span of only 1 month is covered and a shorter total profile length. In 2004 a higher ε_{mean} suggests a lower self similarity of the obtained thickness profiles, and this even with a smaller extent of the survey area than 2007.

In 2001 and 2007 ε_{mod} reached 0.2 m for a subsection length of 50 km. In 2004 the minimum value of ε_{mod} was still as high as 0.6 m for a section length of 100 km. The dependence of ε_{mod} on the subsection length l showed a different behaviour than for ε_{mean}. The modal standard error ε_{mod} was characterised by more abrupt changes (Fig. 5a right), which are based on the fact that the modal thickness reflects just a single thickness out of the distribution, namely the maximum, whereas all others are neglected and it means that there are other frequent thickness classes which differ significantly from the dominant one. The profile length for which ε_{mod} starts to decrease for the first time is probably correlated to the length of deformed sea-ice sections, since modes of level ice sections must dominate those of deformed sections. Positions where a steeper decline of ε_{mod} starts probably mark the minimum length for which the main ice class becomes dominant. The magnitude of the decline reflects the ice-thickness difference between the dominant and the second-most frequent thickness class. This is the difference of the MYI and FYI modes in the 2001 data (see chapter 3.6.) but also the occurrence of thin ice sections with a mode of 0.1 m are a reason for abrupt declines in ε_{mod}. In the MYI regime of 2004 the jump of ε_{mod} occurs at a larger length than in 2001 and 2007 because thickness classes are present which differ significantly from each other but are more equally frequent than in the MYI regime of 2001. This is also indicated by the larger FWHM (Table 1) of the 2004 data. In the more homogeneous FYI regime of 2007 ε_{mod} is generally smaller and shows no abrupt declines because the different dominant thickness classes are similar in thickness (smaller FWHM). Strictly speaking, with an ε_{mod} of more than 0.2 m, like in the 2004 data, the assignment of just a single modal thickness to the study region is not warrantable.

Since mean and mode of a thickness distribution are not equal, modes of short profiles more likely reflect the overall mean thickness than the overall modal thickness (Fig. 5c right). This is easier to understand if we imagine a section length of only one sample. Then the mean of all modes of these one-sample sections is naturally equal to the overall mean thickness. Beyond a certain section length, the mean modal thickness decreases until it is equal to the overall modal thickness. In the less deformed FYI regime of 2007 from 30km length onwards the true modal thickness was achieved, in the 2001 MYI regime from 50km length onwards and in the heterogeneous and more deformed 2004 MYI regime not even at 100km length.

We summarize that for a clear characterization of a sea-ice regime with respect to its mean thickness, survey lengths of 10 to 15 km may be necessary in relatively homogeneous MYI or FYI regimes like 2001 and 2007. In heterogeneous and deformed MYI regimes like 2004 a minimum of 100 km can be required. For a representative modal thickness profile lengths of 50 km are necessary in homogeneous MYI and FYI regimes and at least 500 km may be necessary in heterogeneous MYI regimes, where an assignment of a dominant modal thickness can even be questionable at all.

The standard error ϵ in dependence of section length l for sail height, spacing and density is shown in Figure 5d-e in terms of percent of the mean. Likewise the standard error of mean and modal thickness, a value of 12.75% of the mean was taken as a threshold for representative results. For a section length of 100 km mean sail-spacing could be obtained with the lowest standard error, followed by mean sail-height and mean sail-density which has the highest error. The small standard error for spacing accounts for the clustering of sail heights with a preferred spacing of between 6 to 11 m within each cluster. In other words, only short profile lengths are necessary to obtain typical spacing of sail-heights within deformation zones. A better quantity to describe the distribution of deformation zones as a whole is the sail density. Since the pattern in which deformation zones appear is less regular than sail spacing within a deformation zone, the standard error of sail density is higher. For sail density the length of the data set correlates with the standard error. Hence 2001 shows the lowest standard errors and the longest data set of 2007b the largest ones. This result indicates that compared to sea-ice thickness, the distribution of deformation zones cannot be associated with huge homogeneous regimes of FYI or MYI, as is possible with thickness.

3.5. Melt Ponds

Melt ponds were detected with the method described in chapter 2.3., which is applicable for open melt ponds only. Open melt ponds were present during the 2004 and 2007a surveys whereas almost all of the meltponds were refrozen during 2001 and 2007b. Henceforth only the 2004 and 2007a data were taken for melt pond coverage determination. In Figure 3, positions having melt ponds, which are defined as laser-data drop outs over ice thicker than 0.1 m, are marked with light blue bars. Mean melt-pond concentrations amounted to $15\pm14\%$ for 2004 and $15\pm11\%$ for 2007a, where the errors are standard errors for profile lengths of 35 km. These results can be compared with visual observations of melt-pond concentrations during each expedition, for which the 2001 melt-pond concentration varied between 10% and 30% (all refrozen) [*Haas and Lieser*, 2003], 2004 between 30% and 40% (during the last two flights partially refrozen) [*Lieser*, 2005] and 2007 melt-pond concentration between 20% and up to 50% (2007b all refrozen or transformed to thaw holes) [*Schauer*, 2008]. The difference between laser-derived melt pond concentration and visual observations or aerial photography (Fig. 7) suggests that the

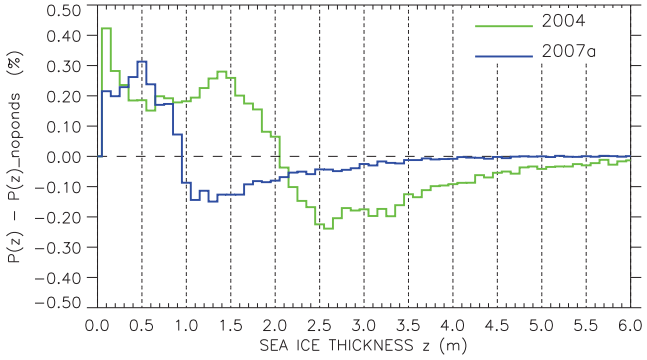

Figure 6. $P(z) - P(z)_{noponds}$ is the difference between sea-ice thickness distributions including ponded ice and excluding ponded ice. Above zero refers to ice-thickness ranges which are over represented in ponded ice and below zero refers to an under representation in ponded ice.

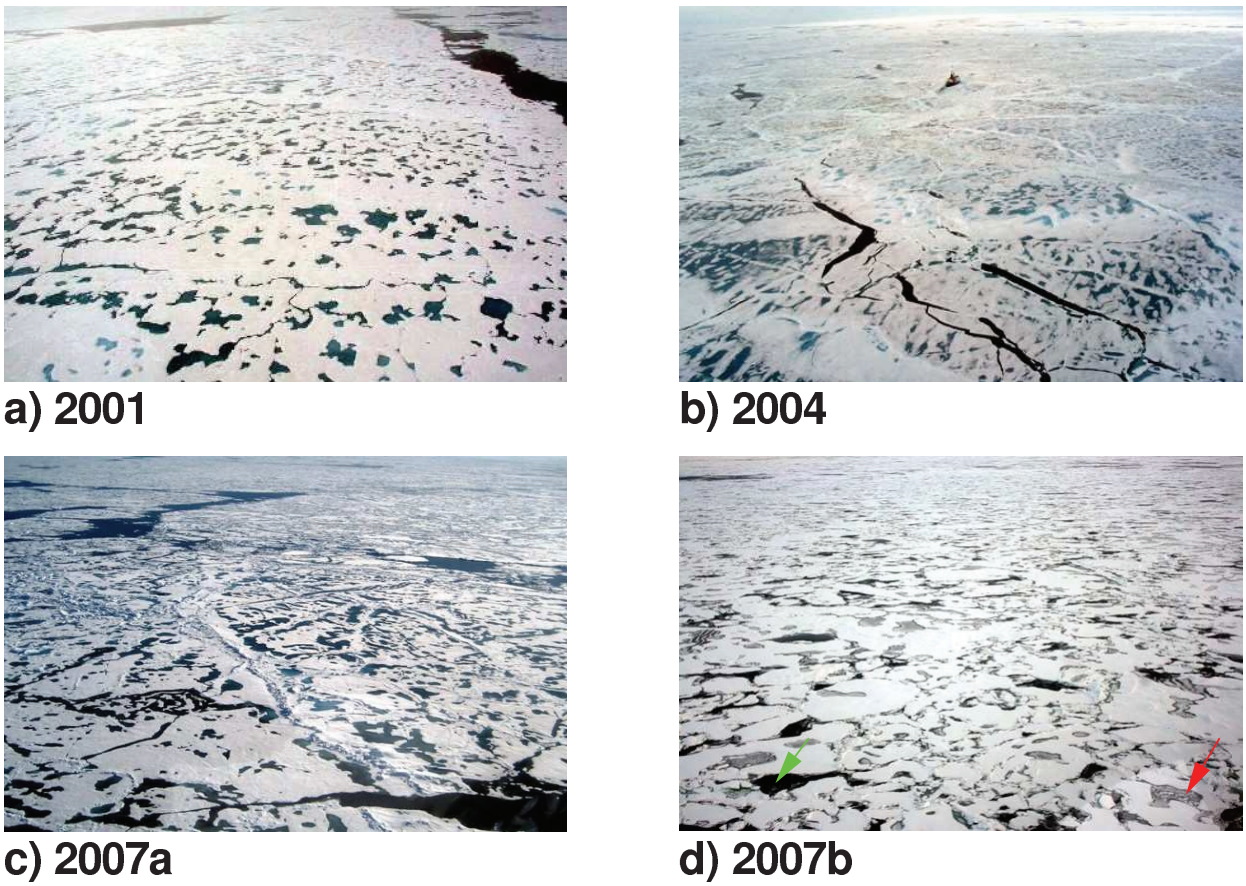

Figure 7. Aerial photographs of typical sea-ice conditions for all four data sets. **a)** Mid-August melt pond concentration is lowest of the four data sets and; all ponds are refrozen., **b)** End of July melt ponds are open, **c)** Beginning of August melt ponds are open and mostly dark coloured, **d)** Mid-September melt ponds are refrozen. The red arrow points to a refrozen melt pond, the green arrow points to a thaw hole.

laser provides an underestimation of the true concentration. In Figure 6 the effect of open melt ponds on the overall thickness distributions of 2004 and 2007a is shown. It can be seen that ponded ice is on average thinner than pond free ice even with the water column of the melt pond included in the ice thickness value, since the HEM instrument measures the distance from the surface of melt ponds to the ice-ocean interface. Furthermore, Figure 6 shows that melt ponds preferably form on ice with a thickness less than or equal to the modal ice thickness, which was 1 meter thicker in 2004 than in 2007. Additional information about the brightness and the colour of melt ponds are known from visual observations. 2007 melt ponds were on average darker than those during 2001 and 2004 (Fig. 7), which accounts for thinner or no ice below the melt pond.

The equal amount of melt pond concentration in 2004 and 2007a suggests that overall surface melting was not stronger in either of the two years. However, since the ice was thinner in 2007 the same amount of melt ponds triggered different processes. Not only are melt ponds on thinner ice more easily transformed into thaw holes, but their darker surface also amplifies the albedo feedback. In 2007b many thaw holes emerged (Fig. 7d) which reduced the ice concentration at some locations, e.g. at the Pacific-Siberian ice edge (Fig. 1d), significantly. Once melt ponds are transformed into thaw holes and the sea ice concentration is lowered, the thinning of ice is even accelerated as described in section 3.7. The question why the ice concentration was lowered close to the ice edge but not over widespread areas of the 2007 FYI cover will be discussed in section 3.8..

Furthermore, we should note that large amounts of thaw holes probably reduce the mechanical strength of the sea-ice cover. Together with the 2007 persistent southerly winds over the Pacific Sector of the Arctic ocean [*Maslanik et al.*, 2007b], the thaw hole related fragmentation of the sea ice cover may be a further reason for the increased drift velocity in 2007, as a fragmented sea ice cover is easier to move [*Rampal et al.*, 2009].

3.6. Level Ice

Level ice was identified using two criteria. First, the numerical differentiation of sea-ice thickness along the profile using a 3-point Lagrangian interpolator must be < 0.04 and second, level-ice sections must extend at least 100 m in length, which is approximately 2 times the footprint of the HEM Bird. Such identified level-ice sections are marked black in Figure 3. Compared to the level-ice definition of former studies [e.g. *Wadhams and Horne*, 1980], which defined a measurement point as level if either of the two points 10 m left or right of it did not differ more than 0.25 m in draft, our criterion is more strict and the amount of level ice identified (see Table 1) is lower than visual observations of the sea-ice cover imply. However, a definition of level ice is always to a certain degree arbitrary, and for our purposes, which is to extract the thermally grown ice thicknesses, we want to minimise the amount of deformed ice passing the level-ice filter as much as possible. With all the deformed sea ice removed, $P(z)$ becomes normally distributed (Fig. 8) and mean and modal thickness agree to within ± 0.1m. The 2004 and 2007b data sets have a second mode at 0.1 m, representing thin ice on refrozen leads. Of particular interest

is the second mode in the 2001 data of 1.1 m, representing sporadically occurring first-year ice. It is sporadic, because the FYI mode ±0.2 m sums up to not more than 6 % of the level ice which is 0.96 % of the total data set. For 2001 and 2004, level ice of even 3 m and thicker occur, which is most probably deformed ice which accidentally fulfil the level ice criterion. The shift of the modal thicknesses in the 2001 and 2007b data from 2.0 m and 0.9 m in the complete thickness distribution to 1.8 m and 0.8 m in the level-ice distribution (Table 1 & 5) can be explained with the strict criterion and the consequence is that not 100 % of the level ice is identified. Another explanation could be the uncertain relation between modal and level-ice thickness. The mean length of level-ice areas is longest for 2001, a little bit shorter for 2007 and shortest in the 2004 data (Table 5).

When we interpret the second mode at 1.1 m in the 2001 level ice histograms as a FYI mode (Fig. 8), the level ice thickness of 2007a and 2007b was only 0.2 m and 0.3 m thinner than level FYI in 2001. Compared to previous studies this lies within the interannual variation of melting and freezing rates. *Haas and Eicken* [2001], for instance, observed changes of level ice thickness within a summer FYI cover in the Laptev Sea of 0.3 m between 1995 and 1996 and *Perovich et al.* [2008] showed yearly melting rates at the North Pole between 0.4 m and 0.7 m. Therefore 2007 was not exceptional with regard to melting rates, at least not within the pack. This result is also supported by *Kwok et al.* [2009], who found a considerably thinner Arctic MYI cover in 2007 but a negligible trend towards thinner FYI.

3.7. Dependence of Thickness on Sea Ice Concentration

Accounting for the lower Albedo of an open ocean, a decreasing sea-ice concentration causes additional heat gain of the ocean via shortwave insolation and therefore causes additional melting. Hence, it is of interest to analyse the relation between level sea-ice thickness and open-water content for all three data sets. According to the instrument accuracy of ±0.1 m our definition of open-water content is the fraction of the thickness distribution function where ice thickness is lower than 0.1 m.

For the analysis of the dependence of level-ice thickness on ice concentration we picked all modal thicknesses emerging for each flight. This time not only the overall maximum in the distribution was picked but every local maximum as well. This highlights the distribution of larger areas with the same level-ice thickness within each flight. Plots of open water fraction versus thickness modes are shown in Figure 9. In 2001 the majority of level-ice modes fell within a range between 1.6 and 2.0 m, independent of sea-ice concentration, although a maximum open-water content of 15 % could be observed (Fig. 9a). The profiles with an open-water content of $> 10\%$ were obtained in the region of the North Pole. Two modes are distinctly thinner and had a thickness of 1.0 and 1.1 m, representing first-year ice. The 2004 data showed a much larger scattering of modal thicknesses, ranging from 0.1 m to 3.6 m, where the majority of the modes lay within 1.5 and 2.0 m (Fig. 9b). Owing to the low fraction of open water (6 %), the variability in sea-ice concentration was too low for the identification of a significant relationship between ice concentration and level-ice thickness. The same applied for 2007a, where no significant amount of open water was present in the data (Fig. 9c). Here the modes were much less scattered and the majority of the modal thicknesses were between 0.6 and 1.0 m. The only significant dependence on open water could be observed in the 2007b data, where modal thickness decreased gradually with an increasing amount of open water (Fig. 9d). For profiles with open-water content of below 10%, the modes were concentrated between 0.6 and 1.0 m, as for 2007a. Ignoring the modes of thin ice, which represent young ice formed in September 2007, this decreasing behaviour can be described by a linear relationship:

$$Z_{2007b}(W) = -0.02 \cdot W + 0.94, \quad \text{with } 10\% < W < 40\%, r = 0.7 \qquad (3)$$

where W is the open-water content and Z the level-ice thickness. There are several explanations for the absence of a thickness dependence on open water content in 2001. First the maximum open water fraction was only 15 %, second open water spots occurred in huge open leads and not in form of a fragmented ice cover as in 2007 and thirdly heat gain of the ocean and downwelling short wave radiation was not as high as in 2007 [*Kay et al.*, 2008] [*Perovich et al.*, 2008]. The gradient of increasing open water content in 2007b was directed towards the Pacific sea ice margin of the 2007 sea ice cover. Therefore we continue the discussion of the thin 2007b sea ice in the next chapter.

3.8. Thickness Gradients towards the Ice Edge

The 2004, 2007a and 2007b data sets allow the study of thickness gradients from the sea-ice edge into the closed ice pack. In Figure 1 the different distributions of sea-ice concentration along the three ice edges are visible. The 2004 sea ice edge north of Fram Strait was exceptionally far north and showed a sharp transition from open water to high ice concentrations (Fig. 1b). Of similar sharp appearance was the sea-ice margin north of the Barents Sea in the 2007a data (Fig. 1c). Moreover, the location of the edge remained stable during the time of rapid sea-ice decline in

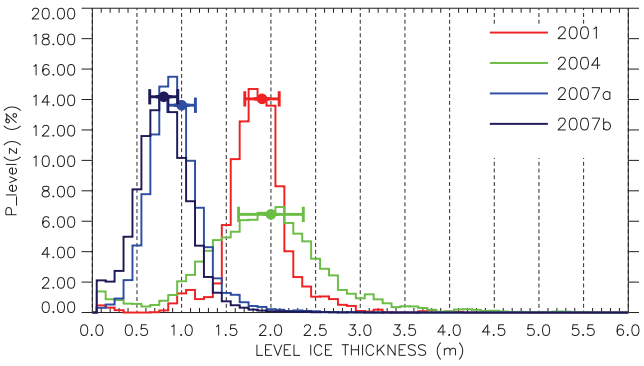

Figure 8. Level-ice-thickness distributions. Circles mark mean sea-ice thicknesses and error bars their standard deviations.

Table 5. Mean and modal thickness of level ice and the mean and maximum length of continuous level-ice sections

Year	Mean Thickness (m)	Modal Thickness (m)	Mean Length (m)	Max Length (m)
2001	1.89 ± 0.37	1.8 1.1 0.1	160 ± 77	552
2004	1.96 ± 0.72	2.1 0.1	148 ± 54	426
2007a	0.97 ± 0.31	0.9	158 ± 69	680
2007b	0.84 ± 0.31	0.8 0.1	154 ± 66	888

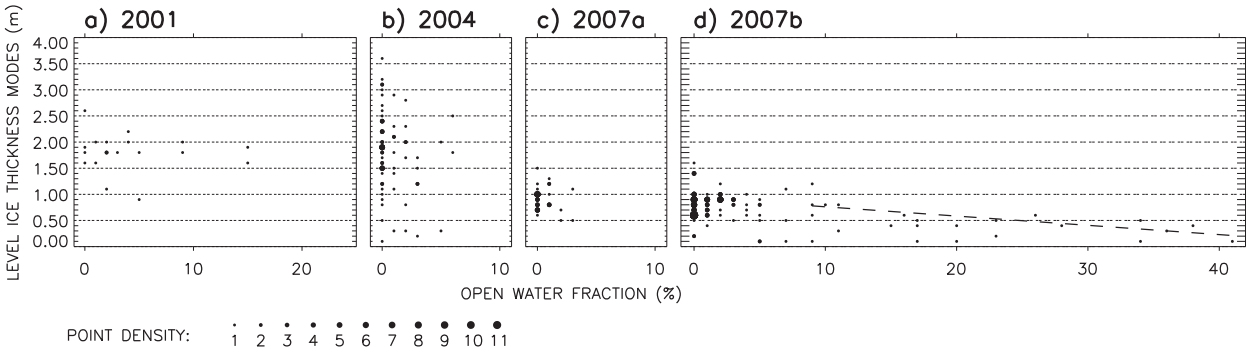

Figure 9. Modes of level-ice thickness of individual 35 km sections (18.5 km in 2001) plotted versus open water fraction. All modes, not only the dominant modes, of all individual sections are plotted. The circle size denotes the point density, i.e. the number of modes plotted on the same position. The dashed line in d.) is a linear fit to level-ice modes thicker than 0.1 m and with an open water content of $> 10\%$

August and September 2007. The 2007 sea-ice decline was rather pronounced at the Pacific-Siberian ice margin, where a widespread decrease in ice concentration was visible already in August (Fig. 1c and Fig. 1d).

The gradients of thickness and open-water fraction $P(0)$ along the ice edge, are shown in Figure 10. On average each sample represents a 35 km long flight track. They are displayed as function of latitude since transects perpendicular to the three ice edges are basically south-north oriented. As we are interested in thickness changes due to melting and freezing, we only considered level-ice thickness. The thickness surveys were performed in time periods of 18 days (2004), 8 days (2007a) and 22 days (2007b) which are time spans where melting and freezing can proceed substantially. To account for temporal changes during the time period of the survey, thickness and open-water samples in Figure 10 are color-coded according to the time progressed. Surface melting could be observed during the first 15 days of 2004 and during 2007a by the presence of open melt ponds. During the last three days of the 2004 surveys and during 2007b thin ice emerged on the melt ponds as an indicator for a decline of surface melting. However, whether these are signs for a thinning or thickening within the survey period cannot easily be answered here, since the amount of bottom melt can be significant even when surface melting comes to a halt [*Perovich et al.*, 2003].

In 2004 a decrease of mean level ice thickness from 2.25 m to 1.75 m could be observed towards higher latitudes between 82°N and 85°N. Open-water content remained lower than 8% and showed no significant gradient but a slightly higher concentration of open leads (8%) around 82.8°N and 84.5°N (Fig. 10a). The 2007a data showed no trend from the margin at 82°N up to 85.5°N, neither in mean level-ice thickness nor in open-water content, which remained lower than 3 % (Fig. 10b). In comparison, 2007b showed significant changes in mean level-ice thickness from values of 0.35 m at the margin at 83°N to values of 0.75 m at 85.5°N, whereas north of 85.5°N level-ice thickness remained constantly scattered around a mean of 0.9 m. The same was true for the open water content, which decreased from a maximum of 40% at the ice margin to a mean of 3% at 85.5°N. Farther north the maximum open water content was lower than 8% (Fig. 10c). This results show that similar to the Beaufort Sea [*Perovich et al.*, 2008] melting rates in the central Arctic in 2007 close to the Pacific sea ice edge were increased, but not within the pack. The thickness gradients in 2004 and 2007b from the edge towards north can be described by the following linear fits:

$$Z_{2004}(L) = -L \cdot 0.27 + 24.35, \quad \text{with } 82^\circ N < L < 85^\circ N, r = 0.63 \tag{2a}$$

$$Z_{2007b}(L) = L \cdot 0.09 - 7.0, \quad \text{with } 82^\circ N < L < 85.5^\circ N, r = 0.53, \tag{2b}$$

where Z is the mean level-ice thickness, L the latitude and r the correlation coefficient. The evolution of ice thickness in time showed no significant correlation in 2004 and 2007a. 2007b implied a thinning of ice during the time period of the survey but this can be explained by a thinning with increasing open water content as well.

Compared to previous studies on meridional sea-ice thickness gradients in the region of the Fram Strait and north of it [*Wadhams and Davis*, 2000a], where the thickness gradient was positive towards the north, the 2004 negative gradient of mean level-ice thickness from 82°N to 85°N (Fig. 10a) is somewhat surprising. It can be interpreted as a situation where older ice was situated in the south and younger north of it. Probably the older ice was advected from north of Greenland whereas the younger ice was advected from the Eurasian side of the TPD.

The reason for the presence of a thickness and concentration gradient at the 2007b ice edge is more difficult to find. Interestingly, the 2007a ice edge did not show such a gradient. Therefore, we pose the question why sea-ice concentration and thickness decreased gradually at the Pacific side but abruptly at the Atlantic side of the 2007 sea-ice cover. An obvious difference between both margins is that the Atlantic margin was stationary whereas the Pacific margin retreated towards the North Pole during August and September (comparison of Fig. 1c and 1d). This was a consequence of the general drift pattern of the TPD in June-October 2007 parallel to the Atlantic sea-ice boundary caused by an anti-cyclonic surface wind anomaly [*Ogi et al.*, 2008]. Considering this wind anomaly, which caused on-ice winds at the 2007 Pacific sea-ice margin, it is contrary to previous studies by *Wadhams* [2000b] that the Pacific sea-ice edge was diffuse instead of compacted and abrupt. Another difference between both sea-ice edges was exceptional heat gain of the surface layer of the Arctic ocean on the Pacific side which could not be observed on the Atlantic side of the ice cover [*Steele et al.*, 2008; *Perovich et al.*, 2008]. Considering both the heat gain and the wind direction, a plausible explanation could be the transport of warmer air masses from the open ocean beyond the Pacific sea-ice margin into the pack. This caused additional surface melting whereby melt ponds were transformed into thaw holes, which amplified the Albedo feedback. Further within the ice-pack the warmer air masses cooled down and melting rates were reduced.

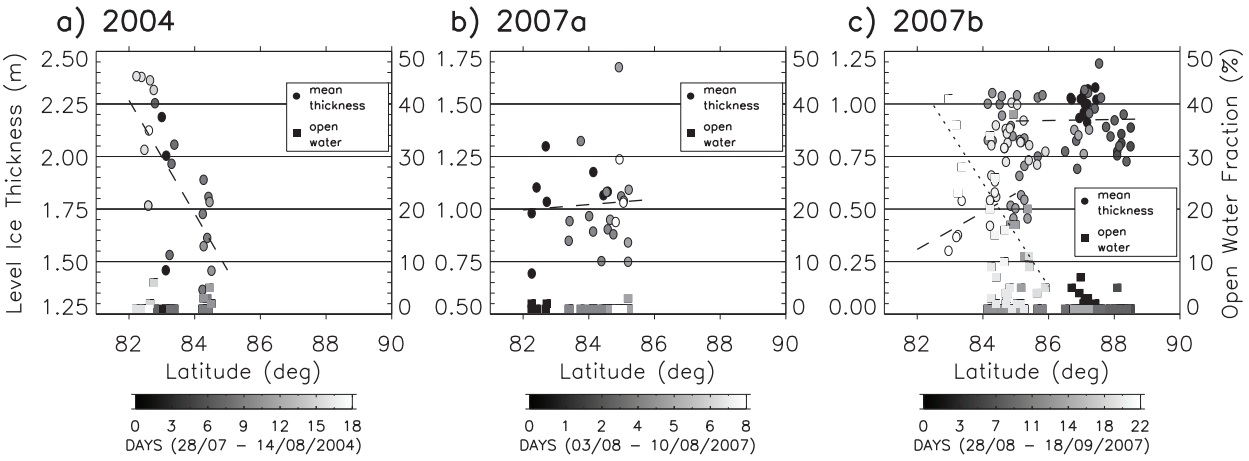

Figure 10. Mean level-ice thickness (circles) of individual 35 km sections and open water fraction (squares) plotted versus latitude. Grey colours indicate the day within the measurement period, where black is the first day and white the last. A circle and square of the same color correspond to one individual section. Dashed lines are linear fits of the level-ice thickness. Dotted line (only in c.) is a linear fit to the open water fraction.

4. Conclusions & Outlook

We have presented high resolution HEM sea-ice thickness data from the Arctic Trans Polar Drift (TPD) in the summers of 2001, 2004 and 2007. These data provided the opportunity to compare thickness distributions and surface properties of sea-ice regimes consisting of predominantly first-year-ice (2007) or predominantly multi-year-ice (2001,2004) with different dynamical histories. Furthermore, the data are of special importance since regular activities of ULS submarine surveys to obtain sea-ice draft became less frequent during the 2000's. These data can be used for validation of various model studies or sea-ice thickness results from satellite altimetry techniques. The 2001 and 2007 surveys were situated more upstream within the TPD, closer to the North Pole and towards the Pacific side of the Arctic Ocean, and the 2004 surveys more downstream within the TPD in the area north of the Fram Strait. September mean sea-ice thickness in the upstream TPD decreased from 2.29m in 2001 to 1.22m in 2007. Downstream TPD mean sea-ice thickness was 2.63m in 2004, which is a continuation of the decreasing trend in the region north of the Fram Strait shown by *Wadhams and Davis* [2000a].

This work focussed on a detailed analysis of sea-ice thickness distributions and surface properties of the sea-ice cover, and is therefore a continuation of the study of *Haas et al.* [2008] which is partially based on the same data sets but focused more on the evolution of summer sea ice thickness in the TPD since 1991. As a major conclusion we found that MYI regimes can show similar modal thicknesses with at the same time different shapes of their distribution functions, for which a less deformed and homogeneous MYI regime was more self consistent with a FYI regime in the same region but six years later. We conclude that the parameters FWHM of a distribution function and the curvature of the tail of a distribution function more depend on the location within the TPD, e.g. locations with different degree of drift convergence, rather than on the age of the ice. For instance, the MYI thickness distribution downstream of the TPD showed a larger FWHM and a lower curvature B, indicating the presence of different types of MYI or a heavier degree of deformation.

The three pressure-ridge parameters sail height, sail spacing and number of sails per kilometer were obtained. We found that sail height is a poor parameter to estimate the mean or modal thickness within a pack since mean sail heights between a thin FYI regime in 2007 and a more than 50% thicker MYI regime in 2004 differed by only 10 %. Likewise small was the difference of modal sail spacings between the studied ice regimes, agreeing within a spacing interval of 6 and 11 m. These small modal spacing values represent the average sail spacing within a deformation zone and not the distance between two of such zones. The sail density showed different behaviour, where both mean and mode increased with transition into the convergent regime north of Fram Strait. Hence sail densities are more appropriate to describe the state of deformation of a regime than sail spacing or sail height.

To ensure the statistical reliability of our measurements standard errors of mean and mode for different profile lengths were calculated. Honoring the 12.75%-of-the-mean criterion of significance of *Wadhams* [1997] the mean thickness of all three years was achieved with an acceptable standard error. The required length of a thickness profile depends on the regional variability of ice-thickness types present in the study area and on the degree of deformation. An absolute standard error of the mean thickness of 0.2 m or below could be achieved for less deformed and homogeneous MYI and FYI regimes in 2001 and 2007 at survey lengths between 10 and 15 km and for a heavier deformed and heterogeneous MYI regime in 2004 at survey lengths of 100 km or more, indicating its larger regional variability due to the presence of different ice-thickness types. Standard errors of modal thickness remained constantly high until a sufficient profile length was reached where the error dropped abruptly to lower values. A standard error for modal thickness of 0.2 m was achieved for profile lengths of 50 km in the MYI and FYI regime of 2001 and 2007 but it remained as high as 0.6 m for 100 km long transects in the heterogeneous and deformed MYI regime in 2004. Most pressure-ridge parameters can be obtained with standard errors lower than 12.75% of the mean, except sail density. Here the standard error increased with the length of the data set in all years, indicating that deformation zones do not distribute as homogeneously as we have observed for sea-ice thickness.

Concentration of open melt ponds was estimated for each year in early August. Later in the year the melt ponds were already refrozen. We observed equal melt pond concentrations of 15% on FYI in 2007 and MYI in 2004; likely an underestimation of the true melt pond coverage. Melt ponds form preferably on ice thinner than the modal thickness. On thin first-year ice they can cause abrupt reductions of sea-ice concentration when the bottom melts through to

the underlying ocean, as we observed for the Pacific Siberian sea-ice edge in 2007.

A comparison of thermodynamically grown sea ice between the years was done by separating level-ice sections from the complete data sets. Level-ice thicknesses of the same type, i.e. FYI or MYI respectively, were normally distributed and mean and mode agreed within 10 cm. Comparison of 2007 level-ice thickness with sporadic FYI in 2001 showed a difference of -0.2m in 2007, which lies within the expected interannual variation of freezing and melting rates. Therefore, thermodynamic growth conditions within the pack seemed not to be much different in 2007 despite the minimum in extent in that summer. This is in agreement with results from *Kwok et al.* [2009] who found no negative trend of the thickness of Arctic FYI between 2003 and 2008.

Meridional gradients of level ice were found in the 2004 and 2007b data. Whereas the first gradient was caused by the advection of different ice types, the latter was a consequence of the proximate and strongly retreating ice edge. We speculate that the combination of persistent southerly winds in the TPD [*Maslanik et al.*, 2007a] [*Ogi et al.*, 2008] and anomalous high sea surface temperatures in the Pacific sector of the Arctic Ocean [*Steele et al.*, 2008] created warm on-ice winds which accelerated the formation of thaw holes on the thin FYI close to the sea ice margin. This lead to accelerated bottom melting [*Perovich et al.*, 2008] and fragmentation of the sea ice cover [*Rampal et al.*, 2009] and to a retreat of the 2007 Pacific-Siberian ice edge. Further, we conclude that sea-ice thickness in the central Arctic Ocean depends more on the surrounding sea-ice concentration than on the latitude, which in turn makes sea-ice thickness measurements in a region with low sea-ice concentration less representative for the whole region.

Some of the results presented here should be considered for future sea ice thickness activities in the Arctic and their interpretations. The fact that satisfactory small standard errors of mean and modal thickness can be obtained on relatively short transects of approximately 15 km and 50 km, at least in the central Arctic, indicates the high representativeness of airborne sea ice thickness profiles in this part of the Arctic Ocean. This can be seen as a justification for an intensified continuation of sea ice thickness monitoring using ice breaker based HEM. Taking remote sensing data or model data of age, concentration or drift of sea ice into account, thickness results from single transects may have a relevance to other regions of the Arctic, where these parameters are similar. On the contrary, in convergent ice regimes, like north of Fram Strait, we suggest not to define obtained mean thicknesses as being representative for that region, when they were recorded on a total transect length of less than 100 km. However, it is worthwhile to continue and expand HEM measurements in the Arctic in order to consolidate the presented results and to assess whether the statistical parameters in other convergent MYI regions are comparable to that of the MYI north of Fram Strait in 2004. Furthermore, laser-derived melt pond concentrations have to be validated by means of ground truthing during future field activities in the Arctic.

Acknowledgments. We thank the crew of *RV Polarstern*, the helicopter crew of *HeliService international GmbH* and all the people who helped with the measurements especially Jan Lieser and Volker Leinweber without whom these data would never have been collected. Additional funding was given by the EU project DAMOCLES. The paper was written during a visit at the University of Alberta which was funded by the German academic exchange service (DAAD). Ice-concentration data were downloaded from CERSAT/IFREMER (http://cersat.ifremer.fr/data/).

References

Bourke, R., and R. Garrett, Sea ice thickness distribution in the arctic ocean, *Cold Reg. Sci. Technol.*, *13*, 259–280, 1987.

Budéus, G., and P. Lemke, The Expeditions ARKTIS-XX/1 and ARKTIS-XX/2 of the Research Vessel "Polarstern" in 2004, *Rep. Polar Res.*, *544*, 242 PP., 2007, http://hdl.handle.net/10013/epic.10549.

Comiso, J. C., C. L. Parkinson, R. Gersten, and L. Stock, Accelerated decline in the Arctic Sea ice cover, *Geophys. Res. Lett.*, *35*, 2008.

Davis, N., and P. Wadhams, A statistical-analysis of Arctic pressure ridge morphology, *J. Geophys. Res.*, *100*, 10,915–10,925, 1995.

Eicken, H., W. Tucker, and D. Perovich, Indirect measurements of the mass balance of summer Arctic sea ice with an electromagnetic induction technique, vol. 33 of *Annals of Glaciology*, pp. 194–200, Int. Glaciological Soc., 2001.

Gerdes, R., and C. Koeberle, Comparison of Arctic sea ice thickness variability in IPCC Climate of the 20th Century experiments and in ocean - sea ice hindcasts, *J. Geophys. Res.*, *112*, 2007.

Giles, K. A., S. W. Laxon, and A. L. Ridout, Circumpolar thinning of Arctic sea ice following the 2007 record ice extent minimum, *Geophy. Res. Lett.*, *35*, 2008.

Haas, C., Late-summer sea ice thickness variability in the Arctic Transpolar Drift 1991-2001 derived from ground-based electromagnetic sounding, *Geophy. Res. Lett.*, *31*, 2004.

Haas, C., and H. Eicken, Interannual variability of summer sea ice thickness in the Siberian and central Arctic under different atmospheric circulation regimes, *J. Geophys. Res.*, *106*, 4449–4462, 2001.

Haas, C., and J. Lieser, Sea ice conditions in the transpolar drift in August/September 2001 : observations during POLARSTERN cruise ARKTIS XVII/2, *Rep. Polar Res.*, *441*, 123 PP, 2003, http://hdl.handle.net/10013/epic.10446.

Haas, C., S. Gerland, H. Eicken, and H. Miller, Comparison of sea-ice thickness measurements under summer and winter conditions in the Arctic using a small electromagnetic induction device, *Geophysics*, *62*, 749–757, 1997.

Haas, C., S. Hendricks, and M. Doble, Comparison of sea ice thickness distribution in the Lincoln Sea and adjacent Arctic Ocean in 2004 and 2005, in *Ann. Glaciol., VOL 44*, edited by Langhorne, P. and Squire, V., vol. 44 of *Ann. Glaciol.*, pp. 247–252, 2006.

Haas, C., A. Pfaffling, S. Hendricks, L. Rabenstein, J.-L. Etienne, and I. Rigor, Reduced ice thickness in Arctic Transpolar Drift favors rapid ice retreat, *Geophys. Res. Lett.*, *35*, 2008.

Haas, C., J. Lobach, S. Hendricks, L. Rabenstein, and A. Pfaffling, Helicopter-borne measurements of sea ice thickness, using a small and lightweight, digital EM system, *J. Appl. Geophys.*, *67*, 234–241, 2009.

Hendricks, S., Validierung von altimetrischen Meereisdickenmessungen mit einem helikopterbasierten elektromagnetischen Induktionsverfahren, Ph.D. thesis, University Bremen, 2009, in german.

Hibler, W., Removal of Aircraft Altitude Variation from Laser Profiles of the Arctic Ice Pack, *J. Geophys. Res.*, *77*, 7190–7195, 1972.

Hoefle, B., M. Vetter, N. Pfeifer, G. Mandlburger, and J. Stoetter, Water surface mapping from airborne laser scanning using signal intensity and elevation data, *Earth Surface Processes and Landforms*, *34*, 1635–1649, 2009.

Holland, M. M., C. M. Bitz, E. C. Hunke, W. H. Lipscomb, and J. L. Schramm, Influence of the sea ice thickness distribution on polar climate in CCSM3, *J. Climate*, *19*, 2398–2414, 2006.

Inoue, J., J. A. Curry, and J. A. Maslanik, Application of Aerosondes to melt-pond observations over Arctic Sea ice, *J. Atmos. Ocean. Tech.* , *25*, 327–334, 2008.

Kay, J., T. L'Ecuyer, A. Gettelman, G. Stephens, and C. O'Dell, The contribution of cloud and radiation anomalies to the 2007 arctic sea ice extent minimum, *Geopy. Res. Lett.*, *35*, 2008.

Kovacs, A., and J. Holladay, Sea-ice thickness measurement using a small airborne electromagnetic sounding system, *Geophysics*, *55*, 1327–1337, 1990.

Kovacs, A., J. Holladay, and C. Bergeron, The footprint altitude ratio for helicopter electromagnetic sounding of sea-ice thickness - comparison of theoretical and field estimates, *Geophysics*, *60*, 374–380, 1995.

Kwok, R., G. F. Cunningham, M. Wensnahan, I. Rigor, H. J. Zwally, and D. Yi, Thinning and volume loss of the Arctic Ocean sea ice cover: 2003-2008, *J. Geophys. Res.-Oceans*, *114*, 2009.

Lieser, J., Sea ice conditions in the northern North Atlantic in 2003 and 2004. Observations during RV POLARSTERN cruises ARKTIS XIX/1a and b and ARKTIS XX/2, *Rep. Polar Res.*, *504*, 197 PP, 2005, http://hdl.handle.net/10013/epic.10509.

Maslanik, J., S. Drobot, C. Fowler, W. Emery, and R. Barry, On the Arctic climate paradox and the continuing role of atmospheric circulation in affecting sea ice conditions, *Geophy. Res. Lett.*, *34*, 2007a.

Maslanik, J. A., C. Fowler, J. Stroeve, S. Drobot, J. Zwally, D. Yi, and W. Emery, A younger, thinner Arctic ice cover: Increased potential for rapid, extensive sea-ice loss, *Geophy. Res. Lett.*, *34*, 2007b.

McLaren, A. J., et al., Evaluation of the sea ice simulation in a new coupled atmosphere-ocean climate model (HadGEM1), *J. Geophys. Res.-Oceans*, *111*, 2006.

Meehl, G., et al., Climate change projections for the twenty-first century and climate change commitment in the CCSM3, *J. Climate*, *19*, 2597–2616, 2006.

Nghiem, S. V., I. G. Rigor, D. K. Perovich, P. Clemente-Colon, J. W. Weatherly, and G. Neumann, Rapid reduction of Arctic perennial sea ice, *Geophy. Res. Lett.*, *34*, 2007.

Ogi, M., I. G. Rigor, M. G. McPhee, and J. M. Wallace, Summer retreat of Arctic sea ice: Role of summer winds, *Geophy. Res. Lett.*, *35*, 2008.

Parkinson, C. L., and D. J. Cavalieri, Arctic sea ice variability and trends, 1979-2006, *J. Geophys. Res.-Oceans*, *113*, 2008.

Percival, D. B., D. A. Rothrock, A. S. Thorndike, and T. Gneiting, The variance of mean sea-ice thickness: Effect of long-range dependence, *J. Geophys. Res.*, *113*, 2008.

Perovich, D., T. Grenfell, J. Richter-Menge, B. Light, W. Tucker, and H. Eicken, Thin and thinner: Sea ice mass balance measurements during SHEBA, *J. Geophys. Res.-Oceans*, *108*, 2003.

Perovich, D., S. Nghiem, T. Markus, and A. Schweiger, Seasonal evolution and interannual variability of the local solar energy absorbed by the Arctic sea ice-ocean system, *J. Geophys. Res.*, *112*, 2006.

Perovich, D. K., J. A. Richter-Menge, K. F. Jones, and B. Light, Sunlight, water, and ice: Extreme Arctic sea ice melt during the summer of 2007, *Geophy. Res. Lett.*, *35*, 2008.

Peterson, I. K., S. J. Prinsenberg, and J. S. Holladay, Observations of sea ice thickness, surface roughness and ice motion in Amundsen Gulf, *J. Geophys. Res.-Oceans*, *113*, 2008.

Pfaffling, A., and J. E. Reid, Sea ice as an evaluation target for HEM modelling and inversion, *J. Appl. Geophys.*, *67*, 242–249, 2009.

Pfaffling, A., C. Haas, and J. E. Reid, Direct helicopter EM - Sea-ice thickness inversion assessed with synthetic and field data, *Geophysics*, *72*, F127–F137, 2007.

Prinsenberg, S., J. Holladay, and J. Lee, Measuring ice thickness with eisflow^{TM}, a fixed-mounted helicopter electromagnetic-laser system, *12th International Offshore and Polar Engineering Conference, Conference Proceedings*, *1*, 737–740, 2002.

Rampal, P., J. Weiss, and D. Marsan, Positive trend in the mean speed and deformation rate of Arctic sea ice, 1979-2007, *J. Geophys. Res.-Oceans*, *114*, 2009.

Reid, J., A. Pfaffling, and J. Vrbancich, Airborne electromagnetic footprints in 1D earths, *Geophysics*, *71*, G63–G72, 2006.

Rothrock, D. A., D. B. Percival, and M. Wensnahan, The decline in arctic sea-ice thickness: Separating the spatial, annual, and interannual variability in a quarter century of submarine data, *J. Geophys. Res.*, *113*, 2008.

Schauer, U., The expedition ARKTIS-XXII/2 of the research vessel "Polarstern" in 2007, *Rep. Polar Res.*, *579*, 271 PP., 2008, http://hdl.handle.net/10013/epic.30947.

Steele, M., W. Ermold, and J. Zhang, Arctic Ocean surface warming trends over the past 100 years, *Geophy. Res. Lett.*, *35*, 2008.

Stroeve, J., M. M. Holland, W. Meier, T. Scambos, and M. Serreze, Arctic sea ice decline: Faster than forecast, *Geophys. Res. Lett.*, *34*, 2007.

Thiede, J., Polarstern Arktis XVII/2 : Cruise Report: AMORE 2001 (Arctic Mid-Ocean Ridge Expedition, *Rep. Polar Res.*, *421*, 390 PP, 2002, http://hdl.handle.net/10013/epic.10426.

Thorndike, A., D. Rothrock, G. Maykut, and R. Colony, Thickness distribution of sea ice, *J. Geophys. Res.- Oc. Atm.*, *80*, 4501–4513, 1975.

Tucker, W., J. Weatherly, D. Eppler, L. Farmer, and D. Bentley, Evidence for rapid thinning of sea ice in the western Arctic Ocean at the end of the 1980s, *Geophysical Research Letters*, *28*, 2851–2854, 2001.

Wadhams, P., Ice thickness in the Arctic Ocean: The statistical reliability of experimental data, *J. Geophys. Res.-Oceans*, *102*, 27,951–27,959, 1997.

Wadhams, P., *Ice in the ocean*, Gordon and Breach Science Publishers, 2000b.

Wadhams, P., and N. Davis, Further evidence of ice thinning in the Arctic Ocean, *Geophy. Res. Lett.*, *27*, 3973–3975, 2000a.

Wadhams, P., and T. Davy, On the Spacing and Draft Distriubtions for Pressure Ridge Keels, *J. Geophys. Res.-Oceans*, *91*, 10,697–10,708, 1986.

Wadhams, P., and R. Horne, An analysis of ice profiles obtained by submarine sonar in the beaufort sea, *J. Glaciol.*, *25*, 401–424, 1980.

Warren, S., I. Rigor, N. Untersteiner, V. Radionov, N. Bryazgin, Y. Aleksandrov, and R. Colony, Snow depth on Arctic sea ice, *Journal of Climate*, *12*, 1814–1829, 1999.

Winsor, P., Arctic sea ice thickness remained constant during the 1990s, *Geophy. Res. Lett.*, *28*, 1039–1041, 2001.

Yu, Y., G. Maykut, and D. Rothrock, Changes in the thickness distribution of Arctic sea ice between 1958-1970 and 1993-1997, *J. Geophys. Res.*, *109*, 2004.

L. Rabenstein, Alfred Wegener Institute of Polar and Marine Research, Bussestr. 24, Bremerhaven, 27570, Germany. (lasse.rabenstein@awi.de)

Paper II

Noise characteristics of an electromagnetic sea-ice thickness sounder on a fixed wing airplane

Lasse Rabenstein[a], Stefan Hendricks[a], John Lobach[b], Christian Haas[c]

[a]*Alfred Wegener Institute for Polar and Marine Research, Bremerhaven, Germany*
[b]*Ferra Dynamics Inc., Mississauga, Ontario, Canda*
[c]*Department of Earth Sciences, University of Alberta, Edmonton, Alberta, Canada*

Abstract

This paper presents a feasibility study for the development of an electromagnetic sea-ice thickness instrument mounted under the wings of an airplane. It comprises test flights with a prototype instrument and 3D finite element model studies. Information is given about technical details of the prototype instrument as well as about processing steps. Corrections for drift, electromagnetic coupling of airplane and ocean, pitch and roll and wing flexure are explained. Drift is corrected on the basis of free space measurements in high altitudes and a transmitter reference signal. With a 3D finite element model study the authors quantified the effect of pitch and roll of the airplane and the electromagnetic coupling between airplane and ocean. Both effects are significantly amplified by the presence of the conducting sea water and for flight heights of 30 m over the ocean these effects can change the signal by about 10 percent or more. For highly quantitative measurements like sea-ice thickness these effects must be taken into account. The by far strongest influence on the signal has wing flexure which can be divided into an inductive and geometric contribution, both equally strong. A wing deflection of 5 degrees relative to the fuselage can cause changes larger than the wanted signal of the ocean. Most of the wing flexure signal appears on the inphase component only, henceforth the quadrature component should be taken for sea ice thickness retrieval. We conclude that a fixed wing electromagnetic instrument for the purpose of measurements in a centimetre scale should include a system to measure the relative position of the antenna coils with an accuracy of 1/10 mm, e.g. lasers pointing from the fuselage to the antennas. The better solution is to mount the antennas on the rigid fuselage and not on the wings.

Keywords: sea-ice thickness, airborne electromagnetics, 3D modelling, noise sources

1. Introduction

With a rapidly changing climate in the Polar regions the need for a long range aircraft equipped with sea-ice thickness sensors emerged. Airborne electromagnetic induction (AEM) is one alternative and was already applied during past sea ice thickness surveys. Such measurements are capable to achieve a high vertical resolution of 0.1 m (Haas et al., 2009; Pfaffling et al., 2007). Their areal coverage depends on the range of the aircraft. During past sea-ice thickness studies mostly helicopter based instruments were used, either with a towed Bird (Kovacs et al., 1987; Haas et al., 2009) or fixed on the nose of a helicopter (Prinsenberg et al., 2002). EM measurements of sea-ice thickness using a fixed-wing aircraft were done for the period of three winters (1991,1993,1994) in the Baltic Sea, with the antennas mounted on the wing tips of a Twin Otter (Multala et al., 1996). The Alfred Wegener Institute (AWI) regularly conducts geophysical and meteorological measurements from an aircraft specially designed for operations in cold regions, the "Polar 2" which is a Dornier 228 (e.g. Steinhage et al., 2001). Based on the experience from five years of successful helicopter EM sea-ice thickness measurements (e.g., Haas et al., 2006, 2008; Rabenstein et al., 2010) the development of a new EM sea-ice system for the "Polar 2" was initiated. The idea was to have an instrument available for long term sea ice thickness studies on a seasonally repeating basis. The "Polar 2" has a significantly larger range than helicopters which offers the possibility to reach even remote areas of the Arctic Ocean where e.g. thicker and older multi year ice can be found. Once constructed, this will be the first fixed wing EM system dedicated to measurements of seasonal and interannual sea ice thickness changes.

The procedure of sea ice thickness retrieval from AEM measurements is described by Pfaffling et al. (2007) and Haas et al. (2009). Basically sea ice thickness is derived by the difference of two distance measurements, a laser altimeter measures the distance to the uppermost snow or ice surface and the actual EM system estimates the distance to the underlying ocean, which can be taken as a homogeneously conductive halfspace. For a conductive halfspace the EM response, which depends on the halfspace conductivity and the height over the halfspace, can be calculated by an analytical 1D model (e,g, Ward and Hohmann, 1988). Hence, with known halfspace conductivity, the distance between instrument and halfspace can be directly derived from the EM signal strength. Whether the 1D model curve can be taken as a reference without any constraints in the case of a fixed wing antenna situation will be clarified here. For the given frequency of 1990 Hz the on average 200 times weaker sea-ice than sea-water conductivity has a neglecting influence. Classical inversion methods which are usually applied for AEM data

turned out to be less accurate than the one described here, even when they account for the sea-ice layer (Pfaffling et al., 2007). Furthermore the AEM method only resolve sea ice thickness features smaller than the footprint of the system, which is for a VCP configuration ∼1.35 times the height over the ocean (Kovacs et al., 1995).

The purpose of this study is to quantify the characteristics of a fixed wing EM system for sea ice thickness measurements including all its noise sources. The system was studied during two test flights. The first flight aimed on the accuracy of the system to measure ice thickness and the second to evaluate the effect of wing flexure. The first flight was performed in different altitudes over open ocean, where sea-ice thickness is zero and sea water conductivity known. Over open ocean the difference between laser and EM distance should be as small as possible and reflects the accuracy of the system to measure ice thickness. The second test flight was performed in high altitudes, where the ocean response signal is negligible. It included alternating descending and ascending manoeuvres in order to trigger inertia forces moving the wings up and down relative to the fuselage. In addition to the test flights the commercial Comsol-Multiphysics® 3D Finite Element (FEM) code was used to simulate the disturbing effects of the "Polar 2" with its complicated 3D geometry.

Generally EM measurements are relative measurements, where the ratio of the secondary magnetic field to the actively transmitted primary magnetic field is calculated. The secondary field emerges from induction in conductive bodies in the range of the transmitter. In this study we consider every signal emerging from induced magnetic fields in the airplane or in the ocean as secondary field signals and quote them in parts per million (ppm) of the primary field. In EM-Bird frequency domain instruments the primary signal usually is attenuated physically by a compensation coil close to the receiver so that a pure secondary field is recorded. Here we follow different approaches by either compensating the primary signal digitally during flight or by subtracting an analytically determined primary field voltage in a post flight processing step. With the post processing approach all signals emerging from the metallic airplane body are included in the secondary signal whereas the digital compensation method tries to compensate the disturbing signals from the airplane during a high altitude adjustment procedure.

Since EM measurements are sensitive to conductive bodies, the metallic airplane in the immediate proximity to the antennas certainly has an influence on the signal. Former studies by Suppala et al. (2005) dealt with the contribution of the conductive airplane to the signal of a fixed wing EM system and found that most effects can be handled by a proper calibration. Furthermore we analyse whether there is an inductive coupling between ocean and airplane. Suppala et al. (2005) found that for the fixed wing EM system of the Finish Geological Survey (GTK) a coupling between airplane and ground can be neglected for the purpose of geological mapping. Nevertheless, for sea-ice thickness measurements, which are performed over a highly conductive ocean, the coupling effect can have a significant contribution. If so, simple 1D models cannot be taken as a reference for the EM response over the ocean. Instead, measurement results have to be compared with 3D models where the conductive airplane body is included. Motivated by previous studies by Fitterman and Yin (2004) another aim is on the effect of pitch, roll and yaw in the presence of the conductive airplane on the EM signal.

The "Data & Method" chapter of this paper introduces the prototype airborne EM instrument, which was used during the test flight, with all important technical parameters and recorded data streams. Furthermore all processing steps, from raw voltage to sea-ice thickness, are explained. The section concludes with a description of the geometry and the settings of the 3D model study. In total three model studies were performed in order to quantify the effect of induced currents in the airplane body, the effect of pitch & roll and the effect of wing flexure.

The "Results" part of this paper is divided into a measurement and modelling part. In the measurement part we show the results of the two test flights and compare the results of the first flight with a theoretical 1D model. Furthermore the potential sea-ice thickness accuracy of the prototype system is presented. Finally the results of the three FEM model studies are presented.

In the "Discussion" part we compare the importance of the particular processing steps and evaluate their relative relevance for the total signal. Furthermore the applicability of the FEM results to the test flight data are discussed. The paper concludes with a short summary and suggestions for future fixed wing sea-ice thickness EM instruments.

2. Data & Methods

2.1. Instrument

The design of the fixed wing system was constraint by available hardpoints and the requirement of easy and inexpensive installation on the Dornier 228 polar airplane of the AWI. Two pylons, one under each wing, already existed on the airplane for installation of several other geophysical instruments, e.g. a ground penetrating radar (Steinhage et al., 2001). The most feasible and cost saving realisation with respect to air certification and aerodynamics was a pair of two vertical coplanar (VCP) coils mounted below each of the pylons, starboard the receiver (Rx) coil and port the transmitter (Tx) coil. The Tx-coil of a VCP configuration creates a horizontal magnetic dipole with the advantage of a weaker coupling with the horizontally oriented wings than a vertical magnetic dipole (Levaniemi et al., 2009). Further technical parameters are listed in Table 1. The signal frequency of 1990 Hz creates an ideal (maximal) response signal over a homogeneous halfspace with conductivities typical for sea-water (2.0-4.5 S/m) and at the same time its sensitivity to the sea-ice layer with typical conductivities of 10-50 mS/m can be neglected. The system itself is shown in Figure 1 together with a wiring diagram of all important electronic components. The fixed wing system uses an electrical compensation method to attenuate the primary field at the receiver coil. Such an approach was already used by e.g. Levaniemi et al. (2009) for the construction of the airborne EM system "AEM-05", operated by the British Geological Survey (BGS)

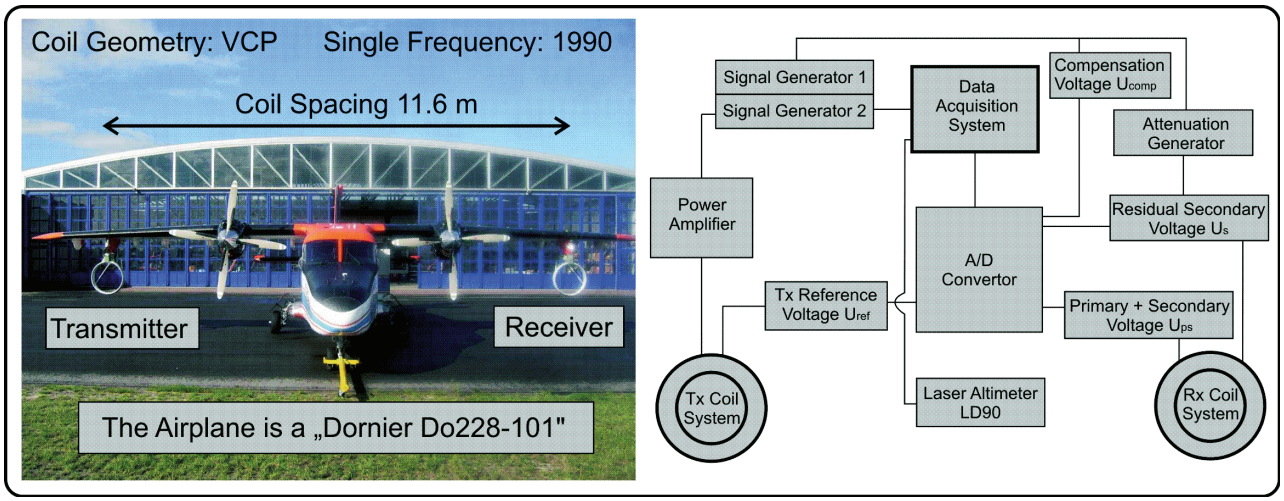

Figure 1: Technical parameters of the prototype fixed wing EM system used for the test flight over the North Sea. **Left:** The "Polar 2" with the installed EM system. **Right:** Data streams and important electronic components. Four data steams are recorded: 1. Tx reference voltag, 2. Rx Primary voltage, 3. Rx Attenuated Primary voltage, 4. Attenuation Signal

Table 1: Technical parameters of the prototype fixed wing EM system.

Altimeter	100 Hz laser altimeter
Domain	Frequency
Frequency Range	One frequency of 1990 Hz
Coil Spacing	11.6 m
Coil Configuration	Vertical Coplanar
Magnetic Moment	495 Am^2
Sampling Rate	10 Hz
Range of Dornier 228	540 to 1400 nautical miles
Operation flight height	Nominally 100 ft
Operation Speed	80 to 100 knots

and the Finish Geological Survey (GTK). In total four EM signals are recorded: The transmitter reference voltage (U_{ref}) by a single loop of wire around the Tx-coil, the compensation voltage (U_{comp}), the primary plus secondary field voltage on the receiver coil (U_{ps}) and the amplified residual secondary field voltage after compensation (U_s). The 1990 Hz voltage of each signal is estimated over a period of 100 ms by the acquisition system. There are 199 periods in each 100 ms measurement period which can be considered a form of stacking to a final sampling rate of 10 Hz. Furthermore a laser altimeter records the altitude of the airplane with an accuracy of 0.02 m. To correct for orientation effects, pitch, roll and yaw of the airplane are recorded. In addition basic meteorological data are routinely recorded during flight.

2.2. Data Processing

2.2.1. Phasing

The receiver signal is divided into two parts, one 180° out of phase with the transmitter signal (called Inphase) and another 90° out of phase with the transmitter signal (called Quadrature). This expression is alternatively to the Phase (Θ) and Amplitude (A) description of time harmonic signals. Calculation of Inphase (I) and Quadrature (Q) follows

$$I = A \cdot sin(\Theta) \quad (1)$$

$$Q = A \cdot cos(\Theta) \quad (2)$$

The relative amplitudes of I and Q depend on the conductivity and distance of the medium causing the EM response. In free space, where no conductors are present, no secondary magnetic field is induced and only voltages due to the primary field are recorded at the receiver coil. Theoretically the primary field is 100% on the I component of the receiver voltage (Telford et al., 1990, p.351). But in reality antenna coils are not perfect conductors, henceforth Q and I components are recorded. Furthermore, with the presence of the metallic airplane a true free space situation cannot be assumed anyway. However, in order to apply equations 1 and 2 Θ has to be known. Every electronic component involved in the signal recording (e.g. amplifiers, A/D converters) and the presence of the airplane body cause additional phaseshifts. To correct for these unknown shifts a pure Q-pulse is sporadically added to the transmitter voltage. During data processing, Θ is adjusted such that the Q-pulse appears on the Quadrature trace only. With these processing steps the system phase can be determined.

2.2.2. Drift Correction

The receiver signal is subject to electronic drift which mainly results from changes of the operating temperature of Tx- and Rx-coil. After a warm-up period this drift becomes weaker and more linear. At the beginning and end of each survey flight several minutes of free space signal are recorded in high altitudes of more than 300 m. The amount of drift can be estimated by comparing the free space signals from the beginning and end of the flight and a drift correction for the entire flight can be done by interpolation. To account for non linear drift behaviour a polynomial curve fit to the free space sections is used for a drift correction of the complete flight. However, a residual amount of drift remains which cannot be removed unless it is visible

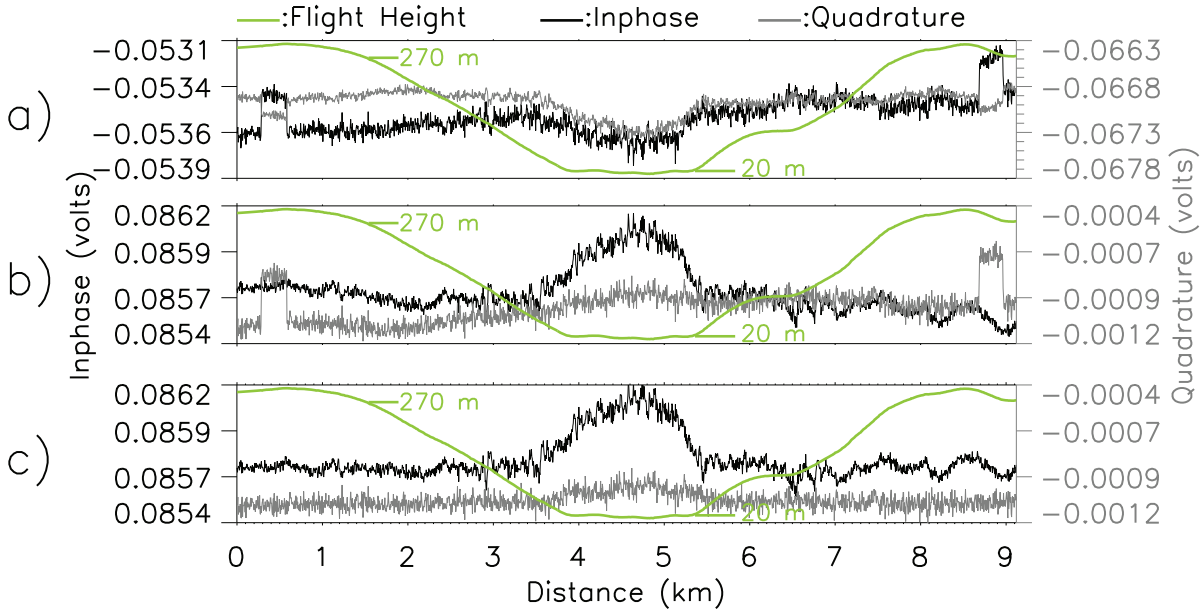

Figure 2: Inphase and Quadrature components of the attenuated Rx primary voltage taken from a test flight over the North Sea. **a.)** Raw voltage, **b.)** Phased voltage, **c.)** Drift and Tx corrected voltage

on the Tx reference signal. Under this circumstances a second drift correction on the basis of the Tx reference voltage is done, the Tx correction. The sensitivity of the single reference loop to the sea water (homogeneous conducting halfspace) is negligible and we consider the reference signal as free of any secondary EM response.

2.2.3. *Conversion to ppm*

After phasing and drift correction the raw receiver voltages are converted to relative secondary field strengths (S) in parts per million (ppm). The conversion is based on the simple formula:

$$\frac{U_{rec}}{10^6(ppm)} = \frac{U_{sec}}{S(ppm)} \tag{3}$$

where $S(ppm)$ is the secondary field signal at the receiver in parts per million of the primary field, U_{rec} is the primary plus secondary receiver voltage in free space recorded in altitudes higher than 300 m and U_{sec} is the secondary voltage either taken from the digitally compensated voltage U_s or determined by a calculated primary voltage U_{calc} (see *Introduction* for further explanation). In the following we take the calculated voltage since it includes the secondary field from the airplane. Then U_{sec} is

$$U_{sec} = U_{PS} - U_{calc} \tag{4}$$

and U_{calc} is the primary voltage which is theoretically induced in the receiver coil in free space under absence of an airplane. U_{calc} is determined using the mutual impedance approach for two loops in free space (Wait, 1955). In other frequency domain EM systems, e.g. helicopter birds, a determination of U_{calc} is not necessary since a bucking coil attenuates the primary field at the location of the receiver physically so that U_{sec} is measured directly. However, the mutual impedance approach is based on the equation:

$$U_{calc} = Z_0 * I_{Tx} \tag{5}$$

where Z_0 is the mutual impedance between transmitter and receiver coil and I_{Tx} is the current strength in the transmitter coil. Z_0 in free space is determined by (Keller and Frischknecht, 1966):

$$Z_0 = \frac{i\omega\mu_0}{4\pi d^3}(N_{Tx}\pi r_{Tx}^2)(N_{Rx}\pi r_{Rx}^2) \tag{6}$$

with ω the circular frequency, μ_0 the magnetic permeability of vacuum, N_{Tx} and N_{Rx} the number of turns of transmitter and receiver coil respectively, r_{Tx} and r_{Rx} the radius of transmitter and receiver coil and d the distance between transmitter and receiver. The transmitter current is determined by

$$I_{Tx} = U_{ref} * N_{Tx}/i\omega L_{Tx} \tag{7}$$

where U_{ref} is the voltage on the reference loop of the transmitter and L_{Tx} the inductance of the transmitter coil.

U_{calc} is smaller than U_{rec} showing that the conductive airplane body has an amplifying effect on the Rx signal. Consequently $S(ppm)$ in free space is not zero but includes the response of the airplane to the primary field. As a first approach we consider this airplane response (S_A) as a constant off set to the signal and simply subtract it from the complete trace in order to eliminate S_A but keep the ocean response S_O for the lower altitudes.

2.2.4. Pitch & Roll Correction

An Inertial Navigation System (INS) records pitch, roll and yaw of the airplane with a sampling rate of 50 Hz. Based on these data the tilted laser height h_m can be corrected for deviations from the nadir direction by a rotation operation (e.g., Fitterman and Yin, 2004):

$$\begin{pmatrix} x \\ y \\ h_c \end{pmatrix} = \mathbf{R_{pitch}}\ \mathbf{R_{roll}} \begin{pmatrix} 0 \\ 0 \\ h_m \end{pmatrix} \tag{8}$$

where h_c is the corrected laser height and $\mathbf{R}$ is the rotation matrix for roll and pitch respectively. Yaw has no influence on the laser height as the problem is symmetrical around the z-axis (=height).

The EM signal itself changes with pitch and roll too. For the half space situation over the ocean yaw again has no influence on the EM signal. To correct for the effect of roll and pitch we developed a system specific chart on the basis of the 3D FEM model results. From this chart EM correction factors can be taken for every combination of roll, pitch and height. The correction factor does not only consider the geometrical displacement of the antenna coils but it additionally takes into account the change of inductive processes in ocean and airplane under tilted conditions. The creation of the chart is explained in Chapter 3.2.2..

2.2.5. Ice thickness retrieval

As mentioned in the *Introduction* a 1D model solution of the EM response for different instrument heights over a homogeneous halfspace can be taken to derive the distance to the sea water from the ocean response signal S_O. Together with every sample of S_O a laser height h_c is recorded. When I and Q of S_O are plotted versus h_c and as long as there is open water under the instrument all data points lie on the respective model curves following an exponential decrease with increasing laser height. When sea ice is present a S_O versus h_c data point do not lie on the model curve any longer. Instead, for a given laser height a smaller S_O is measured. The 1D model curve indicate the true height over the ocean halfspace h_{em} for a given S_O. This height is subtracted from the corresponding laser height which results in ice thickness. However, as described in the *Results* section the 1D model curve is better replaced by a model curve from more complex 3D FEM model.

2.3. Finite Element Model Study

2.3.1. Model Description

For the FEM models the commercial software package Comsol-Multiphysics® was used. All model parameters are shown in Figure 3. The geometry of the FEM model consists of two homogeneous half spaces, the upper one with a conductivity of 0 S/m and the lower one with a sea-water conductivity of 4.2 S/m. Two vertical coils, representing transmitter and receiver, were placed under the two wings of a solid airplane model, which was designed to resemble the geometry of the "Polar2" as good as possible. The aeroplane conductivity was set to the conductivity of Aluminium which is $3.77 \cdot 10^7$ S/m.

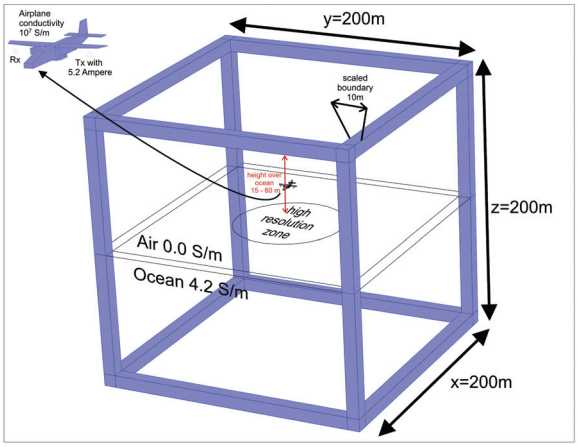

Figure 3: The geometry of the 3D FEM model. The center of the "Polar 2" is placed at x=0, y=0 and at z values between 15 m and 60 m. Below the airplane the resolution of the FE mesh of the conducting halfspace is increased, to account for the higher flux density and stronger gradients. The geometry of the airplane resembles the geometry of a "Do 228-101" as good as possible.

For the given frequency of 1990 Hz this results in a skin depth of below one centimetre. Therefore model results with a solid airplane do not differ from those with a hollow airplane and furthermore the solid airplane solution needs less computing time. The outer boundaries of the model geometry consist of zones were the spatial coordinates are scaled to very large distances in order to simulate an infinite space and to suppress boundary effects (*mapped infinite elements (COMSOL, 2006)*).

The complete problem can be solved for a quasi static case, i.e. displacement currents generally can be neglected. The prerequisite for the quasi static case is a wavelength of the transmitter signal much larger than the dimension of the structures involved. With a frequency of 1990 Hz we obtain a wavelength of approximately 150 km. The model code obtains the magnetic vector potential $\mathbf{A}$ on every gridpoint by solving the following equation:

$$(i\omega\sigma - \omega^2\epsilon_0\epsilon_r)\mathbf{A} + \nabla \times (\mu_0^{-1}\mu_r^{-1}\nabla \times \mathbf{A}) = \mathbf{J} \tag{9}$$

where σ is the electrical conductivity, ϵ_0 the electrical permittivity of vacuum and $\mathbf{J}$ an externally generated current. ϵ_r and μ_r are the relative electrical permittivity and the relative magnetic permeability and are both set to one, with the consequence that the involved structures in the model are neither polarisable nor magnetisable. The magnetic vector potential relates to the magnetic field $\mathbf{B}$ by

$$\mathbf{B} = \nabla \times \mathbf{A}. \tag{10}$$

The Tx-coil is represented by a rectangular wire in the yz-plane with a current I of 5.2 Ampere flowing through it. The receiver (Rx) is defined as a rectangle parallel to Tx with the same dimension. The magnetic flux $\mathbf{\Phi}$ within Rx is determined by the numerical integration of $\mathbf{B}$ over the area A_{Rx} enclosed by the receiver:

$$\mathbf{\Phi} = \int_{A_{Rx}} \mathbf{B} \cdot d\mathbf{a} \tag{11}$$

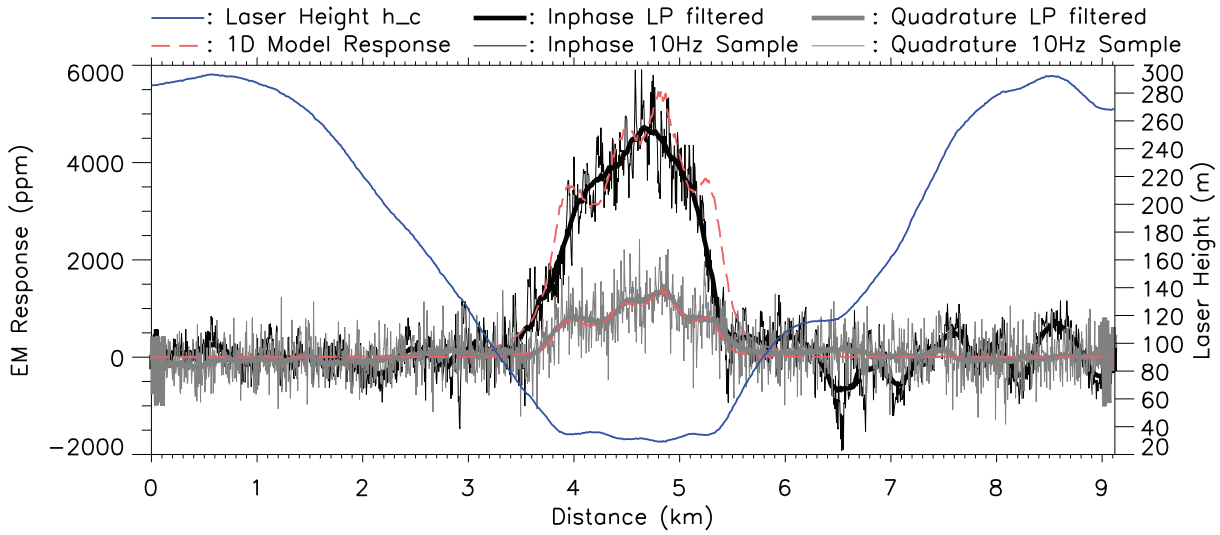

Figure 4: Results of the test flight over the North Sea. For altitudes lower than 50m the response from the ocean half space is detectable. The inphase (black) component causes a stronger response than the quadrature (grey) component. The quadrature component is in better agreement with the theoretical ocean response based on a 1D model.

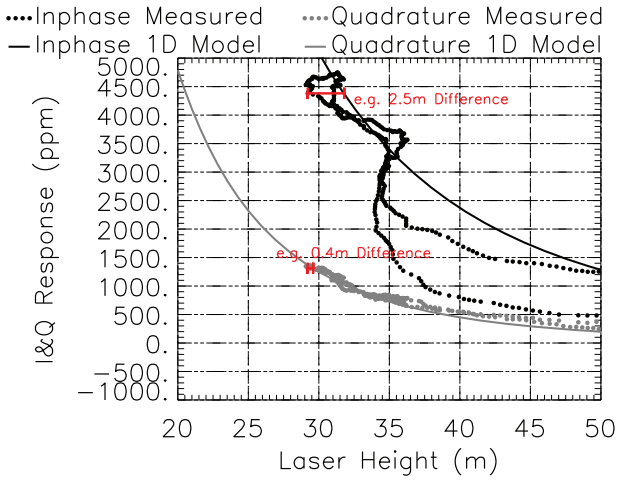

Figure 5: Inphase and quadrature response versus laser height together with 1D model curves. The distance between each sample and the model curve along the x-axis reflects the achievable sea-ice thickness accuracy. For the ideal case (noise free) all data points should lie on the respective model curves. The inphase component deviates strongly due to heavy noise which is particular pronounced when the airplane is descending or climbing (here for the altitude range 35-50 m).

where $d\mathbf{a}$ is the unit vector normal to A_{Rx}.

In total we performed three different model experiments to study the effects of:

1. induction in the airplane body
2. pitch and roll
3. wing deflection

on the EM signal measured by Rx. Every experiment was conducted under four different settings and different flight heights. One setting without ocean and airplane and the output signal S_P (The term S for signal corresponds to the flux density Φ from equation 11), a second setting without an airplane and the output signal S_{PO} (PO for primary and ocean) , a third without an ocean and the output signal S_{PA} and a fourth with all elements shown in Figure 3 switched on and the output signal S_{POA}. The four different settings are necessary in order to determine the different contributions to the EM signal S_{POA} separately: The primary field S_P, the ocean response S_O, the contribution of the airplane S_A and the signal contributing from the coupled airplane-ocean system together S_{AO} which is identical to S in equation 3.

3. Results

3.1. Test Flights

3.1.1. Accuracy Test

In order to examine the system performance under flight conditions several test flights were done over the North Sea in fall 2006. Figure 4 shows results of a flight which started in 300 m height, descended down to 20 m and climbed back again to 300 m. In this way the systems agreement with the calculated response for different flying heights can be evaluated. The sea water conductivity in the study region was measured at the same time by the research ship 'RV Heincke' and amounted to 4.2 S/m. Furthermore open water is a good validation target since ice thickness is zero and henceforth laser height and EM derived height must agree. All processing steps described in chapter 2.2. were applied on these data. In particular the data were corrected for the constant offset caused by the S_A signal. Following equation 3 the amplitude of S_A was in the order of 35,000 ppm. Significant Inphase and Quadrature signal from the ocean emerged for altitudes below 50 m. The 10 Hz signal

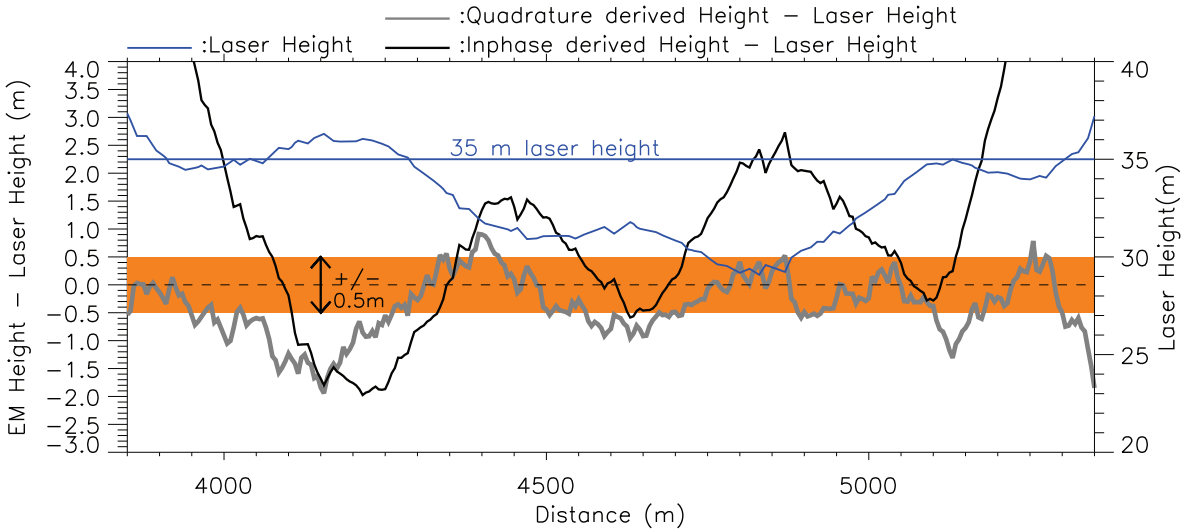

Figure 6: Difference between laser height and EM derived height versus distance for the inphase (black) and quadrature (grey) component. The orange area marks the zone of ±50*cm* accuracy. Only the quadrature derived height is within this accuracy range, but only for flight altitudes below 35m.

is very noisy with signals of on average +/- 500 ppm probably caused by high frequency vibration of the antenna coils. This vibration noise is also present when the airplane is on ground with the engines switched on and is normally distributed. It can be reduced by applying a low pass (LP) filter which also leads to a loss of horizontal resolution. As LP filter a 10 point running window was used. After the averaging filter was applied the Quadrature trace is in good agreement with the 1D model curve, deviating by less than ±20 ppm. In contrast the Inphase trace is subject to variations which are not directly caused by changes in altitude. Possible reasons are pitch & roll of the airplane, wing flexure and/or EM coupling between airplane and ocean. These were examined by the detailed finite-element model study.

In Figure 5 I and Q are plotted against laser height together with the 1D model curve. The deviation of each sample from the model curve along the x-axis is a measure for the accuracy of the system. The data shown in Figure 5 were transferred into ice thickness (which should be zero) as described in section 2.2.5., by the difference between laser height and EM height. The results for the low altitude part of the test flight is shown in Figure 6. Despite its weaker response the Q signal agrees better with the model curve because it is less affected by the disturbing signals mentioned above. However, for a distance of 1.5 km a vertical accuracy of +/- 0.5 m was reached (marked by the orange zone in Fig. 6). This can be considered as the maximum achievable accuracy for the prototype ice thickness system used during the test flights. Furhtermore, these results suggest that a minimum flight height of 35 m is required but even lower flight heights are recommended since the EM response increases exponentially with height and the vertical accuracy should be better than ±0.1 m .

3.1.2. Wing Flexure Test

A second test flight was performed in altitudes of 630 m and aimed on the signal emerging from wing flexure. Up and down flight manoeuvres caused the elastic wings to deflect strongly due to upward and downward directed inertia forces. The inphase and quadrature response for this flight are shown in Figure 7. A strong signal of approximately ±7000 ppm could be detected on the inphase component whereas the quadrature component is almost unaffected. Since the wing positions, and therewith the antenna positions, are not recorded, we further examined the wing flexure effect during the 3D FEM model study.

3.2. 3D Modeling

3.2.1. Induction in the Airplane

In the first model experiment S_O, S_A and S_{AO} were calculated to fully explain all contributions to S_{AO} resulting from induction processes in the airplane body. Our first assumption was that the airplane causes a constant signal independently of the height over the ocean. If this is true, a simple subtraction of S_A from the signal measured in free space would remove the airplane effect. In order to verify this assumption several model runs were performed where the height of the airplane over the ocean changed between 15m and 60m in steps of 2.5m (see Fig. 3). The following equations were used to calculate the response signals in ppm from the model output, where all signals S are taken in their complex form:

$$S_O = \frac{(S_{PO} - S_P) \cdot 10^6}{S_P} \tag{12}$$

$$S_A = \frac{(S_{PA} - S_P) \cdot 10^6}{S_P} \tag{13}$$

$$S_{AO} = \frac{(S_{POA} - S_P) \cdot 10^6}{S_P} \tag{14}$$

S_A amounted to a constant signal of $33,260 \pm 160$ ppm on the inphase and 71 ± 3 ppm on the quadrature where the ± values are related to the numerical accuracy. The much larger inphase response on S_A results from the high conductivity of the airplane

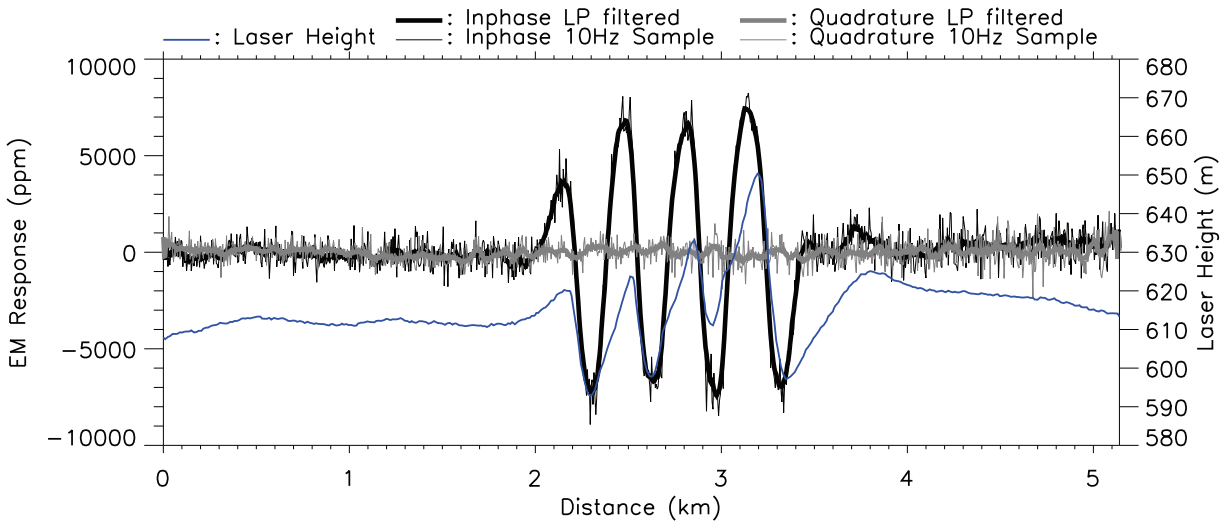

Figure 7: Results of a second test flight with strong up and down manoeuvres in high altitudes. The signal change is primarily on the inphase component and most probably caused by wing deflection

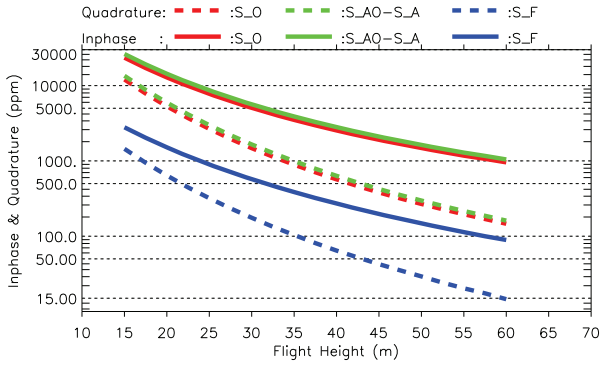

Figure 8: Ocean response without airplane (S_0, red), with airplane ($S_{A0} - S_A$, green) and the difference (S_F,blue) which is the ocean response solely caused by induction currents in the airplane body.

body of $3.77 \cdot 10^7$ S/m causing only a small phase shift relative to S_P. When S_A is constant, it can be removed by subtraction from S_{AO} but surprisingly we found

$$S_{AO} - S_A = S_O + S_F \tag{15}$$

where S_F is the signal caused by a coupling between airplane and ocean. Both, S_O and S_F depend on the height over the ocean. In Figure 8 S_O, S_F and $S_{AO} - S_A$ are plotted. For a typical flight height of 35m S_F amounts to 373 ppm on the inphase and 100 ppm on the quadrature component.

3.2.2. Pitch & Roll

The second model experiment estimated the effect of variable pitch and roll on S_{AO}. For this purpose the conducting halfspace was tilted instead of the airplane (see Fig.9a). The advantage of this approach is that the calculation of **B** at Rx is limited to the easier calculation of $\mathbf{B_x}$. The roll and pitch angle in the model varied between 0 and 17 degrees. During test flights usual pitch and roll angles of ±7 degrees emerged with extreme values of ±15 degrees. Following the study of Fitterman and Yin (2004) we introduce the response ratio R which is the ratio of S_{AO} when pitch and roll is present to S_{AO} when pitch and roll is zero:

$$R(pitch, roll) = \frac{S_{AO}(pitch, roll)}{S_{AO}(0,0)} \tag{16}$$

In Figure 9b R is plotted for a constant flight height of 30m. Obviously pitch has a much stronger effect than roll for the VCP configuration, since roll does not change the orientation of the diploe axis relative to the ocean which is in agreement with the analytical results of Fitterman and Yin (2004). For a HCP configuration both, pitch and roll, would change the axis of the magnetic dipole relative to the ocean and consequently both would affect S_{AO}. With increasing pitch I and Q of S_{AO} both get weaker by for instance 7% and 9% for typical roll and pitch values of 5 degrees. Extremer pitch and roll of 10 degrees occur during ascending, descending or curve manoeuvres, which decrease S_{AO} by about 20% and 15%. These sections are normally cut out from the data set.

For the further construction of a correction chart, roll is neglected and set to zero due to its minor influence. Instead we examined the pitch effect on inphase and quadrature for different heights between 15m and 60m. R is shown for different heights and pitch angles in Figure 9c, which is identical to the correction chart for data processing. For usual pitch angles and flight heights of 25-40m a maximum change of 10% and 13% can be expected for the inphase and quadrature components respectively.

3.2.3. Wing Deflection

In the third model experiment the influence of wing deflection on S_P, S_A and S_O was examined for two different flight heights, 60m and 30m. For both heights 11 model runs, with 11

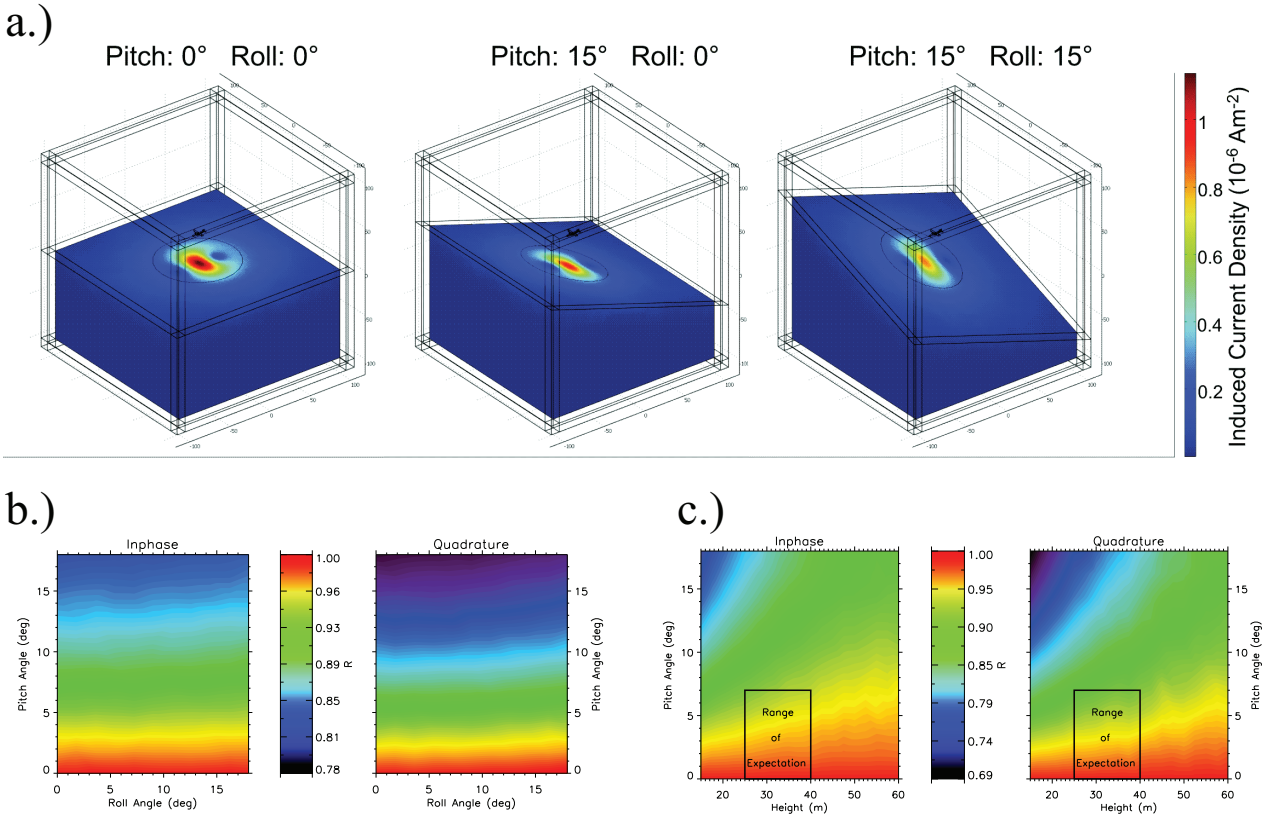

Figure 9: **a.)** Pitch and Roll were simulated by tilting the entire halfspace. The graphs show a weaker induced current density under pitched conditions. **b.)** R plotted over pitch and roll. The effect of pitch dominates over roll for the VCP coil configuration used here. **c.)** R plotted over pitch and height. Range of expectation marks the pitch and height range occurred during the test flight.

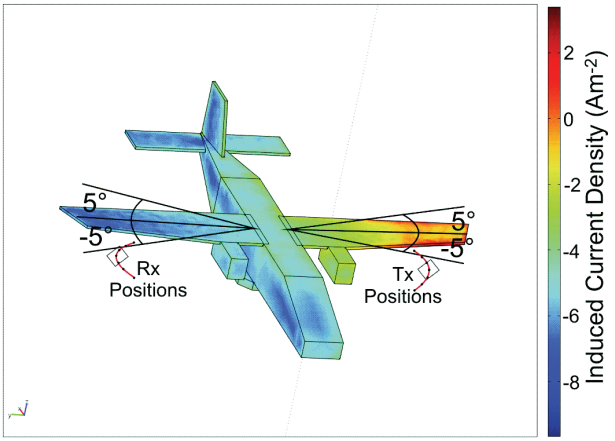

Figure 10: Wing deflections were simulated by a change of the angle between fuselage and wings by up to ±5°. The positions of transmitter and receiver were adjusted accordingly. Colours indicate the induced current density.

different airplane models, were calculated. The airplane models differed in the angle between wings and fuselage within a range of ±5 degrees (Figure 10). The position of the coils were modified accordingly.

In Figure 11 S_P, S_O and S_A are plotted versus deflection angle for both flight heights. From all contributions to the EM signal presented so far, wing deflection has the highest potential to disturb the signal. The inphase component of S_P changes by up to 10,000 ppm just because of the change in system geometry, particularly in the antenna separation distance (d) which influences the signal with d^{-3} (see equation 6). Of the same order of magnitude is the change in the inphase component of S_A (-3500 to 7800 ppm), which can only be attributed to changing induction currents in the airplane body. The influence on the quadrature component of S_A is negligible. Closer to the ocean (30m) even S_O changes with wing deflection, due to an effective height change of the antennas over the ocean halfspace. The change of S_O ranges between -250 ppm and +150 ppm for maximum deflection angles of ±5 degrees.

4. Discussion

A low signal to noise ratio is of special importance for quantitative and high resolution AEM measurements like sea-ice thickness sounding. Here we have shown and quantified noise sources appearing for a fixed wing system over a homogeneous halfspace. Even after a series of standard processing steps of phase-, drift-, pitch- and roll correction, conversion to ppm and low pass filtering residual unwanted signals remain. By means of 3D FEM modelling we quantified three processes contributing to this residual noise. In particular this was the additional

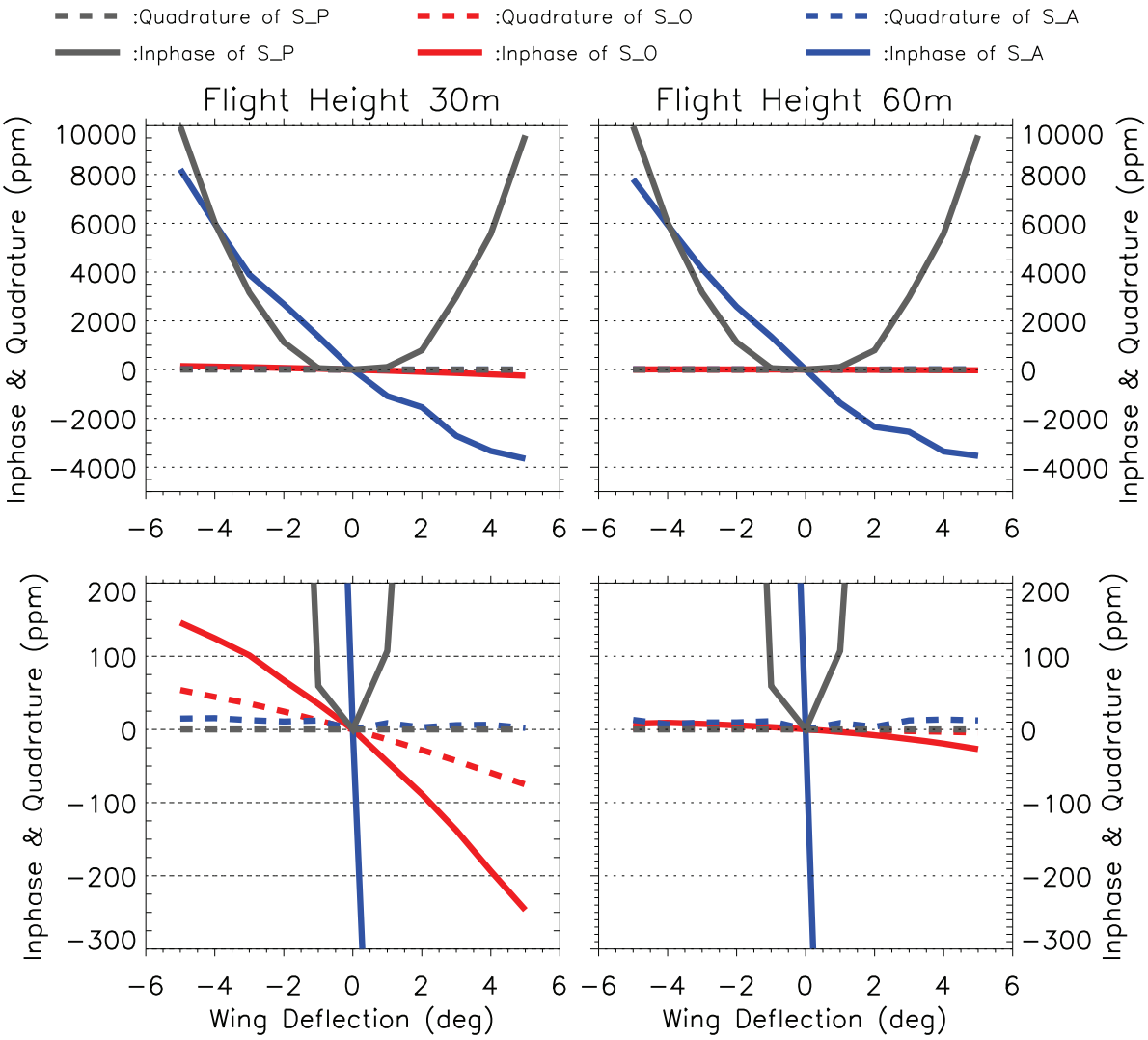

Figure 11: Plotted is the signal change versus wing deflection. The upper two and lower two images show the same curves for different ppm ranges. The primary signal (S_P) changes due to reduced antenna separation distance by up to 10,000 ppm. The changed geometry of wings and antennas produces a significantly different airplane signal (S_A) between -4000 and +8000 ppm. Note that for small angles the change in S_A is even larger than the change in S_P. For the 30m altitude situation a change in the ocean response (S_O) is noticeable primarily caused by a reduced or increased distance of the antennas to the ocean.

ocean response caused by induction currents in wings and fuselage, pitch movement and wing deflection in presence of an airplane over a good conducting halfspace. The first two noise sources could be addressed during data processing whereas wing-deflection noise cannot be corrected since the relative position of antenna coils and wings are not recorded. From this three noise sources the by far strongest contribution comes from wing deflection.

In Figure 12, all processing steps applied to the test data set (the one shown in Figure 4) are evaluated by comparing the difference between FEM model result and measured data after each processing step (Figure 12). The biggest improvement is obtained by the basic drift correction (difference between green and red in Fig.12) showing that in real systems drift has an enormous contribution to the signal. However, the improvement of the corrected signal shows that the majority of the drift can be corrected by a first drift correction as explained in chapter 2.2.2., but certainly a non linear and short term drift component during the time of measurement in low altitudes remains, which is hard or even impossible to correct for unless the same residual drift appears on the reference trace of the transmitter. Under this circumstances a further improvement can be achieved by a Tx reference voltage correction (difference between red and blue (overlayed with grey) in Fig.12). The smallest improvement of the signal is obtained by a pitch (maximum pitch was 7°) correction of the laser height (chapter 2.2.5) and the EM signal (chapter 3.2.2.) which changes the signal by about a maximum of 35 ppm and 75 ppm for the quadrature and inphase respectively. Thus pitch (and also roll for a HCP configuration) is of importance for accurate thickness measurements, but

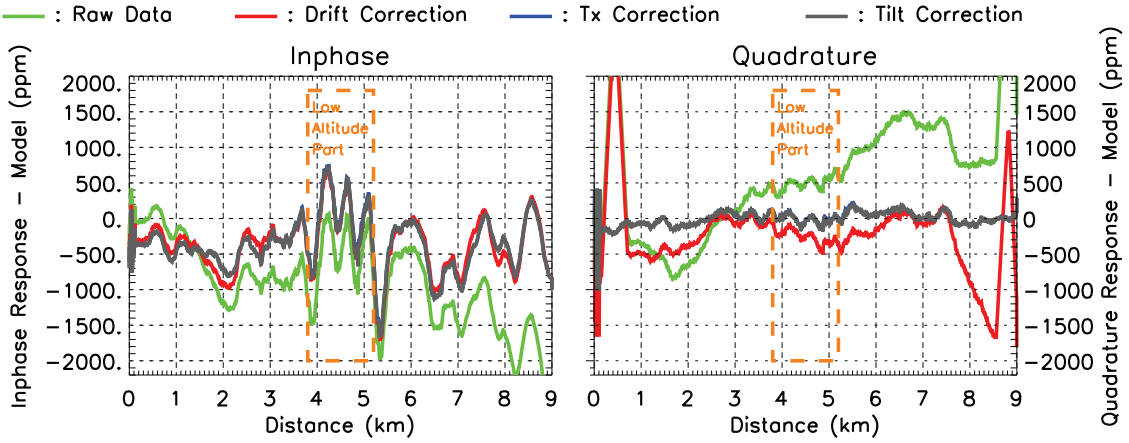

Figure 12: Shown is the difference between the model curve obtained by the FE models (without wing deflection) and the test flight data for the raw case (green), after drift correction (red), after Tx correction (blue) and after pitch correction (grey). The residual noise is caused by wing deflection and non linear drift components.

for a fixed wing system it has a minor effect in comparison to wing deflection. The residual noise (grey in Figure 12) can be assigned to wing deflection and or nonlinear drift components caused by e.g. sensitivity of involved electronic components to temperature changes and air pressure changes.

For the prototype system used in this study wing deflection and/or the relative position of the antenna coils were not recorded. But the second test flight in high altitudes of 630 m supports the wing deflection results from the FE model study 7. In agreement with Figure 11 the wing deflection signal of approximately ±7000 ppm is primarily on the inphase component. The inphase signal change is positive and negative which justifies two conclusions. The first conclusion is that the in-flight wing position and therefore the antenna separation distance differs to the situation on ground even during calm flight conditions with the consequence that deflection in one direction increases the antenna distance and deflection in the other direction decreases the antenna distance. In Figure 11 S_P can only be positive because the antenna separation distance always becomes smaller when we assume the horizontal wing position as the neutral one. The second conclusion is, that wing deflection is below ±2 degrees where S_A has a stronger contribution than S_P. This conclusion is in contradiction to the symmetry of the positive and negative ppm amplitude in Figure 7 because $S_P + S_A$ is not symmetric around the neutral wing position (Fig.11). However, since the in flight antenna position could not be measured, a direct comparison between model results and real data is difficult. But the general comparison of both results show an agreement in the occurring signal magnitudes.

Another interesting point is, why wing deflection influences the inphase component of S_A much stronger than the quadrature component. The answer is given by the following formula in combination with the high conductivity of the aircraft (in the FE model set to $3.77 \cdot 10^7$)(Telford et al., 1990, p.351):

$$\theta_P - \theta_S = \left(\frac{\pi}{2} + tan^{-1}\frac{\omega L_S}{\rho_s}\right) = \left(\frac{\pi}{2} + \phi\right) \quad (17)$$

where θ is the phase of the primary and secondary field respectively and L_S and ρ_S are inductance and resistance of the conductor causing the EM response (in this case the airplane body and/or the ocean halfspace). With a high conductivity (i.e. low resistance) $\omega L_s/\rho_S \rightarrow \infty$ and $\phi \rightarrow \pi/2$ and therefore the overall phaseshift is 180° relative to the primary field i.e. for a perfect conductor all the signal is on the inphase component.

5. Concluding Remarks and Outlook

In this study we quantified the biggest noise contributors occurring with an airplane based frequency domain electromagnetic instrument with the receiver and antenna coils fixed under the wings. Two test flights with a prototype instrument and three finite-element 3D modelling studies were performed. The situation was that of vertical coplanar antenna coils over a conducting homogeneous halfspace in presence of a highly conductive airplane body. The maximun achievable sea-ice thickness accuracy was ±0.5m using the quadrature component. The inphase component is more sensitive to changes in antenna distance and to induction currents in the airplane body and therefore it is less suitable for ice thickness retrieval than the quadrature component (at least for the prototype instrument used here) even when the inphase ocean response is stronger than the quadrature response. The results of this paper are important for the construction and usage of future AEM sea-ice thickness instruments whenever the antennas are mounted close to the body of the aircraft. For the sea-ice application the effects are particularly strong due to mutual induction in the conducting ocean half space but certainly the described effects also influence other quantitative AEM measurements, e.g. all free space effects are of similar importance independently of the measurement target. Finally we suggest that a fixed wing EM sea-ice thickness sounder should not be operated without an adequate measurement of the relative coil position, e.g. by a laser distance meter pointing from the fuselage to the anten-

nas. In order to achieve an ice thickness accuracy of ±0.1 m the antenna separation distance should be measured with an accuracy of more than 1/10 mm. As a conclusion of this study we suggest to mount antennas for such highly quantitative EM measurements on the more rigid fuselage and not on the wings.

Acknowledgements

This work got additional funding by the EU project DAMOCLES, a contribution to the International Polar Year 2007-2008. Furthermore we thank all involved companies and institutions, in particular 'Optimare Sensorsyteme AG' for the technical support and the handling of the licensing procedure, 'Deutsches Zentrum für Luft- und Raumfahrt' (DLR) for the operation of the *Polar2* and 'Leichtwerk AG' for the construction of the outer antenna shells. Furthermore we are indebted to the following persons: Thomas Garbrecht and ... from Optimare AG, Stefan Seydel, Andreas Hahn and Hans Juergen Berns from DLR and finally Andreas Herber for the support from the AWI logistics. Without any of these persons the test flights would never have been successfully conducted.

References

COMSOL, 2006. Comsol Multiphysics, Manual AC/DC Module: Users Guide.

Fitterman, D., Yin, C., Sep-Oct 2004. Effect of bird maneuver on frequency-domain helicopter EM response. Geophysics 69 (5), 1203–1215.

Haas, C., Hendricks, S., Doble, M., 2006. Comparison of sea ice thickness distribution in the Lincoln Sea and adjacent Arctic Ocean in 2004 and 2005. In: Langhorne, P. and Squire, V. (Ed.), Ann. Glaciol. Vol. 44 of Ann. Glaciol. pp. 247–252.

Haas, C., Lobach, J., Hendricks, S., Rabenstein, L., Pfaffling, A., Mar 2009. Helicopter-borne measurements of sea ice thickness, using a small and lightweight, digital EM system. J. Appl. Geophys. 67 (3, Sp. Iss. SI), 234–241.

Haas, C., Pfaffling, A., Hendricks, S., Rabenstein, L., Etienne, J.-L., Rigor, I., SEP 3 2008. Reduced ice thickness in Arctic Transpolar Drift favors rapid ice retreat. Geophys. Res. Lett. 35 (17).

Keller, G., Frischknecht, F., 1966. Electrical methods in geophysical prospecting. Oxford Pergamon Press.

Kovacs, A., Holladay, J., Bergeron, C., MAR-APR 1995. The footprint altitude ratio for helicopter electromagnetic sounding of sea-ice thickness - comparison of theoretical and field estimates. Geophysics 60 (2), 374–380.

Kovacs, A., Valleau, N., Holladay, J., OCT 1987. Airborne electromagnetic sounding of sea ice thickness and sub-ice bathymetry. Cold Reg. Sci. Technol. 14 (3), 289–311.

Levaniemi, H., Beamish, D., Hautaniemi, H., Kurimo, M., Suppala, I., Vironmaki, J., Cuss, R. J., Lahti, M., Tartaras, E., March 2009. The JAC airborne EM system: AEM-05. Journal of Applied Geophysics 67 (3, Sp. Iss. SI), 219–233.

Multala, J., Hautaniemi, H., Oksama, M., Lepparanta, M., Haapala, J., Herlevi, A., Riska, K., Lensu, M., Dec 1996. An airborne electromagnetic system on a fixed wing aircraft for sea ice thickness mapping. Cold Regions Science and Technology 24 (4), 355–373.

Pfaffling, A., Haas, C., Reid, J. E., Jul-Aug 2007. Direct helicopter EM - Sea-ice thickness inversion assessed with synthetic and field data. Geophysics 72 (4), F127–F137.

Prinsenberg, S., Holladay, J., Lee, J., 2002. Measuring ice thickness with eisflow^{TM}, a fixed-mounted helicopter electromagnetic-laser system. 12th International Offshore and Polar Engineering Conference, Conference Proceedings 1, 737–740.

Rabenstein, L., Hendricks, S., Martin, T., Haas, C., 2010. Thickness and surface-properties of different sea-ice regimes within the Arctic Trans Polar Drift: Data from summers 2001, 2004 and 2007. J. Geophys. Res. , in press.

Steinhage, D., Nixdorf, U., Meyer, U., Miller, H., Jul 2001. Subglacial topography and internal structure of central and western Dronning Maud Land, Antarctica, determined from airborne radio echo sounding. Journal of Applied Geophysics 47 (3-4), 183–189.

Suppala, I., Oksama, M., Hongisto, H. in Airo, M. E., 2005. Gtk airborne em system: characteristics and interpretation guidelines. Geological Survey of Finland, Special paper 39, 103–118.

Telford, W., Geldart, L., Sheriff, R., 1990. Applied Geophysics, 2nd Edition. Vol. 2. Cambridge University Press, Cambridge, iSBN 0-521-33938-3.

Wait, J., July 1955. Mutual electromagnetic coupling of loops over a homogeneous ground. Geophysics 20 (3), 630–637.

Ward, S., Hohmann, G.W. in Nabighian, M. E., 1988. Electromagnetic theory for geophysical applications., 1st Edition. Vol. 1 of Electromagnetic methods in applied geophysics. Society of Exploration Geophysicists, iSBN 1-56080-069-0.

Paper III

Journal of Applied Geophysics 67 (2009) 234–241

Contents lists available at ScienceDirect

Journal of Applied Geophysics

journal homepage: www.elsevier.com/locate/jappgeo

Helicopter-borne measurements of sea ice thickness, using a small and lightweight, digital EM system

Christian Haas [a,1,*], John Lobach [b], Stefan Hendricks [a], Lasse Rabenstein [a], Andreas Pfaffling [a,2]

[a] Alfred Wegener Institute for Polar and Marine Research, Bussestrasse 24, D-27570 Bremerhaven, Germany
[b] Ferra Dynamics Inc., 4070 Powderhorn Cres., Mississauga, Ontario, Canada L5L 3B9

ARTICLE INFO

Article history:
Received 13 March 2007
Accepted 26 May 2008

Keywords:
Sea ice thickness
Frequency-domain electromagnetics (EM)
Helicopter EM (HEM) bird

ABSTRACT

Sea ice is an important climate variable and is also an obstacle for marine operations in polar regions. We have developed a small and lightweight, digitally operated frequency-domain electromagnetic-induction (EM) system, a so-called EM bird, dedicated for measurements of sea ice thickness. It is 3.5 m long and weighs only 105 kg, and can therefore easily be shipped to remote places and operated from icebreakers and small helicopters. Here, we describe the technical design of the bird operating at two frequencies of $f1 = 3.68$ kHz and $f2 = 112$ kHz, and study its technical performance. On average, noise amounts to ±8.5 ppm and ±17.5 ppm for $f1$ and $f2$, respectively. Electrical drift amounts to 200 ppm/h and 2000 ppm/h for $f1$ and $f2$, during the first 0.5 h of operation. It is reduced by 75% after 2 h. Calibration of the Inphase and Quadrature ppm signals varies by 2 to 3%. A sensitivity study shows that all these signal variations do affect the accuracy of the ice thickness retrieval, but that it remains better than ±0.1 m over level ice in most cases. This accuracy is also confirmed by means of comparisons of the helicopter EM data with other thickness measurements. The paper also presents the ice thickness retrieval from single-component Inphase data of $f1$.

1. Introduction

Sea ice forms at the surface of polar waters due to cooling by low air temperatures. In September, during the peak of the Southern Hemisphere winter, sea ice covers approximately 10% of the world ocean surface. In spite of its large coverage, the thickness of sea ice ranges only between a few decimetres to a couple of meters. Locally, however, in pressure ridges, ice thickness can amount to more than 50 m as a result of rafting and ridging (Wadhams, 2000). As sea ice forms by thermodynamic processes, its thickness depends primarily on the surface energy balance, which is largely determined by air temperature, short- and long-wave radiation, winds, and ocean heat flux (Maykut, 1986). However, sea ice also moves as a consequence of forces exerted by winds and ocean currents. Therefore, pressure ridges of piled ice blocks above and under the ice form by rafting and ridging in regions of convergent ice drift. Consequently, sea ice floes in a given region are composed of larger areas of level ice with confined regions of pressure ridges in between, and the sea ice thickness distribution is usually characterised by a strong mode representing the thickness and fractional coverage of level ice and a long tail towards larger thicknesses contributed by deformed ice (Haas, 2003, and Fig. 8 below).

Due to its bright surface and snow cover, sea ice plays an important role in the global radiation balance and climate. The ice-albedo-feedback describes the accelerated warming and melting of ice as a consequence of small reductions in sea ice coverage (e.g. Hall, 2004). When sea ice retreats, more dark ocean area is exposed to the surface, thus enhancing absorption of solar radiation and subsequent warming of surface water. This in turn will increase the melting of sea ice, thus contributing to a positive feedback of sea ice retreat.

As most sea salt is expelled from the ice matrix during sea ice formation, sea ice also contributes to the densification of surface sea water, which leads to convection and enhances thermohaline ocean circulation. On the opposite end, when sea ice melts, fresh water is released into the ocean, leading to a more stable stratification.

The development of sea ice is therefore critically observed in the context of global climate change, and sea ice is considered as a climate indicator. Recently, sea ice coverage has strongly decreased in the northern hemisphere, in summer and winter (Meier et al., 2005; Stroeve et al., 2005). However, little is known about ice thickness changes.

The role of sea ice and its thickness is also important for offshore operations and shipping. Sea ice occurs every winter e.g. in the Sea of Okhotsk, Baltic and Caspian Seas, and Gulf of St. Lawrence. In these regions sea ice thickness information is of fundamental importance for

* Corresponding author. Present address: Department of Earth and Atmospheric Sciences, University of Alberta, 1-26 ESB, Edmonton, Alberta, Canada T6G 2E3. Tel.: +1 780 492 8171; fax: +1 780 492 2030.
E-mail addresses: Christian.Haas@ualberta.ca (C. Haas), shendricks@awi.de (S. Hendricks), lrabenstein@awi.de (L. Rabenstein), andreas.pfaffling@ngi.no (A. Pfaffling).
[1] Present address: Department of Earth and Atmospheric Sciences, University of Alberta, 1-26 ESB, Edmonton, Alberta, Canada T6G 2E3.
[2] Present address: Norwegian Geotechnical Institute (NGI), PO Box 3930 Ullevaal Stadion, NO-0806 Oslo, Norway.

0926-9851/$ – see front matter.
doi:10.1016/j.jappgeo.2008.05.005

operational purposes and marine safety as well as for the design of ships, offshore structures, and port facilities.

While sea ice area and extent have been well observed by satellites for more than 30 years, ice thickness is still poorly observed. Most observations come from military nuclear submarine operations or from scientific ocean moorings, where ice thickness has been measured by means of upward-looking sonar (Rothrock et al., 1999; Wadhams, 2000; Haas, 2003). Only since the 1980s, American and Canadian work has established the use of electromagnetic-induction (EM) sounding (Kovacs et al., 1987; Kovacs and Holladay, 1990).

Starting 2001, the German Alfred Wegener Institute for Polar and Marine Research (AWI) commenced with the operation of a purpose-built, small and lightweight, frequency-domain EM bird with digital electronics, which was designed for systematic ice thickness measurements in the context of climate studies and polar oceanography (Fig. 2). It had to be small and lightweight to facilitate operations from helicopter decks of ice breakers with small helicopters, and to be easily shippable to remote places in the Arctic and Antarctic. In this paper, we describe the instrument and its operation, and present its main noise, drift, and calibration characteristics as observed during six summer and winter measurement campaigns between 2004 and 2006. We also review our 1D approach for the ice thickness retrieval, which uses only one channel of the EM data instead of the full set of measurements of the Inphase and Quadrature components of the EM signal (Haas et al., 2006; Pfaffling et al., 2007). Finally, the sensitivity of the thickness estimates to the accuracy of the instrument calibration will be presented.

2. EM sea ice thickness sounding

EM sea ice thickness sounding takes advantage of the fact that sea ice has a very low electrical conductivity, while sea water is a very good conductor. Typical conductivities of sea ice are 0 to 50 mS/m (Haas et al., 1997) and 2400 to 2700 mS/m for sea water. Therefore, a low-frequency, primary EM field generated by the transmitting coil of an EM system penetrates the sea ice almost unaffected, while it generates eddy currents in the sea water below the sea ice underside. In turn, these eddy currents induce a secondary EM field which propagates upwards through the sea ice and whose strength is measured with the receiving coil of the EM system. The strength of the secondary EM field is directly related to the distance h_w between the coils and the conductive sea water surface, which coincides with the ice underside. Normally, the height of the EM system above the ice surface h_i is measured by means of a laser altimeter. Ice thickness Z_i results then from the difference between the electromagnetically determined height above the water surface h_w and the height above the ice surface h_i measured with the laser (Fig. 1; Haas et al., 2006; Pfaffling et al., 2007):

$$Z_i = h_w - h_i \quad (1)$$

Note that Z_i is the total ice thickness, i.e. the sum of snow plus ice thickness.

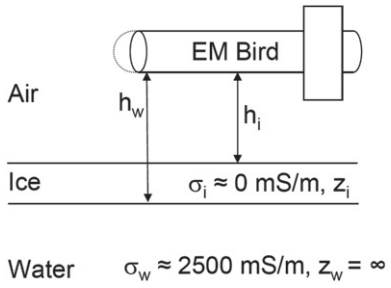

Fig. 1. Principle of EM thickness sounding, using a bird with transmitter and receiver coils and a laser altimeter. Ice thickness Z_i is obtained from the difference of measurements of the bird's height above the water and ice surface, h_w and h_i, respectively. h_w is obtained with the assumption of a negligible ice conductivity σ_i, known water conductivity σ_w, and horizontal layering.

Table 1
Main characteristics of the AWI EM bird

Size (m)	3.5 long, 0.35 diameter
Weight (kg)	105
Operation height (m)	10 to 20
Flying speed (knots)	80 to 90
Signal frequencies (kHz)	3.68 (*f*1) and 112 (*f*2)
Coil spacing (m)	2.77 (*f*1) and 2.05 (*f*2)
Sample frequency (Hz)	10 (EM) and 100 (Laser)
Tx dipole moment (Am^2)[a]	54.5 (*f*1) and 5.3 (*f*2)
Power requirement (W)	400

[a] Calculated as NIA: No. of turns*Current*Coil Area.

Based on the pioneering work of Kovacs et al. (1987),Kovacs and Holladay (1990), and Prinsenberg and Holladay (1993) using a helicopter-towed EM bird, EM sea ice thickness measurements have then been taken forward by Multala et al. (1996) and Prinsenberg et al. (2002). The former study has used a fixed-wing system where the transmitting and receiving coils were mounted at the wingtips of a Twin Otter air plane. Prinsenberg et al. (2002) have developed a fixed-mounted helicopter EM system, where the EM coils are housed in a stinger in front of the helicopter.

In parallel to the technical developments in Canada and the US mentioned in Section 1, Liu and Becker (1990) and Liu et al. (1991) developed numerical 1D and 2D inversion algorithms for the ice thickness retrieval from the EM measurements, partially in real-time. Other sea ice studies used standard Marquart–Levenberg inversion (Rossiter and Holladay, 1994; Multala et al., 1996). However, the results of the inversion are critically dependent on the accuracy and stability of the calibration of the EM instrument, and on low noise characteristics, and can require extensive and tedious data editing. Therefore, we have developed an alternative 1D approach for the ice thickness retrieval, which uses only one channel of the EM data. This will be reviewed in detail in Section 5 and has also been described by Haas et al. (2006) and Pfaffling et al. (2007). As demonstrated by Haas et al. (2006), Pfaffling et al. (2007), and Pfaffling and Reid (2009-this issue) this approach yields quick and accurate ice thickness estimates of level ice in good agreement (±0.1 m) with drill-hole validation measurements. Pfaffling et al. (2007) showed that the sensitivity of these ice thickness estimates to uncertainties of assumed ice and water conductivities is very small for the range of normally occurring ice thicknesses and ice conductivities.

In contrast to their high accuracy over level ice, EM measurements normally underestimate the maximum thickness of deformed ice (Kovacs et al., 1995; Reid et al., 2006). This is due to the footprint of EM measurements over those 3D structures, and due to the high conductivity of the ridge keel, which is composed of ice blocks and interconnected voids filled with sea water. The latter can lead to channelling effects of the electrical currents, preventing any deeper penetration of the EM field. As shown by Haas and Jochmann (2003), the underestimation of ridge thicknesses by EM measurements can therefore exceed 50% of coincident upward-looking sonar measurements. In this paper, we only focus on measurements over level ice.

3. System components

The AWI EM system consists of three main components (Fig. 3): The actual EM bird, the towing cable, and a few devices inside the helicopter for system control and power supply. Main characteristics are summarized in Table 1.

3.1. EM bird

The EM bird is 3.5 m long, has a diameter of 0.35 m, and weighs 105 kg (Fig. 2). Inside the cylindrical kevlar shell, all components are mounted on a rigid plate which is accessible through two lid-closable holes. The plate can also be completely removed from the shell. The bird

Fig. 2. AWI EM bird during take-off from the helicopter deck of an icebreaker, North Pole 2001.

operates at two frequencies of 3.68 (*f*1) and 112 kHz (*f*2). The frequencies were chosen to provide as much sensitivity to changes of ice thickness and ice conductivity as technically possible. As deviations of 1 or 2 kHz do not significantly change the sensitivities, no efforts were undertaken to carefully adjust the resonance frequencies to a specific value. However, as shown by the inversion study of Pfaffling and Reid (2009-this issue), an even higher second frequency would be required for a stable inversion of ice conductivity. Unfortunately this could not be realised due to technical reasons (see below). The coils for each frequency are mounted above and below the rigid plate. Fig. 3 shows the approximate positions of the coils of only one frequency. As usual with frequency-domain EM systems, for each frequency there is a transmitter coil Tx for signal generation, a receiving coil Rx for signal reception, a bucking coil for compensation of the primary EM field at the receiving coil, and a calibration coil which generates very accurate signals of known phase and amplitude if electrically connected. Tx–Rx coil spacing is 2.77 and 2.05 m for *f*1 and *f*2, respectively. At the bird's nose, there is a vertically downward-looking laser altimeter (cf. Fig. 1). A Differential Global Positioning System (DGPS) antenna is mounted on top of the shell. A computer in the centre of the rigid plate performs all required operations. It hosts A/D-converters for the analogue coil output signals, digital signal processing boards, serial communication cards, a network card, a GPS receiver, and a hard disk. The computer processes Inphase and Quadrature of the continuous harmonic signal with a sampling interval of 0.1 s. The laser is operated at 100 Hz. With a typical

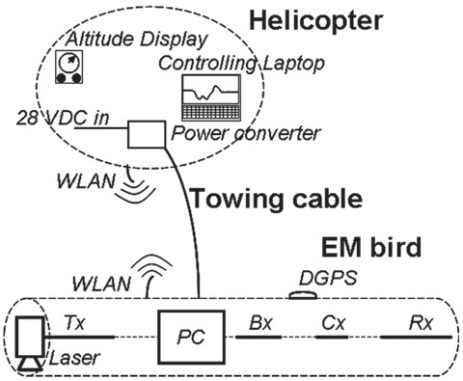

Fig. 3. Sketch of major components of AWI EM bird, consisting of transmitter coil (Tx), bucking coil (Bx), calibration coil (Cx), receiver coil (Rx), computer (PC), differential Global Positioning System (DGPS), wireless network (WLAN). Note that figure is not drawn to scale.

flight speed of 80 knots, this corresponds to a point spacing of approximately 4 m for the EM data, and of 0.4 m for the laser data. The computer is connected to a wireless LAN network antenna, which provides communication with the operator in the helicopter (Section 3.3).

3.2. Towing cable

The towing cable is used to suspend the EM bird under the helicopter, and to transmit the required electrical power. We use tow cable lengths of 20 and 30 m, respectively, depending on the size of the helicopter, and whether the bird needs to be landed on a small helicopter deck or on a large ice floe. With middle-sized helicopters, 20 m is sufficient to avoid disturbances of the measurements by conductive parts of the helicopter or by airflow turbulence.

3.3. Devices inside the helicopter

Three devices are hosted inside the helicopter: A DC/DC-power converter transforms the 28 VDC, 400 W input voltage of the helicopter to approximately 200 VDC fed into the towing cable. All operations are performed with a standard laptop connected to the bird by wireless LAN. It is used to store and display the Inphase,

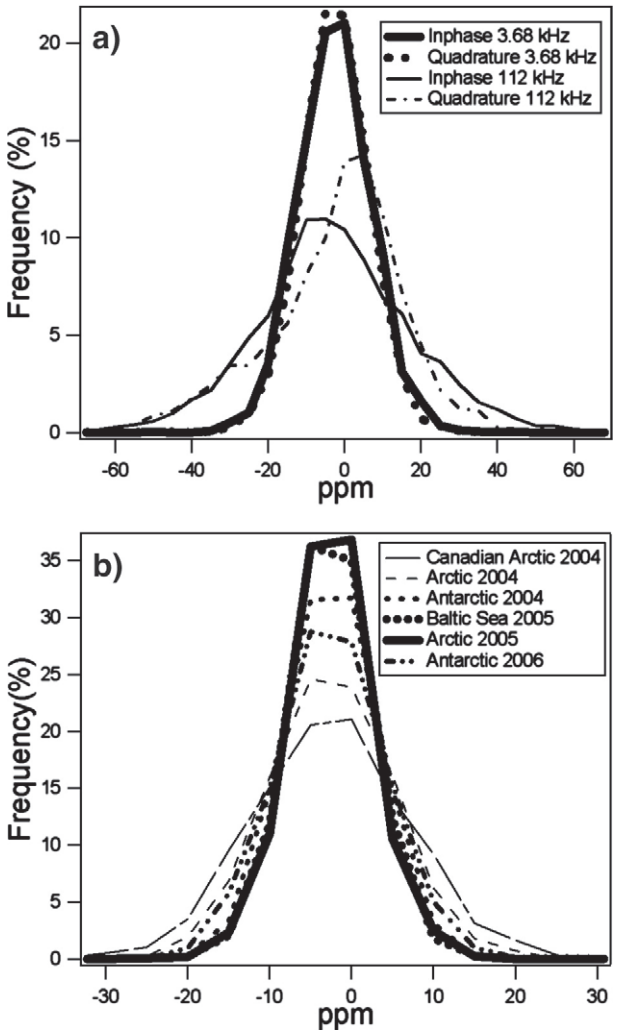

Fig. 4. Histograms of 40 s long sections of EM measurements of relative secondary EM field strength at altitudes greater than 100 m. a) Inphase and Quadrature components of *f*1 = 3.68 kHz and *f*2 = 112 kHz measured in the Arctic during winter 2004 (cf. Fig. 4b). b) Inphase component of *f*1 measured on different summer and winter campaigns between 2004 and 2006.

Quadrature, laser, and GPS data in real-time, and to perform the required operations on the bird, e.g. nulling, phasing, and calibration. Via serial link, the raw laser data is forwarded to an analogue altimeter display visible for the pilot to control flying altitude. With this, pilots are comfortably flying the bird at typical altitudes of 10 to 20 m above the ice surface. Because of the bird's compactness and simplicity we have so far operated it from various different helicopter types like MD500, AS350, Bell 206, BO 105, Bell 212 and MI-8.

4. Noise, drift, and stability of calibration

The accuracy, sensitivity, and lateral resolution of EM measurements depend critically on the signal-to-noise ratio of the measurements, on the drift of the electronic components, as well as on the stability of the calibration. Fig. 4 shows typical histograms of measurements of the relative secondary EM field strength at high altitudes > 100 m. At these heights, the relative secondary field strength of the Inphase component of *f*1 is <5 ppm, and <1 ppm for all other components. Therefore, the histograms are centred around approximately 0 ppm. However, it can be seen that there are large numbers of measurements with secondary field strengths significantly smaller or larger than 0 ppm. These measurements are due to noise. The noise distributions closely resemble Gaussian distributions (Fig. 4). As can be seen from their widths, the standard deviation of the noise amounts to approximately ±9, ±8, ±20, and ±15 ppm for the Inphase and Quadrature components of *f*1 and *f*2, respectively. However, the skewness of the distributions of the measurements at *f*2 is due to the sporadic presence of spikes of unknown origin in those measurements. These also lead to the non-zero modes after nulling of the *f*2 histograms in Fig. 4a. Fig. 4b shows that the noise of one component can vary between ±5 ppm (Arctic, summer 2005) and ±10 ppm (Arctic winter 2004) during different measurement campaigns.

Fig. 5 shows a 2.25 h long record of raw unphased complex voltage measurements at *f*1. The typical sequence of measurements at high and low altitude can be seen. While the latter are performed to actually measure ice thickness, ascents to more than 100 m above sea level are made every 15 to 20 min to monitor and correct for electrical system drift in the absence of any significant signal from the sea water. Ideally, the measurements at high altitude should yield a voltage of 0 mV, if the compensation by the bucking coils was perfect. However, it can be seen that voltages of approximately −200 mV and −230 mV remain for the complex components of *f*1, respectively, due to incomplete compensation. In addition, these zero-voltages are not constant, but vary for each ascent due to electrical drift. This offset and drift is removed by nulling with the data acquisition software during each ascent. For the drift correction, linear drift is assumed between ascents. The validity of this approach can be validated over sections of open water along the flight track (Sections 5 and 7).

Fig. 6 provides a summary of the typical drift of measurements representative of all campaigns between 2004 and 2006. It can be seen that there is no systematic drift behaviour. The same components might have a negative or positive drift, and the drift can be as high under summer conditions with warm air temperatures as under cold winter conditions. In fact, in all cases shown, the bird was already operated on the ground for 1 h or more to achieve thermal balance of the transmitter coil components before take-off. During take-off, the bird was switched off for as short a time as possible. Analysis of the curves in Fig. 6 shows that within the first 0.5 h of measurements, typical maximum drift rates are below ±200 ppm/h for both components of *f*1 and below ±2000 ppm/h for *f*2, respectively. After 2 h of operation, the drift is usually lower than ±50 ppm/h for *f*1 and ±500 ppm/h for *f*2, i.e. reduced by 75%.

During the high altitude flight sections and after nulling, the calibration coils are electrically connected for a few seconds and generate well defined Inphase and Quadrature voltage offsets (cf. spikes in Fig. 5). The absolute value of the calibration signal has been both calculated (Fitterman, 1998) and verified by means of flights over open sea water with a precisely known conductivity. The measured strength of the calibration voltage offsets is first used to phase the raw complex voltage components and then to convert the voltage measurements into ppm. Typical values of the calibration coefficients derived over the period of our 6 campaigns were 95.27 ± 1.98 μV/ppm, 97.76 ± 1.45 μV/ppm, 27.06 ± 0.64 μV/ppm, and 32.51 ± 0.93 μV/ppm for the Inphase and Quadrature signals of *f*1 and *f*2, respectively. The standard deviations of the calibration coefficients reflect some drift of the calibration constant, but results also from the noise superimposed on the short calibration signals. The values show that the calibration has an uncertainty of less than ±2% for *f*1, and of approximately ±3% for *f*2. These are equivalent to uncertainties of ±2% and ±3% in the Gain of *f*1 and *f*2, and less than 1° in the Phase.

5. Ice thickness retrieval

As also shown by Haas et al. (2006) and Pfaffling et al. (2007), ice thickness can be retrieved from one component of the complex EM signal alone if the conductivities of ice and water are known within certain bounds. For normal sea water with conductivities between 2000 and 2800 mS/m, we invert only measurements of the Inphase component of *f*1, as this is the strongest signal, and has also the lowest noise (Fig. 4) and smallest drift (Fig. 6). However, for brackish water of a few hundred mS/m only, like, e.g. in the Baltic and Caspian Seas, the

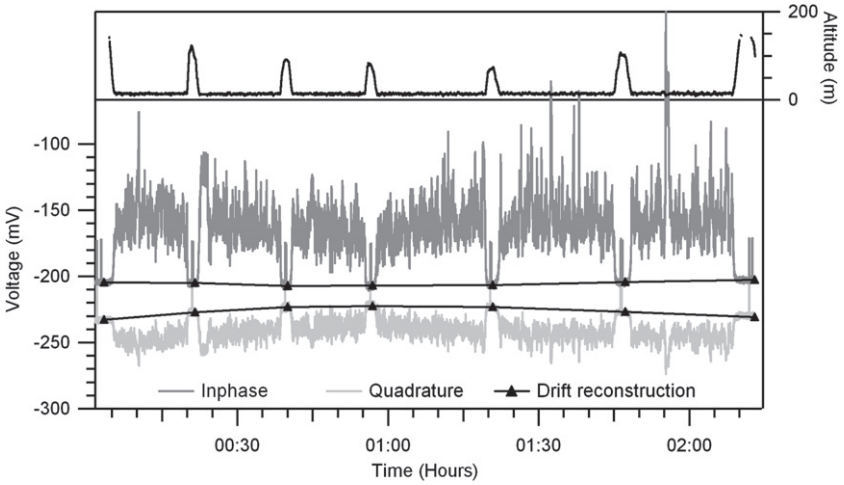

Fig. 5. 2.25 h long records of Inphase and Quadrature voltages at *f*1 = 3.68 kHz, and flight altitude. Thick triangles mark the electrical drift determined during ascents to altitudes > 100 m above the sea surface. Note variations of high altitude measurements due to noise (cf. Fig. 4). Singular spikes during high altitude flights are due to calibration signal induced by calibration coils.

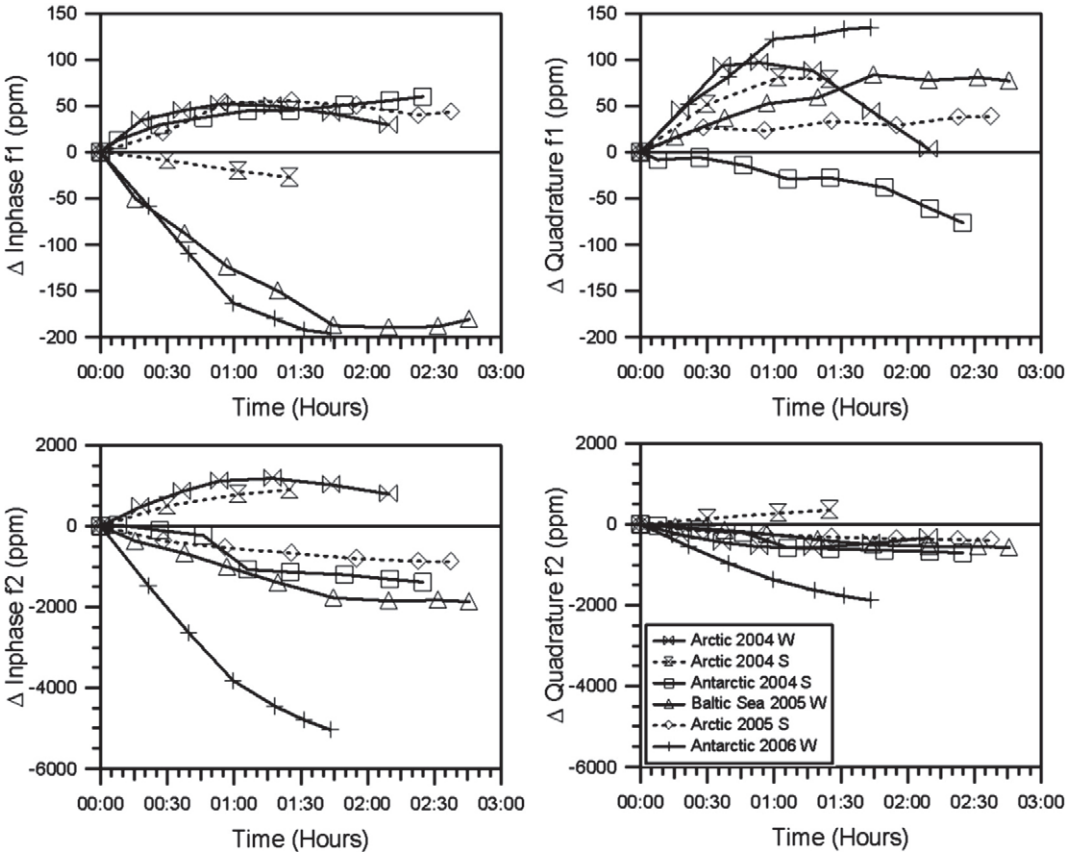

Fig. 6. Typical drift behaviour of Inphase and Quadrature components of *f*1 and *f*2 obtained from high altitude sections of flights during all campaigns between 2004 and 2006 (cf. example in Fig. 5). Measurements are split into winter (W, solid lines) and summer campaigns (S, stippled lines).

Inphase of *f*2 is the strongest signal and can be used as well (Haas, 2004, 2006; Pfaffling et al., 2007). The method is described in detail below.

Fig. 7 shows the relationship between bird height above the ice surface and measured and modelled EM responses for a flight over the Lincoln Sea, a marginal sea of the Arctic Ocean north of Ellesmere Island in Canada. Data and model show the Inphase response of *f*1. The model results (Ward and Hohmann, 1988) have been computed for open water (ice thickness 0 m) with a sea water conductivity of 2500 mS/m, representative of in-situ salinity measurements. The model curve provides the general means of computing the height of the bird above the water surface h_w or ice underside from a measurement of Inphase EM field strength at a certain height above the water (Fig. 1; Haas, 1998). Measurements at different heights are obtained because the altitude of the helicopter and bird vary between 10 and 25 m during the flight (Figs. 7 and 8). The data can be separated into two sections: while open water measurements at different bird heights agree well with the model curves, the presence of sea ice leads to a reduction of the measured EM signal at a given laser height (Fig. 7). Therefore the scattered cloud of data points below the model curve represents measurements over ice. Ice thickness is computed by subtracting the laser height measurement over sea ice from the model curve (Haas, 1998). It can also be visually estimated from the horizontal distance between each EM measurement and the model curve (Fig. 7). The thickness computation assumes a negligible sea ice conductivity of <20 mS/m, which is likely for the multiyear ice in the study region (Haas et al., 1997; Pfaffling et al., 2007).

Fig. 8 illustrates the two steps of determining the height above the ice and water surfaces h_i and h_w, and obtaining ice thickness from the difference of these measurements. The example is from the Transpolar Drift in August 2001. Fig. 8c shows the thickness distribution computed from the resulting ice thickness profile with a bin width of 0.1 m. The modes of the distribution represent the fraction of open water along the profile, first-year ice with a modal thickness of 1.2 m, and 2 m thick second and multiyear ice.

Due to the uncertainty of the calibration explained in Section 4, sometimes a slight recalibration of Inphase and Quadrature components, *I* and *Q*, of the chosen frequency, is required during post-processing, after drift correction and before ice thickness can be calculated as described above (Figs. 7 and 8). The Gain is corrected manually by aligning the open water measurements of both Inphase

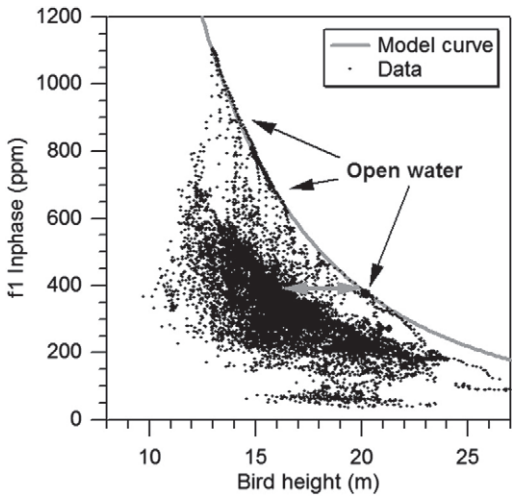

Fig. 7. Inphase component of relative secondary field strength of *f*1 = 3.68 kHz versus bird height h_i(Fig. 1). A model curve for open water with a conductivity of 2500 mS/m and data over a typical ice surface with some leads are shown. The horizontal arrow illustrates how ice thickness (4 m) is obtained for a single data point from the difference between h_i and the model curve h_w for a given EM field strength (see Section 5; Fig. 1; Eq. (1)).

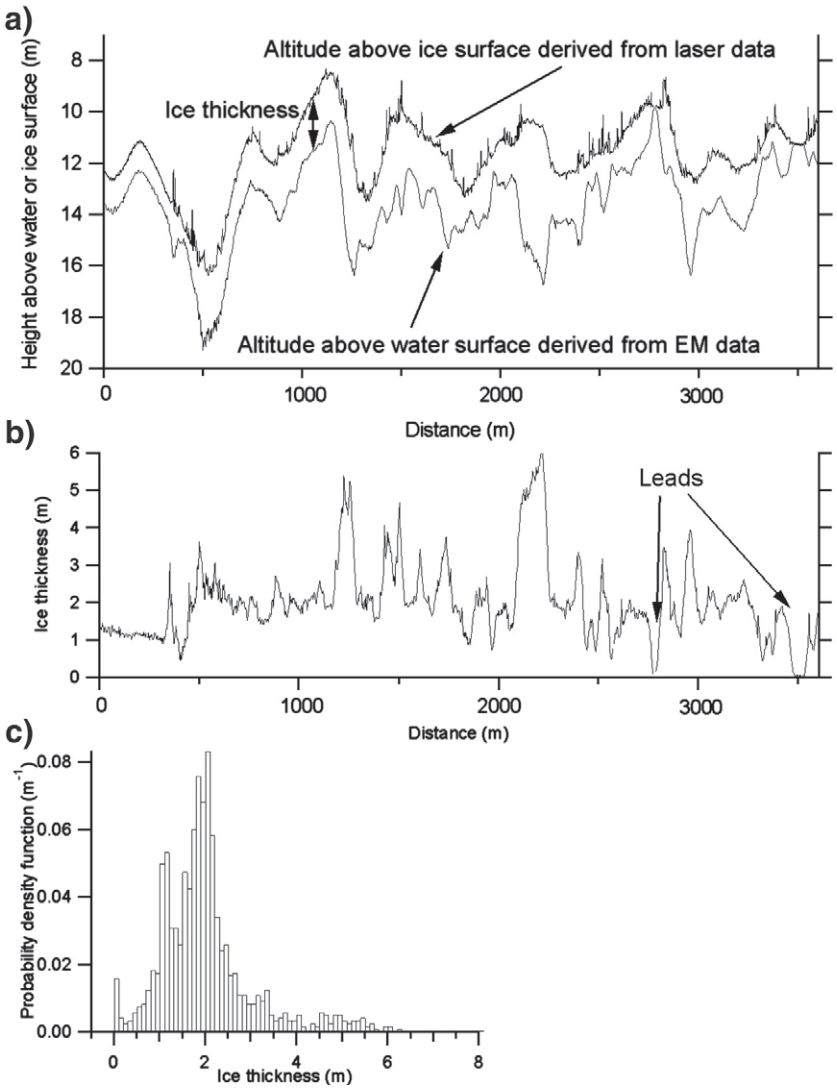

Fig. 8. (a) EM and laser derived bird height above the water h_w and ice surface h_i, respectively, and (b) ice thickness profile resulting from subtraction of the latter from the former. (c) Resulting thickness distribution.

and Quadrature components visually with the model curves for open water. The Phase is adjusted by aligning the measurements with modelled I and Q responses in a Phasor diagram, a cross-plot of I and Q (Pfaffling and Reid, 2009-this issue). The recalibration of Inphase, I_{recal}, and Quadrature, Q_{recal}, is performed by changing the Gain A and Phase P by ΔA and ΔP according to

$$I_{recal} = A_{recal} * \cos(P_{recal}) \quad (2a)$$

$$Q_{recal} = A_{recal} * \sin(P_{recal}) \quad (2b)$$

Where $A_{recal} = A*(1+\Delta A)$ and $P_{recal} = P+\Delta P$. A and P are derived from the original measurement of I and Q according to

$$A = \mathrm{SQRT}(I^2 + Q^2) \quad (3a)$$

and

$$P = \mathrm{atan}(Q/I). \quad (3b)$$

Typical values resulting from the recalibration range between 1.00 to 1.03 for $(1+\Delta A)$ and 0° to 3° for ΔP, slightly exceeding the uncertainty of the calibration coefficients described in Section 4. This deviation is due to other additional factors determining the agreement with the model curves, including the correct knowledge of the seawater conductivity.

6. Accuracy

Noise, drift, and accuracy of the calibration affect the accuracy of the electromagnetically derived height above the water surface h_w and therefore the ice thickness calculation (Eq. (1)). The dependence of h_w on variations of noise, drift and accuracy of the calibration is shown in Fig. 9 for the Inphase component I of $f1$. For an ice thickness of 0 m, I agrees with the model curve for open water, and application of Eq. (1) correctly results in an ice thickness of 0 m. I has subsequently been varied by a constant offset of 5 and 10 ppm, by variable gain of 1.01 to 1.02, and by a phase shift of 1 to 3°, according to the variations observed and described in Sections 4 and 5. The resulting deviations from an ice thickness of 0 m show the inaccuracy due to the uncertainty of the respective parameter.

As can be seen from Fig. 9, the errors resulting from noise and insufficient drift correction, as well as from inaccurate gains and phases are all dependent on the flying height above the water surface. For offsets of the Inphase component of $f1$ of 10 ppm, the error exceeds 0.1 m for flying heights above 17 m. Gain variations of between 0.99 and 1.01 result in thickness errors of less than 0.1 m. The thickness retrieval is least sensitive on variations of phase, where variations of ±2° result in errors of about 0.1 m. In summary, we conclude that the observed errors caused by the normal range of

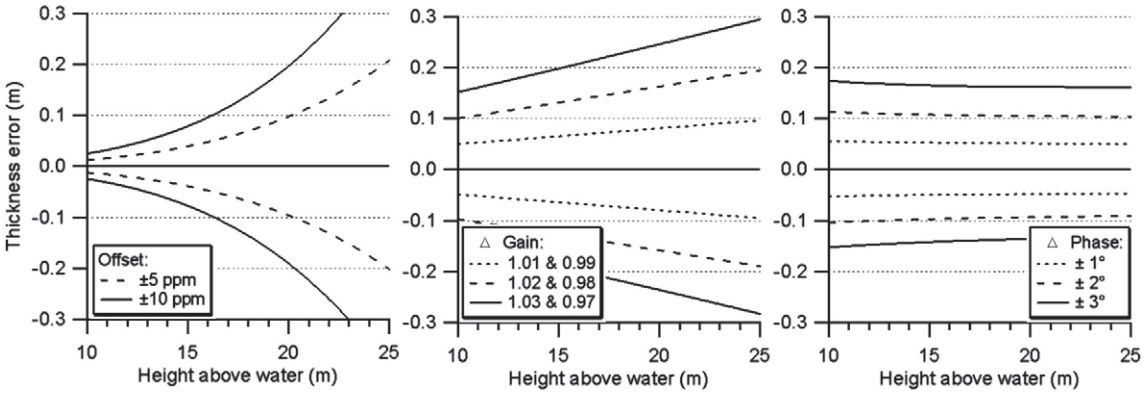

Fig. 9. Sensitivity of the ice thickness estimate in Eq. (1) to offsets of the measured Inphase component of $f1 = 3.68$ kHz and inaccurate Gain and Phase. For the computation, an ice thickness of 0 m was taken and the panels show the difference between the true thickness and the thickness resulting from wrong offset, Gain and Phase.

noise, insufficient drift correction, and inaccurate calibration shown above all result in thickness errors of less than ±0.1 m. These may partially compensate each other, but can also add up in worst cases.

Finally, we compare ice thicknesses derived by means of HEM surveying with ice thicknesses derived by other means. Reid et al. (2006) and Pfaffling et al. (2007) have shown a good agreement within ±0.1 m between extensive drill-hole and HEM measurements along the same profile. In Fig. 10, we compare thickness distributions derived by means of HEM and ground-based EM surveying over the same regions of Arctic and Antarctic sea ice. The ground-based profiles have been obtained on individual ice floes using a Geonics EM31 instrument (Haas et al., 1997). The histograms show the generally good agreement between both measurements. While most deviations can be explained by the largely different sample numbers and non-coincident profiles, characteristic modes can be found in both data sets in close agreement. In Fig. 10a, both histograms show a mode of 1.6 m representing first-year ice (Haas et al., 2006). Similarly in Fig. 10b, 1.2 m thick first-year ice resulted in clear modes in both data sets, disagreeing by only 0.1 m (Haas et al., 2008). Both distributions also have local maxima at 2.6 and 2.9 m, representing thick first-year and second year ice of the same origin.

All thickness distributions in Figs. 8 and 10 show rather narrow thickness modes less than 0.2 m wide for profile sections over open water and uniform first-year ice. This, as well as the results presented above, leads us to the conclusion that our ice thickness estimates have an accuracy of at least ±0.1 m.

7. Discussion and conclusions

We have presented the design and characteristics of a purpose-built, small and lightweight digital EM bird for sea ice thickness measurements, and have summarized our approach to compute sea ice thickness from single-component EM data. This approach was taken because it is largely independent of effects of sea ice conductivity (Pfaffling et al., 2007), and because it provides as accurate ice thickness results as a full geophysical inversion using all EM channels (Pfaffling and Reid, 2009-this issue). In addition, its accuracy can easily be verified by plotting the EM signal versus laser height as in Fig. 7.

In this paper, we show that the errors resulting from system properties like noise, drift, and accuracy and stability of the calibration remain mostly below ±0.1 m of ice thickness. Pfaffling et al. (2007) show that variations of sea ice conductivity result in ice thickness uncertainties of the same order. However, there are additional error sources e.g. from bird pitch and roll (Fitterman and Yin, 2004) not discussed here. These are due to both, changes of the electromagnetic dipole orientation with respect to the water surface, as well as due to slant angle changes of the laser altimeter. However, for roll angles of $<< 10°$ typical for normal flight patterns along straight lines with little wind, and for the operating altitude of our bird of 10 to 20 m, these do not result in much larger errors than those described here (Holladay et al., 1997; Kratzer and Vrbancich, 2007).

Even during winter, there is usually some open water along the flight track, with an ice thickness of 0 m (Figs. 7 and 10). These open water sections are important for the verification of a correct drift correction

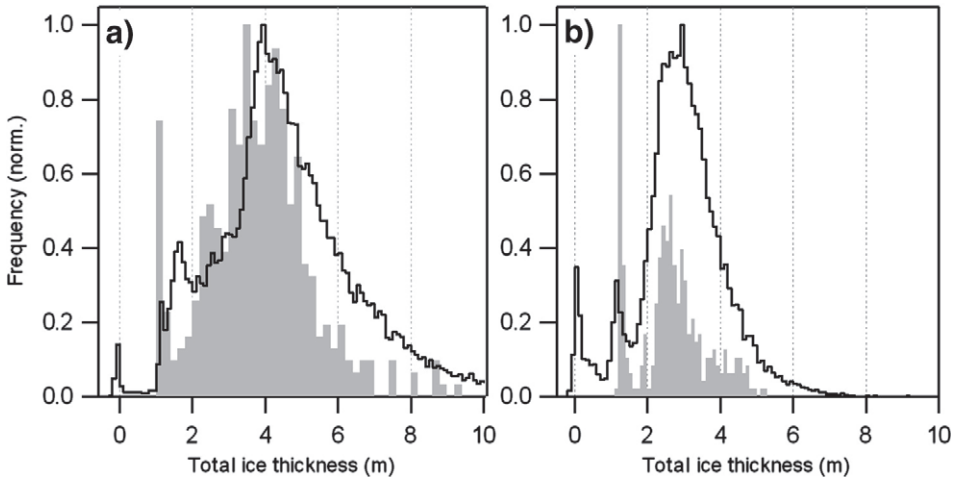

Fig. 10. Comparison of ice thickness distributions derived by means of HEM (solid line) and ground-based EM surveying (grey shade). a) Histograms derived from a 150 km long HEM and 2 km long ground-based profile from the same region of the Lincoln Sea (Haas et al., 2006); b) Histograms derived from the same ice floe in the Weddell Sea, with a grid of 140 km of HEM data and 4 km of ground-based data (Haas et al., 2008).

and calibration, as the estimated ice thickness has to be 0 m over these regions as well. When there is no open water, drift, gain, and phase should be within the range of adjacent profile sections. The sensitivity study presented here (Section 6) shows that this can be done with little error.

Figs. 4 and 6 point to problems with spikes and strong drift of the high frequency of 112 kHz. That frequency is technically challenging because it exceeds the normal audio frequency range and therefore standard electronic components operate close to their technical limits. This is unfortunate, as the Inphase of the high frequency is superior in the case of measurements over brackish water. We have successfully measured ice thickness with sea water conductivities as low as 300 mS/m (Haas, 2004, 2006). The combination of frequencies of 3.68 and 112 kHz is also sensitive to the bathymetry of shallow, brackish water (Haas, 2006).

Unfortunately, the performance of the high frequency measurements is also hampered by the low dipole moment and small coil spacing (Table 1). The former is due to the high AC resistance of coils at those frequencies. In fact, for even better sensitivity to ice conductivity, our original goal was to design *f*2 as high as 200 kHz. However, no useful signals could be generated at this frequency at all. Although coil spacing was optimized for both frequencies, it is of course largely confined by the small size of the bird, which poses a great constraint. In fact, a small increase in coil spacing from 2.7 to 3.5 m would double the in-phase sensitivity of *f*1 (Pfaffling et al., 2007).

Due to the great success of our bird operations, we have actually built a second bird. This operates only at one frequency of 4.1 kHz, but is otherwise identical to the first bird. Its behaviour and performance are very similar to that of the first bird presented here.

Future improvements of the birds should include means for measuring the exact bird orientation and pitch and roll, e.g. with several differential GPS antennas (Holladay et al., 1997) or with an inertial navigation system. Combination with a radar for snow thickness measurements would also be desirable (Lalumiere, 1998), as snow is an independent climate variable and strongly influences sea ice thermodynamics.

Although we operate our bird several times per year and also for systematic ice thickness monitoring projects, it should not be forgotten that most accurate results can only be obtained over level ice, and that conclusions from this paper are also only valid for level ice. For a better judgment of the bird performance over deformed and porous ice with a 3D structure, coincident measurements of the true underside topography are required. These can be obtained by upward-looking sonar measurements with submarines or autonomous underwater vehicles, or by divers. During the present International Polar Year (IPY) in 2007 and 2008, we are very hopeful to obtain an extensive coincident underwater and EM ice thickness data set.

Acknowledgements

We are most grateful to E. Augstein and H. Miller for initiating this work, and for funding and continued support by the Alfred Wegener Institute. K.P. Sengpiel and the staff of Aerodata AG and Optimare Sensorsysteme AG are greatly acknowledged for their geophysical and technical guidance and advice. Numerous students improved the data processing procedures. We also acknowledge the patience and cooperation of pilots and staff of Helicopter Service Wasserthal and Helitransair during extensive tests flights. Careful comments of James Macnae and the Editor Niels B. Christensen improved the manuscript significantly.

References

Fitterman, D.V., 1998. Sources of calibration errors in helicopter EM data. Exploration Geophysics 29, 65–70.

Fitterman, D.V., Yin, C., 2004. Effect of bird maneuver on frequency-domain helicopter EM response. Geophysics 69 (5), 1203–1215. doi:10.1190/1.1801937.

Haas, C., 1998. Evaluation of ship-based electromagnetic-inductive thickness measurements of summer sea-ice in the Bellingshausen and Amundsen Seas, Antarctica. Cold Regions Science and Technology 27, 1–16.

Haas, C., 2003. Dynamics versus thermodynamics: the sea-ice thickness distribution. In: Thomas, D.N., Dieckmann, G.S. (Eds.), Sea Ice—An Introduction to its Physics, Biology, Chemistry and Geology. Blackwell Scientific, pp. 82–111.

Haas, C., 2004. Airborne EM sea-ice thickness profiling over brackish Baltic sea water. Proceedings of the 17th international IAHR Symposium on Ice, June 21–25, 2004, 2. All-Russian Research Institute of Hydraulic Engineering (VNIIG), Saint Petersburg, Russia, pp. 12–17.

Haas, C., 2006. Airborne electromagnetic sea ice thickness sounding in shallow, brackish water environments of the Caspian and Baltic Seas. Proceedings of OMAE2006 25th International Conference on Offshore Mechanics and Arctic Engineering. Hamburg, Germany. 6 pp.

Haas, C., Jochmann, P., 2003. Continuous EM and ULS thickness profiling in support of ice force measurements. Proceedings of the 17th International Conference on Port and Ocean Engineering under Arctic Conditions POAC '03, 2. Department of Civil and Transport Engineering, Norwegian University of Science and Technology NTNU, Trondheim, Norway, pp. 849–856.

Haas, C., Gerland, S., Eicken, H., Miller, H., 1997. Comparison of sea-ice thickness measurements under summer and winter conditions in the Arctic using a small electromagnetic induction device. Geophysics 62, 749–757.

Haas, C., Hendricks, S., Doble, M., 2006. Comparison of the sea ice thickness distribution in the Lincoln Sea and adjacent Arctic Ocean in 2004 and 2005. Annals of Glaciology, 44, 247–252.

Haas, C., Nicolaus, M., Willmes, S., Worby, A.P., Flinspach, D., 2008. Sea ice and snow thickness and physical properties of an ice floe in the western Weddell Sea and their changes during spring warming. Deep Sea Research II 55 (8-9), 963–974. doi:10.1016/j.dsr2.2007.12.020.

Hall, A., 2004. The role of surface albedo feedback in climate. Journal of Climate 17, 1550–1568.

Holladay, J.S., Lo, B., Prinsenberg, S.J., 1997. Bird orientation effects in quantitative airborne electromagnetic interpretation of pack ice thickness sounding. Conference Proceedings of the Oceans Conference 1997, 2. Marine Technology Society, Institute of Electrical and Electronics Engineers Inc., pp. 1114–1119.

Kovacs, A., Holladay, J.S., 1990. Sea-ice thickness measurements using a small airborne electromagnetic sounding system. Geophysics 55, 1327–1337.

Kovacs, A., Valleau, N.C., Holladay, J.S., 1987. Airborne electromagnetic sounding of sea ice thickness and sub-ice bathymetry. Cold Regions Science and Technology 14, 289–311.

Kovacs, A., Holladay, J.S., Bergeron, C.J., 1995. The footprint/altitude ratio for helicopter electromagnetic sounding of sea-ice thickness: comparison of theoretical and field estimates. Geophysics 60, 374–380.

Kratzer, T., Vrbancich, J., 2007. Real-time kinematic tracking of towed AEM birds. Exploration Geophysics 38, 132–143. doi:10.1071/EG07012.

Lalumiere, L.A., 1998. Implementation of a prototype real-time snow thickness radar. Canadian Contractor Report of Hydrography and Ocean Sciences 48 81 pp.

Liu, G., Becker, A., 1990. Two-dimensional mapping of sea ice keels with airborne electromagnetics. Geophysics 55, 239–248.

Liu, G., Kovacs, A., Becker, A., 1991. Inversion of airborne electromagnetic survey data for sea-ice keel shape. Geophysics 56, 1986–1991.

Maykut, G.A., 1986. The surface heat and mass balance. In: Untersteiner, N. (Ed.), The Geophysics of Sea Ice. Martinus Nijhoff Publ., Dordrecht, pp. 395–463 (NATO ASI B146).

Meier, W., Stroeve, J., Fetterer, F., Knowles, K., 2005. Reductions in arctic sea ice cover no longer limited to summer. Eos, Transactions of the American Geophysical Society 86, 326.

Multala, J., Hautaniemi, H., Oksama, M., Leppäranta, M., Haapala, J., Herlevi, A., Riska, A., Lensu, M., 1996. An airborne electromagnetic system on a fixed wing aircraft for sea ice thickness mapping. Cold Regions Science and Technology 24, 355–373.

Pfaffling, A., Reid, J.E., 2009. Sea ice as an evaluation target for HEM modelling and inversion. Journal of Applied Geophysics 67, 242–249 (this issue).

Pfaffling, A., Haas, C., Reid, J.E., 2007. A direct helicopter EM sea ice thickness inversion, assessed with synthetic and field data. Geophysics 72, F127–F137.

Prinsenberg, S.J., Holladay, J.S., 1993. Using air-borne electromagnetic ice thickness sensor to validate remotely sensed marginal ice zone properties. In: HSVA (Ed.), Port and Ocean Engineering under Arctic Conditions (POAC 93), 2, pp. 936–948.

Prinsenberg, S.J., Holladay, J.S., Lee, J., 2002. Measuring ice thickness with EISFlowTM, a fixed-mounted helicopter electromagnetic-laser system. Proceedings 12th International Offshore and Polar Engineering Conference, 1, pp. 737–740.

Reid, J., Pfaffling, A., Vrbancich, J., 2006. Airborne electromagnetic footprints in one-dimensional earths. Geophysics 71 (2), G63–G72. doi:10.1190/1.2187756.

Rossiter, J.R., Holladay, J.S., 1994. Ice-thickness measurement. In: Haykin, S., Lewis, E.O., Rainey, R.K., Rossiter, J.R. (Eds.), Remote Sensing of Sea Ice and Icebergs. John Wiley & Sons Inc., pp. 141–176.

Rothrock, D.A., Yu, Y., Maykut, G.A., 1999. Thinning of the Arctic sea-ice cover. Geophysical Research Letters 26, 3469–3472.

Stroeve, J., Serreze, M.C., Fetterer, F., Arbetter, T., Meier, W., Maslanik, J., Knowles, K., 2005. Tracking the Arctic's shrinking ice cover; another extreme September sea ice minimum in 2004. Geophysical Research Letters 32, L04501. doi:10.1029/2004GL021810.

Wadhams, P., 2000. Ice in the Ocean. Gordon & Breach Science Publishers. 351 pp.

Ward, S.H., Hohmann, G.W., 1988. Electromagnetic theory for geophysical applications. In: Nabighian, M.N. (Ed.), Electromagnetic Methods in Applied Geophysics, Volume 1 Theory. SEG Monograph, vol. 3, pp. 131–313.

Paper IV

GEOPHYSICAL RESEARCH LETTERS, VOL. 35, L17501, doi:10.1029/2008GL034457, 2008

Reduced ice thickness in Arctic Transpolar Drift favors rapid ice retreat

Christian Haas,[1,2] Andreas Pfaffling,[1,3] Stefan Hendricks,[1] Lasse Rabenstein,[1] Jean-Louis Etienne,[4] and Ignatius Rigor[5]

Received 24 April 2008; revised 27 June 2008; accepted 17 July 2008; published 3 September 2008.

[1] Helicopter-borne electromagnetic sea ice thickness measurements were performed over the Transpolar Drift in late summers of 2001, 2004, and 2007, continuing ground-based measurements since 1991. These show an ongoing reduction of modal and mean ice thicknesses in the region of the North Pole of up to 53 and 44%, respectively, since 2001. A buoy derived ice age model showed that the thinning was mainly due to a regime shift from predominantly multi- and second-year ice in earlier years to first-year ice in 2007, which had modal and mean summer thicknesses of 0.9 and 1.27 m. Measurements of second-year ice which still persisted at the North Pole in April 2007 indicate a reduction of late-summer second-year modal and mean ice thicknesses since 2001 of 20 and 25% to 1.65 and 1.81 m, respectively. The regime shift to younger and thinner ice could soon result in an ice free North Pole during summer. **Citation:** Haas, C., A. Pfaffling, S. Hendricks, L. Rabenstein, J.-L. Etienne, and I. Rigor (2008), Reduced ice thickness in Arctic Transpolar Drift favors rapid ice retreat, *Geophys. Res. Lett.*, *35*, L17501, doi:10.1029/2008GL034457.

1. Introduction

[2] The summer of 2007 saw another record low sea-ice coverage of the Arctic Ocean, with a minimum monthly ice extent of 4.28×10^6 km^2, 23% less than during the previous minimum in 2005 [*Stroeve et al.*, 2008]. Questions arise whether this drastic reduction of ice extent is just the result of natural variability superimposed on a generally declining trend, or if the Arctic sea ice cover has transitioned into a different climatic state where completely ice-free summers would soon become normal [*Lindsay and Zhang*, 2005; *Holland et al.*, 2006]. The rapidity of the Arctic summer sea ice decline is also surprising as it is much faster than predicted by any of the Intergovernmental Panel of Climate Change model scenarios [*Stroeve et al.*, 2007]. A better representation of sea ice in these models is complicated by the variety of different processes contributing to the presence of sea ice. For example, anomalous wind patterns, air temperatures, and radiation regimes have all been considered as causes for the minimum ice coverage in 2007 [*Stroeve et al.*, 2008]. It is unclear how much the warming of the Atlantic layer contributes to increases in ocean heat flux and therefore ice reduction [*Polyakov et al.*, 2007]. These factors all overlay a general, continued reduction of the fraction of older ice in the Arctic Ocean, as shown by drifting buoys and satellite radar maps [*Nghiem et al.*, 2007]. The latter also implies an overall shrinkage of ice volume, as the thickness of sea ice generally increases with age [*Thorndike et al.*, 1975].

[3] However, due to methodological and logistical constraints, little is known about recent changes of ice thickness. The ice thickness distribution includes important information about both, thermodynamic and dynamic boundary conditions of ice formation and development [*Thorndike et al.*, 1975]. The mode of the thickness distribution, or modal thickness, represents level ice thickness, which is a result of winter accretion and summer ablation. Mean ice thickness is dominated by the tail of the thickness distribution which represents the thickness and amount of deformed ice as a result of ice convergence and shear.

[4] Electromagnetic-inductive (EM) measurements by *Haas* [2004] showed that between the summers (August/September) of 1991 and 2001 the modal (and mean) thickness of large numbers of individual ice floes in the region of the North Pole had decreased from 2.50 m (3.11 m) to 1.95 m (2.41 m), or by 22% (22.5%). Here, we update those findings with more recent measurements performed by means of helicopter-borne EM sounding in the same geographical region in 2001, 2004 and 2007. These show a continued thinning of the ice of the Transpolar Drift. However, as results were obtained in the same geographical region, i.e., in an Eulerian reference system, changes of ice regime and age [*Nghiem et al.*, 2007] have to be considered in their interpretation. Therefore, we include information about the age of the surveyed ice obtained from a buoy-based Drift-Age Model (DM) [*Rigor and Wallace*, 2004]. In 2007, some measurements were also performed during April, i.e., at the end of the freezing season. These will be compared with the summer measurements taking into account and revealing the magnitude of the seasonal thickness cycle.

2. Data

[5] Extensive helicopter-borne EM ice thickness surveys have been performed during cruises of the German icebreaker RV Polarstern in August and September of 2001, 2004 and 2007, representing the minimum ice thickness at the end of the ablation season. In total, 280, 540, and 3140 km of profile data were obtained during 5, 6, and 21 flights in 2001, 2004, and 2007. Each flight was typically performed

[1] Alfred Wegener Institute for Polar and Marine Research, Bremerhaven, Germany.
[2] Now at Department of Earth and Atmospheric Sciences, University of Alberta, Edmonton, Alberta, Canada.
[3] Now at Norwegian Geotechnical Institute, Oslo, Norway.
[4] Septieme Continent, Paris, France.
[5] Polar Science Center, Applied Physics Laboratory, University of Washington, Seattle, Washington, USA.

0094-8276/08/2008GL034457$05.00

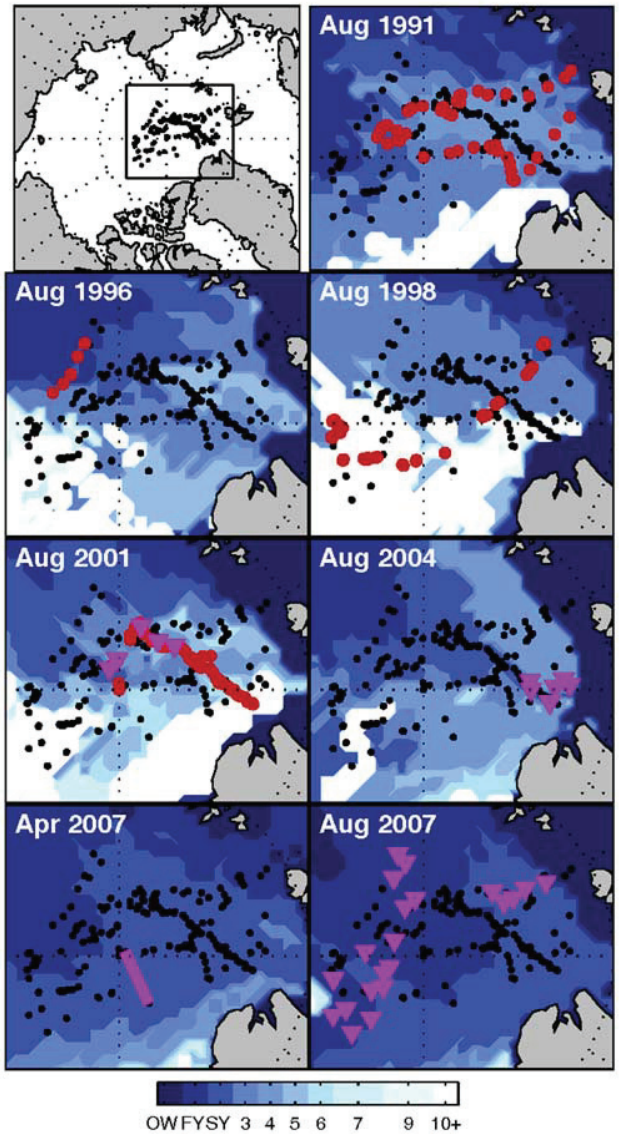

Figure 1. Maps of locations of ground-based (red circles) and helicopter-borne (magenta triangles/line) ice thickness surveys and buoy-derived ice age (color scale) during the measurement campaigns. Black dots show the location of all measurements for comparison.

along a triangular track with a side length of 40 to 80 km, including measurements over thin and thick ice and open water. Figure 1 shows the center location of each flight. Data from the marginal ice zone were excluded from the analysis to limit bias due to low ice concentration which would have enhanced bottom melt [*Perovich et al.*, 2008]. Thickness distributions for each year were derived by averaging over normalized distributions of individual flights, to prevent bias due to different profile lengths. Figure 1 also includes the track of one 350 km long flight performed in April 2007 between the North Pole and 87°N, 58°W, as well as the locations of individual floes profiled by ground-based EM sounding in 1991, 1996, 1998, and 2001 (same as given by *Haas* [2004]).

[6] EM sounding is a classical geophysical method to detect the distance between an EM instrument and the boundary between the resistive sea ice and the conductive sea water. With ground-based measurements, an EM instrument is placed onto the snow or ice surface, and the measured distance to the ice-water interface corresponds to the ice-plus-snow thickness [*Haas and Eicken*, 2001]. These measurements can only be performed on ice which is accessible to walking, i.e., not on very thin or heavily rubbled ice. With helicopter-borne EM (HEM) measurements, the EM instrument is operated at an altitude of 15 to 20 m above the snow or ice surface, and its altitude is measured with a laser altimeter. Ice-plus-snow thickness (hereafter referred to as ice thickness) results from the difference between the altitude above the ice/water-interface and above the snow or ice surface [*Haas et al.*, 2008]. Note that almost all surveys were performed in the summer when the ice was snow-free. Point-spacing of all ground-based and helicopter-borne measurements ranged between 3 and 5 m.

[7] The accuracy of EM measurements is better than ±0.1 m over level ice [*Haas and Eicken*, 2001; *Pfaffling et al.*, 2007]. However, the maximum thickness of pressure ridges is generally underestimated due to their porosity and the lateral extent of electromagnetically induced eddy currents of up to 3.7 times the instrument altitude [*Reid et al.*, 2006]. Measured ridge thickness can deviate by as much as 50% from the "true" thickness. Therefore, obtained thickness distributions are most accurate with respect to their modal thickness, while mean ice thickness can still be used for relative comparisons between regions and campaigns.

[8] In April 2007, in addition to the airborne survey, a 1.78 km long ground-based EM and snow thickness profile was obtained with a point spacing of 8 m. Snow thickness was measured with a meter stick. Results from the snow thickness measurements will be used for comparisons between the April 2007 data and all other summer measurements.

[9] An estimate of the Arctic sea ice age distribution was obtained from the DM [*Rigor and Wallace*, 2004]. It tracks a grid of points (ice parcels) as they move about the Arctic Ocean. This model defines new, first year sea ice in areas of open water in September (the month of the climatological annual minimum in sea ice extent), and advects these ice parcels using the monthly gridded fields of ice motion based on buoy and ice-camp data. If these drifting parcels lie within the limit of the ice edge in September of the following year, they are said to have survived the summer melt, and these parcels are marked as one year older. The process is repeated for each year since 1955. Because of the limited number of buoys, variations in sea ice motion may not be adequately captured in some regions, resulting in uncertainties in the final results.

3. Results

[10] Figure 1 shows that all measurements between 1991 and April 2007 have been performed over ice older than one year. The disagreement in 1996 points to some uncertainty of the ice age maps in the region of the previous summers ice edge, which had been taken as the 90% ice concentration isoline. For an ice concentration threshold of 50% the areas of the 1996 measurements would also be estimated to be

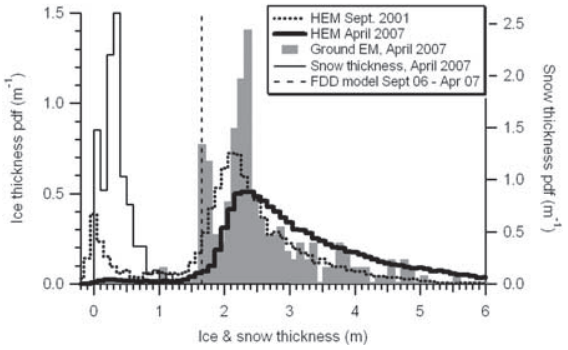

Figure 2. Thickness distributions (probability density functions, pdf; bin width 0.1 m) of ice and snow obtained from HEM sounding in September 2001 and April 2007 in the same region of the Transpolar Drift (cf. Figure 1), and ground EM and snow stake measurements on an individual ice floe at the North Pole in April 2007. Dashed vertical line shows ice thickness of 1.65 m derived from a FDD model.

older than 1 year. Results presented by *Eicken et al.* [1995], *Haas and Eicken* [2001], and *Haas* [2004] showed that ice thicknesses over each study region were remarkably uniform, although the age of the older ice might have been variable, as suggested by Figure 1. This has justified their summary into a single thickness distribution for each observational campaign. In August/September 2007 however, measurements over the generally same geographical region including the North Pole were performed mainly over first-year ice (FYI), as a result of the fundamental regime shift due to the replacement of second-year and older ice by FYI [*Nghiem et al.*, 2007].

[11] Figure 2 summarizes the measurements performed in April 2007. Mean and modal thicknesses along the 350 km long HEM profile were 3.31 ± 1.51 m (mean ± 1 standard deviation) and 2.35 m, respectively. There was only a very small thickness gradient of 0.19 m/° Latitude towards Ellesmere Island in the South, confirming the result of Figure 1 that the flight was exclusively performed over ice of the same, second-year age. Although not measured over the same ice fields nor in the same season, and neglecting interannual variations, Figure 2 compares this thickness distribution with an individual HEM profile obtained on September 8, 2001, close to the North Pole as well (cf. Figure 1), to contrast typical summer and winter ice thickness distributions in a certain region. Modal thickness was only 2.05 m in 2001, in agreement with ground-EM results of *Haas* [2004]. Mean ice thickness amounted to 2.21 ± 1.12 m, including 8 % open water. In contrast, there was only 0.3 % of open water in April 2004. The comparison nicely demonstrates different characteristics of seasonal ice thickness distributions, with large amounts of open water during summer, and much more deformed ice during winter [*Thorndike et al.*, 1975].

[12] When comparing modal thicknesses observed in August/September of 2001 with the one from April 2007, the seasonal thickness cycle and the winter snow thickness have to be taken into account. Figure 2 shows a snow thickness distribution obtained on an individual ice floe close to the North Pole in April 2007. Mean snow thickness was 0.32 ± 0.21 m. There were two modes of 0.05 and 0.3 m, representing snow on FYI and second-year ice (SYI). This corresponded to the ground-based ice thickness distribution, which was also bimodal with modes of 1.65 and 2.35 m for the FYI and SYI, respectively, and a mean thickness of 2.56 ± 0.80 m. The modal thickness of 1.65 m is in good agreement with ice thickness results from a freezing-degree-day (FDD) model [*Lebedev*, 1938]. The model was forced with air temperature observations from surrounding drifting buoys of the International Arctic Buoy Programme between September 2006 and March 2007. Note that the good agreement between modeled and observed thickness is partially due to the thin FYI snow, because it hardly acted as an insulating layer. The large fraction of first-year ice was a local phenomenon, as part of the profiled ice floe had been selected as a landing strip for large supply aircrafts. Otherwise, FYI was hardly present along the HEM profile (Figure 2). However, the modal SYI thicknesses of ground-based and HEM measurements are in very good agreement.

[13] Subtraction of the modal SYI snow thickness of 0.3 m from the modal (total) SYI HEM thickness results in an ice-only modal thickness of 2.05 m, which is very similar to the modal thickness observed in September 2001. Observations of *Perovich et al.* [2008] show that summer surface and bottom ablation amount to 0.3 to 0.5 m in the region of the North Pole. Therefore, our observations suggest that modal SYI thicknesses in our study region would have reduced to 1.75 to 1.55 m in the summer of 2007, i.e., approximately 0.4 m or 20% less than in 2001. If we assume an Arctic seasonal mean thickness cycle of 1.5 m between April and September [*Rothrock et al.*, 1999], mean ice

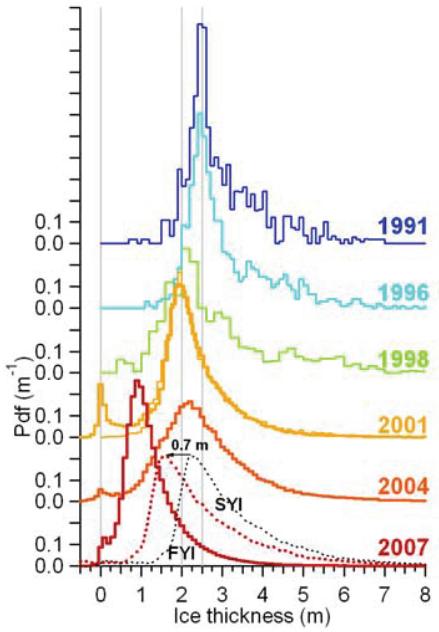

Figure 3. Late summer ice thickness pdfs of the Transpolar Drift, between 1991 and 2007, obtained by means of ground-based (thin lines) and HEM sounding (thick lines), see Figure 1 for measurement locations. The 2007 SYI thickness distribution has been obtained in April 2007 (dotted black line) and was seasonally adjusted by 0.7 m (stippled red line; see text). Vertical grey lines mark ice thicknesses of 2.0 and 2.5 m for reference.

Table 1. Summary of Late Summer Ice Thicknesses in the Transpolar Drift Shown in Figure 3

Year	Mean Thickness Including Water[b] (m)	Open Water Fraction (%)	Mean Thickness, Ice Only[b] (m)	Modal Thickness (m)
1991[a]	N/A[d]	N/A	3.11 ± 1.03	2.50
1996[a]	N/A	N/A	3.11 ± 1.12	2.45
1998[a]	N/A	N/A	2.88 ± 1.49	2.10
2001[a]	N/A	N/A	2.41 ± 0.98	1.95
2001	2.20 ± 1.05	5	2.31 ± 0.95	1.90
2004	2.59 ± 1.27	1	2.63 ± 1.24	2.20
2007 (April)[c]	1.81[c] (3.31 ± 1.51)	0.3	1.82[c] (3.32 ± 1.35)	1.65[c] (2.35)
2007	1.27 ± 0.77	2	1.30 ± 0.76	0.90

[a]From *Haas* [2004].
[b]Mean ± 1 standard deviation.
[c]Values are seasonally adjusted. Parentheses show original April thickness.
[d]N/A: Not applicable.

thickness would have reduced to 1.81 m, i.e., 0.59 m or 25% less than the ice-only mean thickness in the summer of 2001.

[14] Figure 3 shows a comparison of all thickness distributions obtained in the Transpolar Drift since 1991. Since 2001, airborne measurements were performed, and the excellent agreement of the 2001 ground-based [*Haas*, 2004] and HEM thickness distributions show how well both methods are comparable.

[15] Table 1 summarizes the results of all HEM thickness measurements, and compares them with the earlier results of *Haas* [2004]. In contrast to the ground-based measurements, the HEM data also include information about the thickness and fraction of thin ice and open water. Here, all measurements less than 0.15 m thick have been defined as open water, and the open water fraction and ice-only thicknesses are listed separately.

[16] In 2001, overall modal thickness was 1.90 m, and mean thicknesses amounted to 2.20 ± 1.05 m including 5% of open water. In 2004 modal and mean ice thicknesses amounted to 2.20 and 2.59 ± 1.27 m including 1% open water. This was slightly thicker than in 2001, probably as a result of the more downstream location of the study region along the Transpolar Drift and the older age of the ice (Figure 1). Therefore, the 2004 data is not discussed in more detail. In Figure 3, the April 2007 SYI thickness distribution has been shifted by 0.7 m towards thinner ice, corresponding to the seasonal adjustment for snow ablation (0.3 m) and summer ice thinning (0.4 m) outlined above.

[17] Figure 3 also includes the thickness distribution obtained from all flights in August/September 2007 over vast regions of predominantly FYI (cf. Figure 1). As in previous years and despite the partial contribution of SYI according to Figure 1, ice thicknesses of all profiles were remarkably similar, with modal and mean thicknesses of individual flights ranging between 0.65 and 0.95 m, and 1.01 and 1.48 m respectively. Overall, modal and mean ice thicknesses amounted to 0.90 m and 1.27 ± 0.77 m (1.30 ± 0.76 m) including (excluding) measurements over the 2% coverage of open water. This is a drastic thinning of 53% and 44% modal and mean (ice only) thickness of the ice in the region of the North Pole between 2001 and 2007. However, it is largely due to the replacement of predominantly second-year and older ice by FYI in the study region. Therefore, the August/September 2007 results can best be compared with ground-based thickness measurements over FYI performed further south in the Laptev Sea in the summer of 1995, which marked a previous ice thickness and extent minimum with a similar atmospheric pressure pattern as in the summer of 2007 [*Haas and Eicken*, 2001; *Stroeve et al.*, 2008]. In 1995 the ice had modal and mean thicknesses of 1.25 m and 1.80 ± 1.10 m, respectively, i.e., 28% and 30% thicker than in 2007.

[18] The modal FYI thickness of 1.65 m in April 2007 in Figure 2 and its good agreement with the FDD-model can be considered as some maximum thickness of ice grown between the fall of 2006 and April 2007. If compared with the modal thickness of 0.9 m measured in August/September 2007, the difference of 0.75 m could be considered as a measure of the seasonal thinning during the summer.

4. Discussion and Conclusions

[19] Our ice thickness data set is very heterogeneous as it has been obtained during sporadic expeditions to varying but overlapping regions of the Transpolar Drift. However, the uniformity of the derived thickness distributions and the inclusions of ice age information in our interpretations justify the conclusion of a rapidly thinning ice cover. Both, modal and mean SYI and FYI thicknesses have decreased in the region of the North Pole. The reduction of modal thicknesses is a result of increased atmospheric and ocean heat fluxes to the ice. Unfortunately, we are not able to distinguish between the individual processes. However, the good agreement with the FDD model suggests an important role of increased air temperature, while increases in ocean heat flux might have played a minor role in the present thinning. Ice concentration was remarkably high in our study region in 2004 and 2007, limiting the deposition of heat in the mixed layer [*Perovich et al.*, 2008]. The presented results provide valuable information for the validation and improvement of numerical sea ice models.

[20] Ice concentration in the summers of 2004 and 2007 was also significantly higher than in 2001. In contrast, there were large open areas in the region of the North Pole in 2001, and overall Arctic ice extent assumed a local small temporal maximum. In 2007, high ice concentrations could have been a result of ice compression in the study region by the general atmospheric circulation over the Arctic, which was also responsible for the strong northward retreat and advection of the ice edge and resulting minimum ice extent [*Stroeve et al.*, 2008; *Kwok*, 2008]. One can speculate that this intensification of ice drift and the displacement of SYI towards North America have increased ice thickness north

of the coasts of Greenland and Canada. Future surveys should be extended over that region to allow better observations of the overall ice mass balance.

[21] Clearly, the thinner ice cover favors a stronger areal retreat of the ice during summer. The uniformity of the observed thickness distribution points to the possibility of further rapid reductions once that vast uniform region has thinned further below certain thresholds, e.g., due to the amplitude of the average or melt-pond related seasonal summer thinning. Unfortunately, we cannot demonstrate any causal relation between ice thickness and ice drift, but it is likely that the thinner and weaker ice cover also facilitates a faster ice drift, which resulted in the occurrence of FYI at the North Pole in the summer of 2007, and is still ongoing as of this writing (July 2008).

[22] Our measurements mark a technological milestone with the onset of regional HEM surveying. Now, observations of the fractions and thicknesses of thin ice and open water are included in the results, in contrast to the earlier ground-based measurements [*Haas and Eicken*, 2001; *Haas*, 2004]. With this, the measurements are also better comparable with other thickness estimates, e.g., from upward-looking sonars (ULS) or satellite altimetry. We hope that we will soon be able to perform more systematic surveys, e.g., by employing the EM method from fixed-wing aircraft, airships, or hovercrafts.

[23] **Acknowledgments.** We thank the station team of the Barneo Ice Camp as well as the helicopter crew of RV Polarstern for their great logistical support, as well as Jan Lieser, Volker Leinweber, and many other people for help with the measurements. Buoy data were obtained from the International Arctic Buoy Programme. Measurements were partially funded by Total and the EU project DAMOCLES. Rigor is funded by ONR, NASA, NOAA, and NSF.

References

Eicken, H., M. Lensu, M. Leppäranta, W. B. Tucker, A. J. Gow, and O. Salmela (1995), Thickness, structure and properties of level summer multi-year ice in the Eurasian sector of the Arctic Ocean, *J. Geophys. Res.*, *100*(C11), 22,697–22,710.

Haas, C. (2004), Late-summer sea ice thickness variability in the Arctic Transpolar Drift 1991–2001 derived from ground-based electromagnetic sounding, *Geophys. Res. Lett.*, *31*, L09402, doi:10.1029/2003GL019394.

Haas, C., and H. Eicken (2001), Interannual variability of summer sea ice thickness in the Siberian and central Arctic under different atmospheric circulation regimes, *J. Geophys. Res.*, *106*(C3), 4449–4462.

Haas, C., J. Lobach, S. Hendricks, L. Rabenstein, and A. Pfaffling (2008), Helicopter-borne measurements of sea ice thickness, using a small and lightweight, digital EM system, *J. Appl. Geophys.*, in press.

Holland, M. M., C. M. Bitz, and B. Tremblay (2006), Future abrupt reductions in the summer Arctic sea ice, *Geophys. Res. Lett.*, *33*, L23503, doi:10.1029/2006GL028024.

Kwok, R. (2008), Summer sea ice motion from the 18 GHz channel of AMSR-E and the exchange of sea ice between the Pacific and Atlantic sectors, *Geophys. Res. Lett.*, *35*, L03504, doi:10.1029/2007GL032692.

Lebedev, V. V. (1938), Rost l'da v arkticheskikh rekakh i moriakh v zavisimosti ot otritsatel'nykh temperatur vozdukha, *Probl. Arkt. Antarkt.*, *5, 9–25.*

Lindsay, R. W., and J. Zhang (2005), The thinning of Arctic sea ice, 1988–2003: Have we passed a tipping point?, *J. Clim.*, *18*, 4879–4894.

Nghiem, S. V., I. G. Rigor, D. K. Perovich, P. Clemente-Colón, J. W. Weatherly, and G. Neumann (2007), Rapid reduction of Arctic perennial sea ice, *Geophys. Res. Lett.*, *34*, L19504, doi:10.1029/2007GL031138.

Perovich, D. K., J. A. Richter-Menge, K. F. Jones, and B. Light (2008), Sunlight, water, and ice: Extreme Arctic sea ice melt during the summer of 2007, *Geophys. Res. Lett.*, *35*, L11501, doi:10.1029/2008GL034007.

Pfaffling, A., C. Haas, and J. E. Reid (2007), A direct helicopter EM sea ice thickness inversion, assessed with synthetic and field data, *Geophysics*, *72*, F127–F137.

Polyakov, I., et al. (2007), Observational program tracks Arctic Ocean transition to a warmer state, *Eos Trans. AGU*, *88*(40), 398, doi:10.1029/2007EO400002.

Reid, J., A. Pfaffling, and J. Vrbancich (2006), Airborne electromagnetic footprints in one-dimensional earths, *Geophysics*, *71*, G63–G72, doi:10.1190/1.2187756.

Rigor, I. G., and J. M. Wallace (2004), Variations in the age of Arctic sea-ice and summer sea-ice extent, *Geophys. Res. Lett.*, *31*, L09401, doi:10.1029/2004GL019492.

Rothrock, D. A., Y. Yu, and G. A. Maykut (1999), Thinning of the Arctic sea-ice cover, *Geophys. Res. Lett.*, *26*, 3469–3472.

Stroeve, J., M. M. Holland, W. Meier, T. Scambos, and M. Serreze (2007), Arctic sea ice decline: Faster than forecast, *Geophys. Res. Lett.*, *34*, L09501, doi:10.1029/2007GL029703.

Stroeve, J., M. Serreze, S. Drobot, S. Gearheard, M. Holland, J. Maslanik, W. Meier, and T. Scambos (2008), Arctic sea ice extent plummets in 2007, *Eos Trans. AGU*, *89*(2), 13, doi:10.1029/2008EO020001.

Thorndike, A. S., D. A. Rothrock, G. A. Maykut, and R. Colony (1975), The thickness distribution of sea ice, *J. Geophys. Res.*, *80*(33), 4501–4513.

J.-L. Etienne, Septieme Continent, 11, rue Caulaincourt, Paris F-75018, France.

C. Haas, Department of Earth and Atmospheric Sciences, University of Alberta, 1-26 Earth Sciences Building, Edmonton, AB T6G 2E3, Canada. (chaas@ualberta.ca)

S. Hendricks and L. Rabenstein, Alfred Wegener Institute for Polar and Marine Research, Bussestrasse 24, D-27570 Bremerhaven, Germany.

A. Pfaffling, Norwegian Geotechnical Institute, Sognsveien 72, Oslo N-0806, Norway.

I. Rigor, Polar Science Center, Applied Physics Laboratory, University of Washington, 1013 NE 40th Street, Seattle, WA 98105, USA.